The Astrophysical Journal, 753:156 (38pp), 2012 July 10 doi:10.1088/0004-637X/753/2/156

FURTHER DEFINING SPECTRAL TYPE "Y" AND EXPLORING THE LOW-MASS END OF THE FIELD BROWN DWARF MASS FUNCTION

J. Davy Kirkpatrick[1], Christopher R. Gelino[1], Michael C. Cushing[2], Gregory N. Mace[3], Roger L. Griffith[1], Michael F. Skrutskie[4], Kenneth A. Marsh[1], Edward L. Wright[3], Peter R. Eisenhardt[5], Ian S. McLean[3], Amanda K. Mainzer[5], Adam J. Burgasser[6], C. G. Tinney[7], Stephen Parker[7], and Graeme Salter[7]
[1] Infrared Processing and Analysis Center, MS 100-22, California Institute of Technology, Pasadena, CA 91125, USA; davy@ipac.caltech.edu
[2] Department of Physics and Astronomy, MS 111, University of Toledo, 2801 W. Bancroft St., Toledo, OH 43606-3328, USA
[3] Department of Physics and Astronomy, UCLA, Los Angeles, CA 90095-1547, USA
[4] Department of Astronomy, University of Virginia, Charlottesville, VA 22904, USA
[5] NASA Jet Propulsion Laboratory, 4800 Oak Grove Drive, Pasadena, CA 91109, USA
[6] Department of Physics, University of California, San Diego, CA 92093, USA
[7] Department of Astrophysics, School of Physics, University of New South Wales, NSW 2052, Australia
Received 2012 April 1; accepted 2012 May 9; published 2012 June 25

ABSTRACT

We present the discovery of another seven Y dwarfs from the *Wide-field Infrared Survey Explorer* (*WISE*). Using these objects, as well as the first six *WISE* Y dwarf discoveries from Cushing et al., we further explore the transition between spectral types T and Y. We find that the T/Y boundary roughly coincides with the spot where the $J-H$ colors of brown dwarfs, as predicted by models, turn back to the red. Moreover, we use preliminary trigonometric parallax measurements to show that the T/Y boundary may also correspond to the point at which the absolute H (1.6 μm) and W2 (4.6 μm) magnitudes plummet. We use these discoveries and their preliminary distances to place them in the larger context of the solar neighborhood. We present a table that updates the entire stellar and substellar constituency within 8 pc of the Sun, and we show that the current census has hydrogen-burning stars outnumbering brown dwarfs by roughly a factor of six. This factor will decrease with time as more brown dwarfs are identified within this volume, but unless there is a vast reservoir of cold brown dwarfs invisible to *WISE*, the final space density of brown dwarfs is still expected to fall well below that of stars. We also use these new Y dwarf discoveries, along with newly discovered T dwarfs from *WISE*, to investigate the field substellar mass function. We find that the overall space density of late-T and early-Y dwarfs matches that from simulations describing the mass function as a power law with slope $-0.5 < \alpha < 0.0$; however, a power law may provide a poor fit to the observed object counts as a function of spectral type because there are tantalizing hints that the number of brown dwarfs continues to rise from late-T to early-Y. More detailed monitoring and characterization of these Y dwarfs, along with dedicated searches aimed at identifying more examples, are certainly required.

Key words: brown dwarfs – solar neighborhood – stars: low-mass – stars: luminosity function, mass function – surveys – techniques: spectroscopic

Online-only material: color figures

1. INTRODUCTION

The coldest field brown dwarfs hold important clues that span a variety of astronomical fields. In the field of star formation, these coldest brown dwarfs contain a historical record of the formation process at very low masses and at epochs many Gyr before the active formation regions we observe today. In the field of planetary atmospheric theory, they represent low-temperature atmospheres that can be used as simple test cases for predictions because they lack the complications of photochemical processes produced through irradiation by a host sun. In the field of exoplanet searches, they provide interesting, nearby targets that may harbor planetary systems in their own right.

The *Wide-field Infrared Survey Explorer* (*WISE*; Wright et al. 2010) was built in part to identify these coldest brown dwarfs by using their signature methane absorption bands as a photometric diagnostic to distinguish them from myriad background sources. Specifically, the shortest wavelength *WISE* band, hereafter denoted W1, has a central wavelength of 3.4 μm, which falls in the middle of the strong fundamental methane absorption band near 3.3 μm. The second shortest *WISE* band, hereafter denoted W2, has a central wavelength of 4.6 μm, which detects light arising from deeper, hotter layers in the brown dwarf atmosphere; at this wavelength, the atmosphere is fairly transparent to radiation, a direct analog being the 5 μm "holes" in the atmosphere of Jupiter (Westphal 1969). As a result, the W1–W2 color can be used to identify cold brown dwarfs because that color should be very red. *WISE* also observes in two other bandpasses, hereafter denoted as W3 and W4, centered at 12 and 22 μm, that can be used to eliminate sources with longer-wavelength flux inconsistent with that of brown dwarfs. In addition to color discrimination, *WISE* also benefits from observations at wavelengths where cold brown dwarfs are emitting most of their light. The all-sky nature of the survey means that the closest and brightest examples in the solar neighborhood will be imaged.

In this paper, we present the discovery of another seven Y dwarfs—the coldest class of brown dwarfs recognized (Cushing et al. 2011)—which brings the total found with *WISE* to thirteen. In Section 2, we discuss their selection as cold brown dwarf candidates along with their confirmation as Y dwarfs. In Section 3, we discuss further the definition of spectral type Y. In Section 4, we place the Y dwarfs in context with other spectral classes by comparing their relative fluxes and space densities,

the latter of which is also used to divine clues regarding the shape of the low-mass end of the (sub)stellar mass function. In that section, we also compare those results to several other studies that have, either directly or indirectly, probed this same mass regime.

2. NEW Y DWARF DISCOVERIES

2.1. Candidate Selection

To support the All-Sky data release in 2012 March, the *WISE* four-band cryogenic data were reprocessed using an improved version of the reduction pipeline, as described in the *WISE* All-Sky Data Release Explanatory Supplement.[8] The individual W1, W2, W3, and W4 frames were rerun and atlas images rebuilt by stacking the individual, reprocessed frames. Source detections were made on the atlas images themselves, and source extractions were made on both the individual frames and the atlas images. Our query for cold brown dwarfs used the database of extractions from the atlas images, this database being a union of the *WISE* All-Sky Source Catalog and the *WISE* All-Sky Reject Table. This query attempts to improve upon the search we used earlier (Kirkpatrick et al. 2011) and is aimed toward identifying mid-T or later brown dwarfs for further follow-up. The search constraints are given below.

1. The W1–W2 color from profile-fit photometry is greater than 2.0 mag, where the W2 measurement is an actual detection. (This criterion guarantees that the W2 signal-to-noise ratio is greater than three.) As Figure 1 of Kirkpatrick et al. (2011) shows, this color is typical of objects of type mid-T and later.
2. The source is detected with a signal-to-noise ratio greater than three in at least eight individual W2 frames going into the co-add stack or, if detected only five, six, or seven times, is still detected at a signal-to-noise ratio greater than three in at least 40% of all frames. This criterion is meant to eliminate spurious, co-aligned artifacts in the co-adds.
3. The source is either undetected in W3 or, if detected, has a W2–W3 color less than 3.5 mag. This criterion is meant to eliminate very red extragalactic contaminants or sources embedded in star formation regions.
4. The source is not flagged as a diffraction spike, star halo, optical ghost, or latent artifact in bands W1 and W2. This criterion is meant to remove known spurious sources. Real sources that are flagged in W1 and W2 as impacted by spikes, halos, ghosts, or latents are, however, retained.
5. The source is not blended with another source. This criterion is meant to reduce the number of objects with poorly determined photometry.
6. The source has a reduced χ^2 value from profile-fit photometry that lies between 0.5 and 3.0. This criterion is meant to eliminate sources that are not point-like.
7. The source has an absolute Galactic latitude greater than 3° if its Galactic longitude falls within 20° of zero. This criterion is meant to eliminate confused areas toward the Galactic center.

With this list of sources in hand, images of the field were constructed using Digitized Sky Survey 2 (DSS2) *BRI* (epoch ∼1980s), Sloan Digital Sky Survey (SDSS) *ugriz* (where available; epoch ∼2000), Two Micron All Sky Survey (2MASS) JHK_s (epoch ∼2000), and *WISE* four-band data (epoch ∼2010). These image sets, an example of which is shown in Figure 1, show the source across time and across wavelength. By using these images, sources that cannot possibly be cold brown dwarfs, because they are extended, spurious, or detected at wavelengths shortward of 1.0 μm (unless very bright in the *WISE* W1 and W2 bandpasses), were eliminated from further consideration.

To select objects within 20 pc of the Sun, we further restricted the W2 magnitude depending on the color of the source:[9] W2 $\leqslant$ 14.5 mag for 2.0 $\leqslant$ W1–W2 $<$ 2.4, W2 $\leqslant$ 14.8 mag for 2.4 $\leqslant$ W1–W2 $<$ 2.8, and W2 $\leqslant$ 15.2 mag for 2.8 $\leqslant$ W1–W2 $<$ 2.9. For colors redder than this—W1–W2 = 2.9 being the color of the standard T9 dwarf UGPS J072227.51−054031.2—no W2 magnitude constraint was applied because at the time of candidate selection, the absolute magnitudes of objects with types $\geqslant$T9 were very poorly known. This search results in 534 candidates along with 30 re-discovered T dwarfs identified earlier by other surveys. Candidates have been placed on our photometry and spectroscopy campaigns, as described in the next section. To date, 189 of these 534 candidates have been followed up via ground-based or *Hubble Space Telescope* imaging, All 534 are on our *Spitzer Space Telescope* follow-up imaging campaign, and 130 have been observed spectroscopically. This paper focuses on the new Y dwarf discoveries; for newly found T dwarfs, the reader is referred to G. N. Mace et al. (in preparation), C. G. Tinney et al. (in preparation), and Wright et al. (2012).

2.2. Follow-up

Cushing et al. (2011) identified the first six Y dwarfs using *WISE* data, and we confirm seven more here. Coordinates and photometry from the *WISE* All-Sky Release are given in Table 1 for all 13 of these Y dwarfs. In order to facilitate future investigations, we also provide finder charts for all 13 in Figure 2. These charts show the W1, W2, and W3 discovery images from *WISE* as well as a deep near-infrared (1.2–1.6 μm) view at higher resolution.

Photometry of the new Y dwarfs is listed in Table 2 along with (in some cases, revised) photometry for the six Y dwarfs from Cushing et al. (2011). Six ground-based instruments and two space-based facilities—in addition to *WISE*, whose imaging identified these objects originally—were used for this imaging follow-up. Spectra of the new Y dwarfs were obtained in the ∼1.0–1.8 μm region with three different instruments. Details for the spectroscopic observations are given in Table 3.

2.2.1. Mt. Bigelow/2MASS

The 2MASS camera on the 1.5 m Kuiper Telescope on Mt. Bigelow, Arizona, observes simultaneously in 2MASS *J*, *H*, and K_s filters (Milligan et al. 1996) using three 256 × 256 NICMOS3 arrays. The plate scale for all three arrays is 1.″65 pixel^{-1}, resulting in a 7′ × 7′ field of view. The only new Y dwarf in Table 2 whose photometry we report from the Bigelow/2MASS camera is WISE 0146+4234.[10] Data acquisition and reduction for this instrument have been described earlier in Kirkpatrick et al. (2011).

2.2.2. AAT/IRIS2

The IRIS2 instrument (Tinney et al. 2004) at the 3.9 m Anglo-Australian Telescope (AAT) at Siding Spring Observatory,

[8] See http://wise2.ipac.caltech.edu/docs/release/allsky/.

[9] Our team also maintains ancillary lists of candidates with bluer colors or fainter magnitudes, but those are beyond the scope of this paper.

[10] Hereafter, we abbreviate the full WISE Jhhmmss.ss±ddmmss.s designations in the text as WISE hhmm±ddmm.

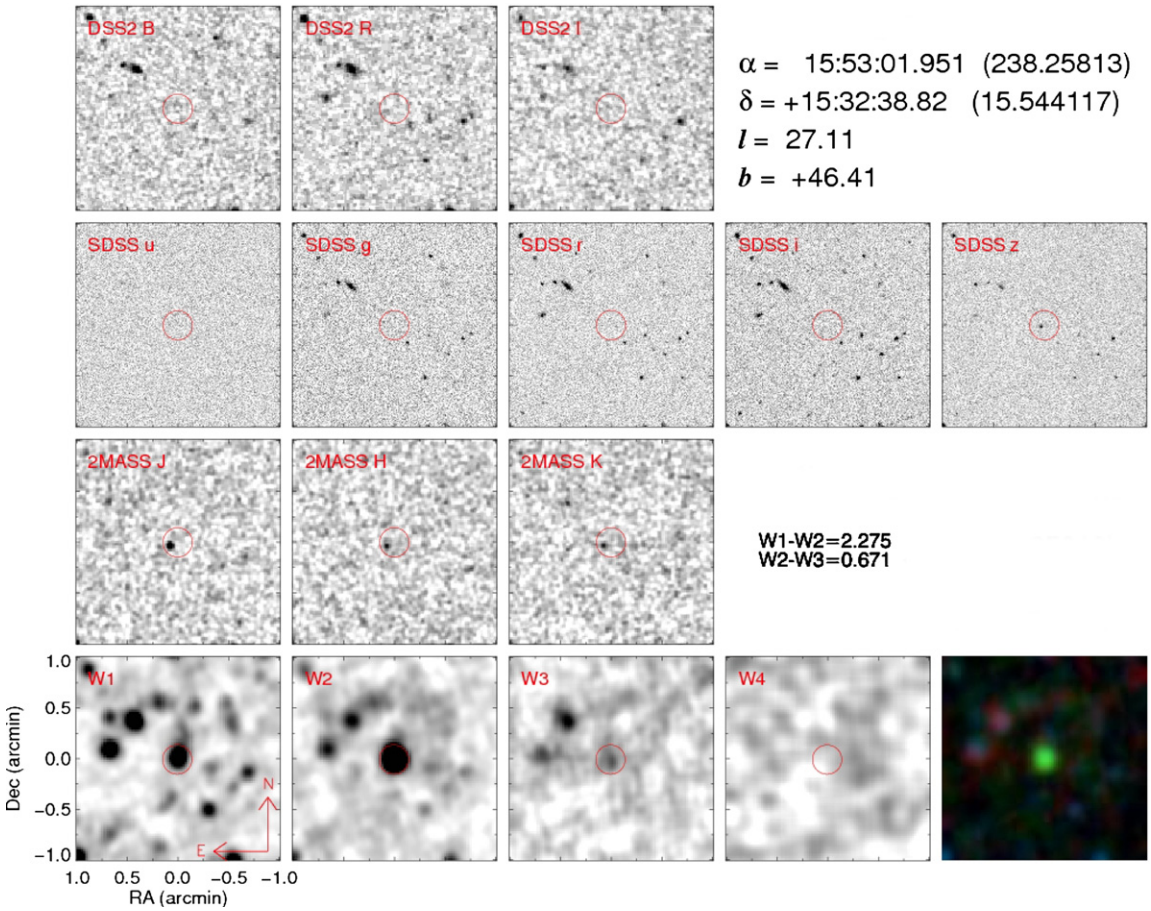

Figure 1. Images of one of our brown dwarf candidates, the previously known T7 dwarf 2MASSI J1553022+153236 from Burgasser et al. (2002). Each row in this image represents a different survey and each image shows a 2 × 2 arcmin region at a different wavelength. The top row shows *B*, *R*, and *I* images from the Digitized Sky Survey 2 (DSS2). The second row shows *u*, *g*, *r*, *i*, and *z* images from the Sloan Digital Sky Survey (SDSS; York et al. 2000). The third row shows *J*, *H*, and K_s images from the Two Micron All-Sky Survey (2MASS; Skrutskie et al. 2006). The last row shows the W1, W2, W3, and W4 images from *WISE* along with a three-color image comprised of W1 (blue), W2 (green), and W3 (red). Sexagesimal and decimal R.A. (α) and decl. (δ) coordinates of the source are given in the upper right, along with the Galactic longitude (l) and latitude (b) in decimal degrees. Also shown are the W1–W2 and W2–W3 colors from *WISE*. A red circle is shown at the location of the candidate identified in *WISE*. For this object, the source is detected only at SDSS *z*, all three 2MASS bands, and the three shortest wavelength bands of *WISE*; detections at these wavelengths are common for nearby, bright T dwarfs. Motion is seen from the earliest epochs (2MASS and SDSS) to the latest (*WISE*), further confirming this as a good candidate.

(A color version of this figure is available in the online journal.)

Table 1
WISE All-Sky Release Photometry of *WISE* Y Dwarfs

WISE Designation	W1 (mag)	W2 (mag)	W3 (mag)	W4 (mag)	W1–W2 (mag)	W2–W3 (mag)	Spec. Type
(1)	(2)	(3)	(4)	(5)	(6)	(7)	(8)
WISE J014656.66+423410.0	>18.99	15.08 ± 0.07	13.20 ± 0.51	>9.41	>3.91	1.88 ± 0.51	Y0
WISE J035000.32−565830.2	>18.90	14.73 ± 0.06	12.53 ± 0.29	>9.00	>4.17	2.20 ± 0.30	Y1
WISE J035934.06−540154.6	>19.29	15.42 ± 0.07	>13.02	>9.76	>3.87	<2.40	Y0
WISE J041022.71+150248.4[a]	>18.33	14.18 ± 0.06	>11.86	>8.90	>4.15	<2.32	Y0
WISE J053516.80−750024.9	>18.92	15.06 ± 0.07	13.12 ± 0.45	>9.00	>3.86	1.94 ± 0.46	⩾Y1:
WISE J071322.55−291751.9	>18.35	14.48 ± 0.06	12.67 ± 0.43	>9.22	>3.87	1.81 ± 0.43	Y0
WISE J073444.02−715744.0	>19.42	15.36 ± 0.06	13.65 ± 0.42	9.65 ± 0.33	>4.06	1.71 ± 0.42	Y0
WISE J140518.39+553421.3[a]	>18.82	14.10 ± 0.04	12.43 ± 0.27	>9.40	>4.72	1.67 ± 0.27	Y0 pec?
WISE J154151.65−225024.9[a]	16.74 ± 0.17[b]	14.25 ± 0.06	>12.31	>8.89	2.49 ± 0.18[b]	<1.94	Y0.5
WISE J173835.53+273259.0[a]	>18.41	14.55 ± 0.06	11.93 ± 0.19	>8.98	>3.86	2.62 ± 0.20	Y0
WISE J182831.08+265037.7[a]	>18.47	14.39 ± 0.06	>12.53	>8.75	>4.08	<1.86	⩾Y2
WISE J205628.91+145953.2[a]	>18.25	13.93 ± 0.05	12.00 ± 0.27	>8.78	>4.32	1.93 ± 0.27	Y0
WISE J222055.31−362817.4	>18.65	14.66 ± 0.06	>12.81	>9.30	>3.99	>1.85	Y0

Notes.

[a] For details about these sources, please see Cushing et al. (2011).

[b] This source has a bluer W1–W2 color than it did in earlier *WISE* processing—W1–W2 = 2.49 ± 0.18 now versus W1–W2 > 3.04 before (Kirkpatrick et al. 2011). In both cases, the strong W2 detection would have driven the photometry, but in the newer processing, the code appears to have erroneously assigned to this object some of the W1 flux from the bright star to the north, therefore producing a brighter W1 detection for WISE 1541−2250 than actually exists.

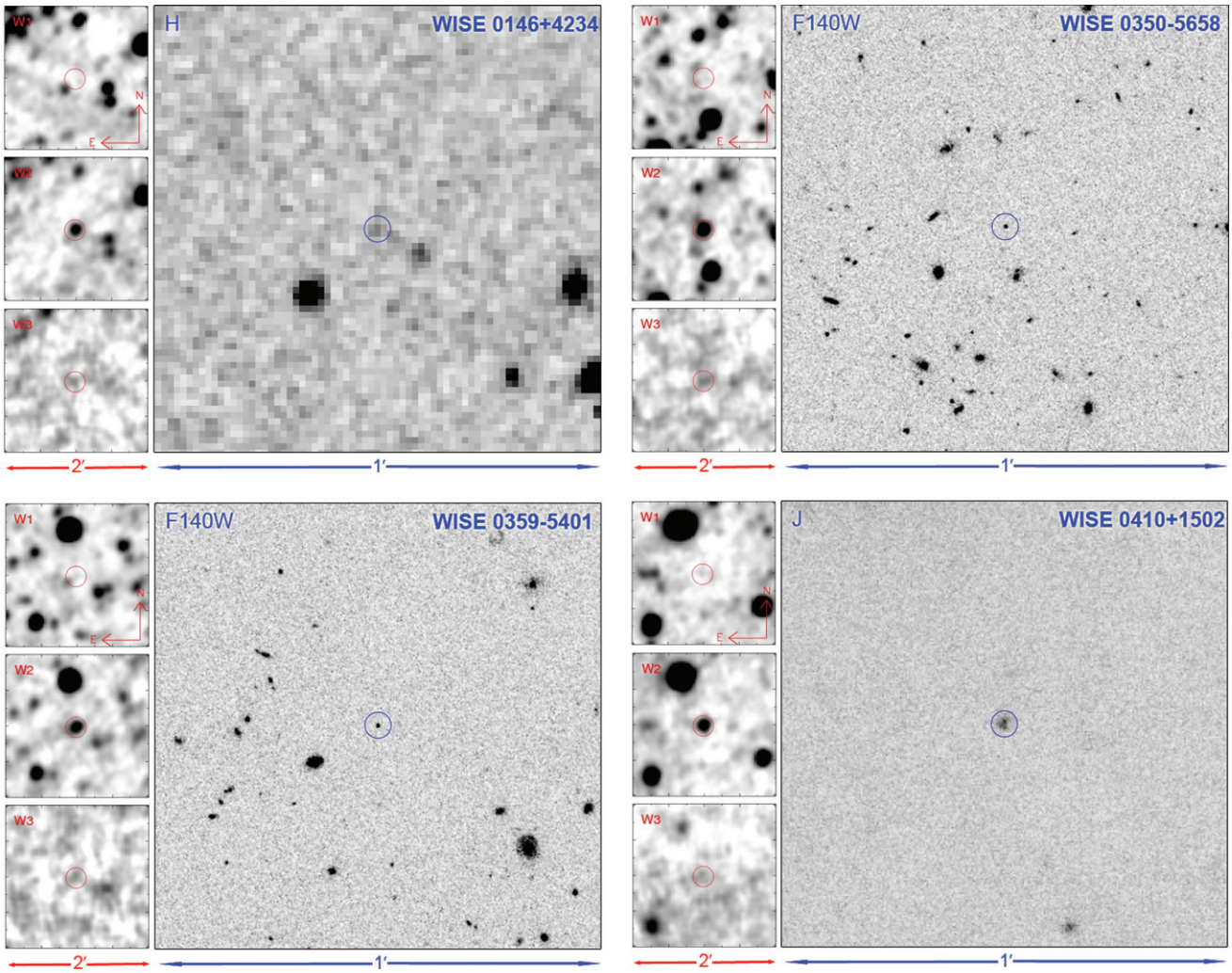

Figure 2. Finder charts for all 13 known *WISE* Y dwarf discoveries. Along the left are 2 × 2 arcmin images from *WISE* in bands W1, W2, and W3 with the location of the Y dwarf shown by the red circle. The large image on the right is a 1 × 1 arcmin zoom taken in the near-infrared; the Y dwarf is circled in blue. In all images, north is up and east is to the left. Note that the field for WISE 0535−7500 is located toward the outskirts of the Large Magellanic Cloud, which is the reason for the high source density. For WISE 0713−2917, our near-infrared image on the right does not completely fill the 1 × 1 arcmin field allotted for it. For WISE 1541−2250, the prominent white ring on the large image is a latent artifact caused by a bright star during the dithering process.

(A color version of this figure is available in the online journal.)

Australia, provides wide-field imaging (7.′7 × 7.′7) using a 1024 × 1024 (0.″4486 pixel^{-1}) Rockwell HAWAII-1 HgCdTe infrared detector. Our observation of WISE 2220−3628 used only the *J* filter, which is on the MKO-NIR system (Tokunaga et al. 2002). Data collection and reduction for this instrument are described in C. G. Tinney et al. (in preparation).

2.2.3. CTIO/NEWFIRM

The NOAO Extremely Wide Field Infrared Imager (NEWFIRM; Swaters et al. 2009) at the 4 m Victor M. Blanco Telescope on Cerro Tololo, Chile, uses four 2048 × 2048 InSb arrays arranged in a 2 × 2 grid. With a pixel scale of 0.″40 pixel^{-1}, this grid covers a total field of view of 27.′6 × 27.′6. Only one of our new Y dwarfs, WISE 0734−7157, was acquired with this instrument and it was observed only at *J* band, which is on the MKO-NIR system. Observing and reduction strategies are described in Kirkpatrick et al. (2011).

2.2.4. SOAR/SpartanIRC

The Spartan Infrared Camera (SpartanIRC; Loh et al. 2004) at the 4.1 m Southern Astrophysics Research (SOAR) Telescope on Cerro Pachón, Chile, uses four 2048 × 2048 pixel HAWAII-2 arrays arranged in a 2 × 2 grid. The field of view can be set to cover either a 3′ × 3′ (0.″043 pixel^{-1}) or 5′ × 5′ (0.″073 pixel^{-1}) area per array. Our only observation, of WISE 0713−2917, was done with the larger field of view in the *J* and *H* filters, which are on the MKO-NIR system. Observing strategy and data reductions followed the same prescription discussed in Burgasser et al. (2011).

2.2.5. SOAR/OSIRIS

The Ohio State Infrared Imager/Spectrometer (OSIRIS), also at SOAR, uses a 1024 × 1024 HAWAII HgCdTe array. The field of view can be set to cover either a 2.′4 × 2.′4 (0.″139 pixel^{-1}) or 5.′6 × 5.′6 (0.″331 pixel^{-1}) area. The Y dwarf WISE 0713−2917 was observed at both *J* and *H*, and the Y dwarf WISE 2220−3628 was observed only at the *H* band. These are Barr filters; for *H* band, the filter curve[11] has half-power points near 1.48 and 1.78 μm. Comparison of this

[11] See http://www.ctio.noao.edu/instruments/ir_instruments/osiris2soar/config/index.html.

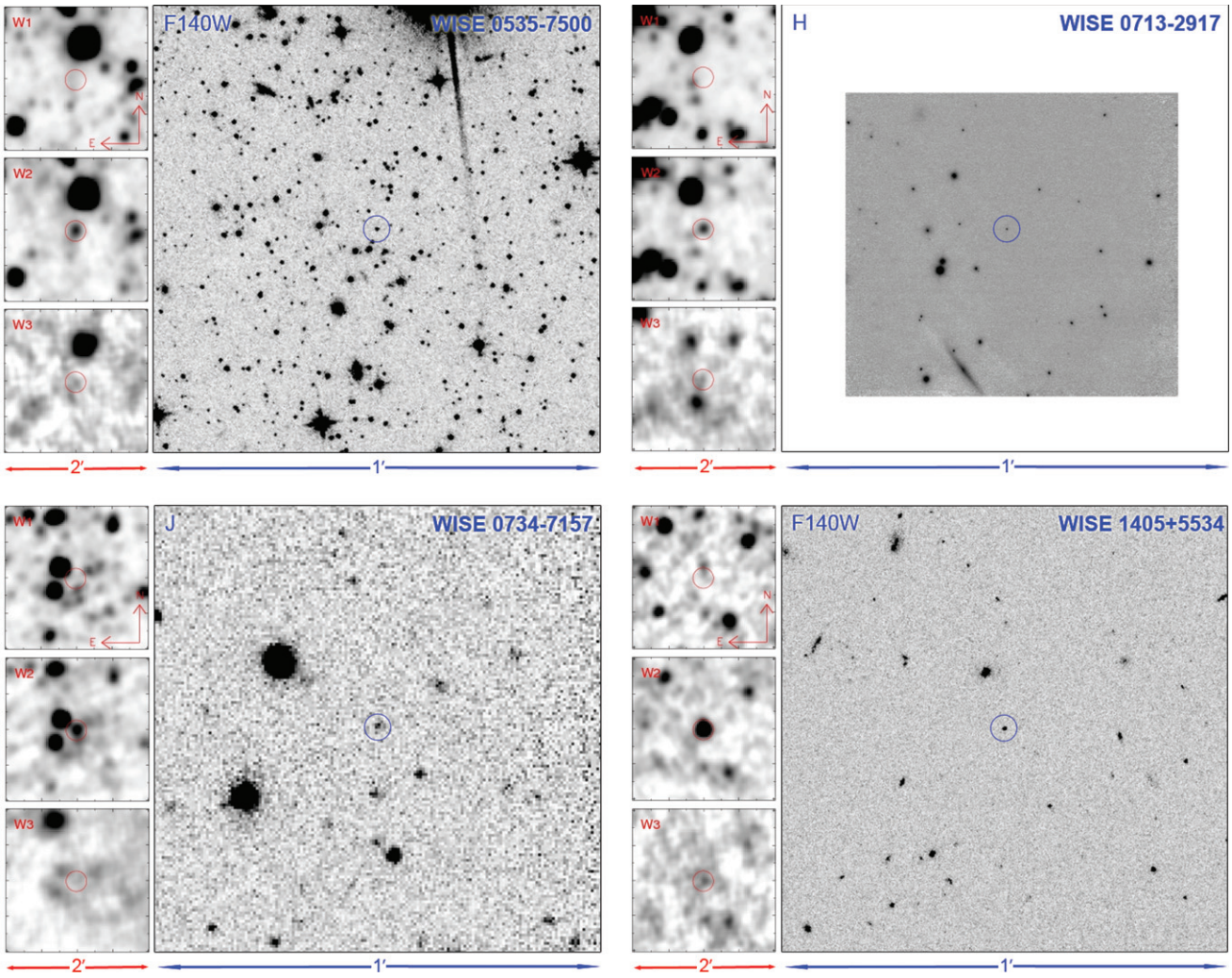

Figure 2. (Continued)

filter curve to the filter curves illustrated in Figure 4 of Bessell (2005) shows that it is very similar to the MKO-NIR *H*-band filter. Observing strategy and data reductions followed the same prescription as those of SpartanIRC (discussed in Burgasser et al. 2011).

2.2.6. Magellan/PANIC

Persson's Auxiliary Nasmyth Infrared Camera (PANIC; Martini et al. 2004) at the 6.5 m Magellan Baade Telescope on Cerro Manqui at the Las Campanas Observatory, Chile, has a 1024 × 1024 HAWAII array with a plate scale of 0.″125 pixel^{-1}, resulting in a 2′ × 2′ field of view. Observations of three of our new Y dwarfs—WISE 0350−5658, WISE 0359−5401, and WISE 0535−7500—were obtained at *J* and *H* bands on the Carnegie (essentially MKO-NIR) filter system. Details regarding standard data acquisition and reduction methods can be found in Kirkpatrick et al. (2011).

2.2.7. Spitzer/IRAC

The Infrared Array Camera (IRAC; Fazio et al. 2004) on board the *Spitzer Space Telescope* employs 256 × 256 pixel detector arrays to image a field of view of 5.′2 × 5.′2 (1.″2 pixel^{-1}). IRAC was used during the warm *Spitzer* mission to obtain deeper photometry in its 3.6 and 4.5 μm channels (hereafter, ch1 and ch2, respectively) than *WISE* was able to take in its W1 and W2 bands. Such observations give us more definitive colors over this wavelength regime because the WISE W1–W2 colors (Table 1) are limits only. These observations were made as part of Cycle 7 and Cycle 8 programs 70062 and 80109 (PI: Kirkpatrick) and include all 13 of our Y dwarf discoveries (Table 2). Our standard data acquisition and reduction methodology for IRAC observations is outlined in Kirkpatrick et al. (2011).

2.2.8. HST/WFC3

The Wide Field Camera 3 (WFC3[12]) on board the *Hubble Space Telescope* employs a 1024 × 1024 HgCdTe detector with a plate scale of 0.″13 pixel^{-1} to image a field of view of 123″ × 126″. It was used to obtain deep near-infrared photometry in the F140W filter (a broad bandpass encompassing most of the *J* and *H* bands) for seven of our Y dwarfs, as listed in Table 2. These observations were made as part of our Cycle 18 program 12330 (PI: Kirkpatrick). Photometry was measured on the drizzled images, and magnitudes were measured on the Vega system. For the brighter sources, a comparison of the photometry measured from the drizzled images to that measured from the individual, direct images showed a systematic difference that was sometimes as large as 0.20 mag. To be conservative, we have adopted 0.20 mag as the uncertainty for all sources

[12] See http://www.stsci.edu/hst/wfc3.

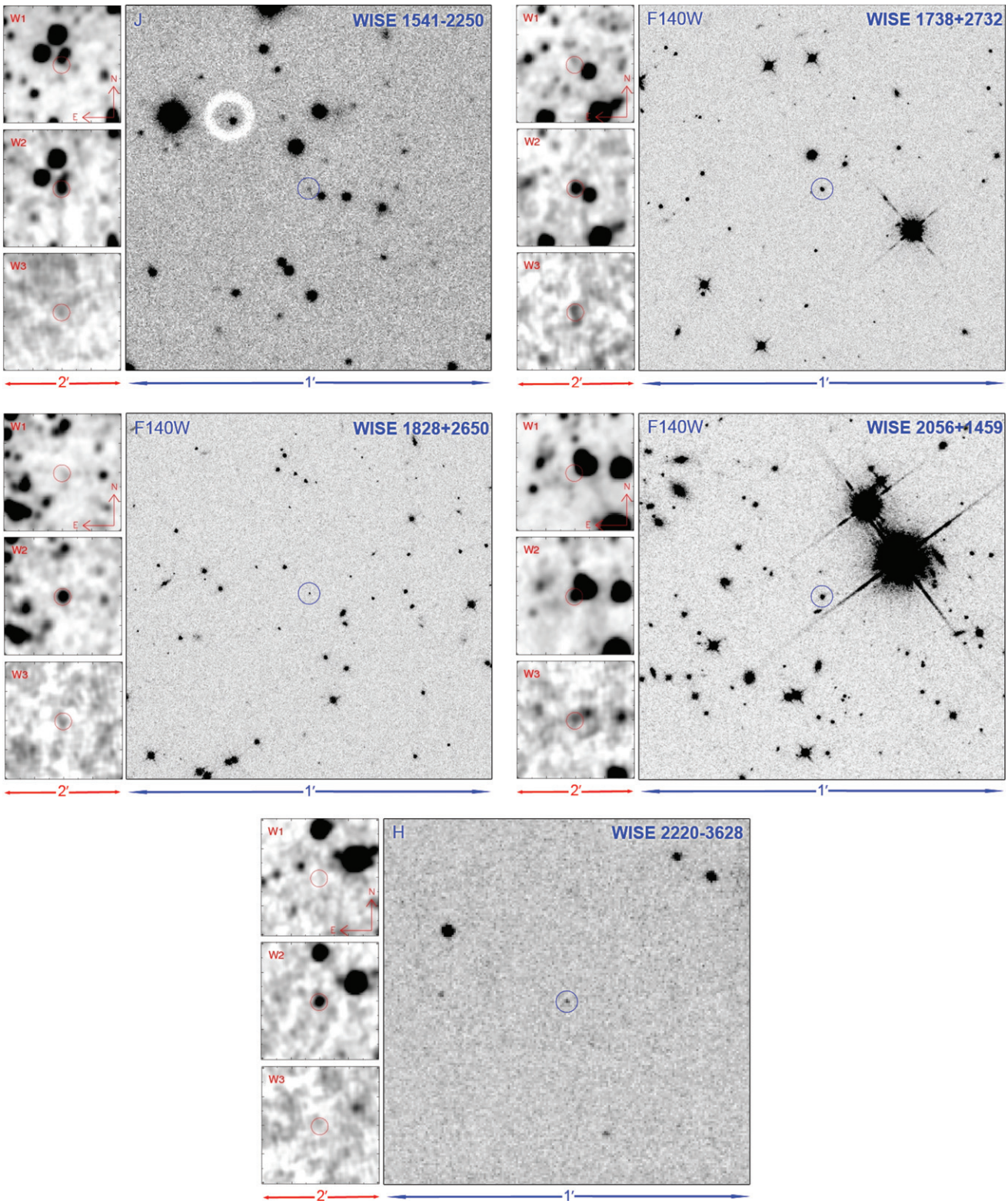

Figure 2. (Continued)

since this systematic difference is believed to be the dominant error term.

This same program also used the G141 grism to acquire slitless spectroscopy over the 1.1–1.7 μm range. This was done to confirm three new brown dwarf discoveries as well as to obtain better signal for a fourth, WISE 2056+1459, in addition to those WFC3 spectra already discussed in Cushing et al. (2011) and Kirkpatrick et al. (2011). Each target was observed over a single orbit, and the integration times were selected to best fill the time available between Earth occultations. Integration times were 2212 s for all objects except WISE 2056+1459, for which only 2012 s could be obtained. Details of data acquisition and reduction are given in Kirkpatrick et al. (2011). Spectra of the program objects were free of contamination by other field

Table 2
Photometric Follow-up of Y Dwarfs

WISE Designation	F140W (mag)	*J* (mag)	*H* (mag)	Ref	ch1 (mag)	ch2 (mag)	ch1–ch2 (mag)	F140W–W2 (mag)	*J*-W2 (mag)	*H*-W2 (mag)	Spec. Type
(1)	(2)	(3)	(4)	(5)	(6)	(7)	(8)	(9)	(10)	(11)	(12)
WISE J014656.66+423410.0	...	*19.40 ± 0.25*	*18.71 ± 0.24*	1	17.50 ± 0.07	15.08 ± 0.02	2.42 ± 0.07	...	*4.32 ± 0.26*	*3.63 ± 0.25*	Y0
WISE J035000.32−565830.2	22.30 ± 0.20	>22.8	>21.5	2	17.94 ± 0.10	14.69 ± 0.02	3.25 ± 0.10	7.57 ± 0.21	>8.1	>6.8	Y1
WISE J035934.06−540154.6	21.84 ± 0.20	21.56 ± 0.24	22.20 ± 0.43	2	17.55 ± 0.07	15.33 ± 0.02	2.22 ± 0.08	6.42 ± 0.21	6.14 ± 0.25	6.78 ± 0.44	Y0
WISE J041022.71+150248.4	...	19.24 ± 0.05[a]	19.05 ± 0.09	3	16.64 ± 0.04	14.18 ± 0.02	2.46 ± 0.05	...	5.06 ± 0.08	4.87 ± 0.11	Y0
WISE J053516.80−750024.9	22.42 ± 0.20	>21.1	>21.6	2	17.77 ± 0.09	15.01 ± 0.02	2.76 ± 0.09	7.36 ± 0.21	>6.0	>6.5	⩾Y1:
WISE J071322.55−291751.9	...	19.64 ± 0.15	>19.3	4	16.67 ± 0.04	14.22 ± 0.02	2.45 ± 0.05	...	5.16 ± 0.16	>4.8	Y0
	...	*20.06 ± 0.21*	*21.16 ± 0.66*	10	...	...	...	...	*5.58 ± 0.22*	*6.68 ± 0.66*	...
WISE J073444.02−715744.0	...	20.41 ± 0.27	...	5	17.69 ± 0.08	15.21 ± 0.02	2.47 ± 0.08	...	5.05 ± 0.28	...	Y0
WISE J140518.39+553421.3	21.22 ± 0.20	20.09 ± 0.12	>20.5[a]	6	16.88 ± 0.05	14.06 ± 0.02	2.82 ± 0.05	7.12 ± 0.20	5.99 ± 0.13	>6.4	Y0 pec?
WISE J154151.65−225024.9	...	20.74 ± 0.31[a]	>20.2[a]	5	16.73 ± 0.04	14.23 ± 0.02	2.50 ± 0.05	...	6.49 ± 0.32	>6.0	Y0.5
WISE J173835.53+273259.0	19.87 ± 0.20	19.51 ± 0.08[a]	20.39 ± 0.33[a]	3	17.10 ± 0.05	14.48 ± 0.02	2.62 ± 0.06	5.32 ± 0.21	4.96 ± 0.10	5.84 ± 0.34	Y0
WISE J182831.08+265037.7	23.12 ± 0.20	23.57 ± 0.35	22.85 ± 0.24	7	16.92 ± 0.02	14.32 ± 0.02	2.60 ± 0.03	8.73 ± 0.21	9.18 ± 0.36	8.46 ± 0.25	⩾Y2
WISE J205628.91+145953.2	19.56 ± 0.20	19.23 ± 0.13[a]	19.62 ± 0.31[a]	8	16.04 ± 0.03	13.92 ± 0.02	2.11 ± 0.04	5.63 ± 0.21	5.30 ± 0.14	5.69 ± 0.31	Y0
WISE J222055.31−362817.4	...	20.38 ± 0.17	*20.81 ± 0.30*	9	17.20 ± 0.06	14.73 ± 0.02	2.46 ± 0.06	...	5.72 ± 0.18	*6.15 ± 0.31*	Y0

Notes. All *J* and *H* data are on the MKO-NIR filter system except for those in italics. See the text for details.
References for photometry: (1) Bigelow/2MASS on 2010 November 20 UT; (2) Magellan/PANIC on 2010 November 25 UT except for the *J*-band measurement of WISE 0359−5401, which was taken on 2010 August 1 UT; (3) Palomar/WIRC on 2010 July 26 except for the *J* measurement of WISE 0410+1502, which was taken on 2010 August 29 UT; (4) SOAR/Spartan-IRC on 2012 January 13 UT; (5) CTIO4m/NEWFIRM on 2011 April 17 UT; (6) Palomar/WIRC combined—*J* is from 2010 July 26 UT and *H* is from a mosaic made from data taken on 2010 July 26, August 28, 30, and 31 UT; (7) Keck/NIRC2+LGSAO on 2010 July 1 UT; (8) Palomar/WIRC 2010 August 29 UT for *J* and 2011 May 16 UT for *H*; (9) AAT/IRIS2 on 2011 September 12 UT for *J* and SOAR/OSIRIS on 2011 September 18 UT for *H*; (10) SOAR/OSIRIS on 2012 March 13 UT for *J* and 2012 March 12 UT for *H*.
[a] These values have been updated using an aperture with radius set to 1.5 times the full width at half maximum of the observed point spread function, as opposed to the use of a standard, fixed aperture size for all observations, as had been done in Cushing et al. (2011).

Table 3
New Follow-up Spectroscopy of Y Dwarfs

WISE Designation	Instrument	Obs. date (UT)	Int. Time (s)	Spec. Type
(1)	(2)	(3)	(4)	(5)
WISE J014656.66+423410.0	Keck/NIRSPEC-N3	2011 Aug 8	6000	Y0
	Keck/NIRSPEC-N5	2011 Sep 6	3600	Y0
WISE J035000.32−565830.2	*HST*/WFC3	2011 Aug 13	2212	Y1
WISE J035934.06−540154.6	*HST*/WFC3	2011 Aug 9–10	2212	Y0
WISE J053516.80−750024.9	*HST*/WFC3[a]	2011 Sep 27	2212	⩾Y1:
WISE J071322.55−291751.9	Keck/NIRSPEC-N3	2011 Oct 7–9	12000	Y0
WISE J073444.02−715744.0	Magellan/FIRE	2012 Jan 5	1775	Y0
WISE J205628.91+145953.2	Keck/NIRSPEC-N3	2011 Aug 9	1200[b]	Y0
	HST/WFC3	2011 Sep 4	2012	Y0
WISE J222055.31−362817.4	Keck/NIRSPEC-N3	2011 Sep 5/Oct 9	5400	Y0
	Keck/NIRSPEC-N5	2011 Sep 6	3600	Y0

Notes.
[a] This spectrum suffers heavy contamination from a field object.
[b] This spectrum was added to the 2400 s NIRSPEC-N3 spectrum previously reported in Kirkpatrick et al. (2011).

spectra and had uncomplicated reductions except for WISE 0535−7500, whose first-order spectrum falls coincident with the second-order spectrum of a field star. The blended spectrum of this source was extracted in the same way as the others, and a correction (discussed in Section 3) was applied to mitigate the effects of the contaminating object.

2.2.9. Keck/NIRSPEC

The Near-Infrared Spectrometer (NIRSPEC; McLean et al. 1998, 2000) on the 10 m telescope at W. M. Keck Observatory on Mauna Kea, Hawai'i, was used to confirm three of our new Y dwarfs and to obtain additional signal for a fourth, WISE 2056+1459 (Cushing et al. 2011). For spectroscopy, NIRSPEC uses a 1024 × 1024 InSb array. In low-resolution mode, use of the 42″ × 0.″38 slit results in a resolving power of $R \equiv \lambda/\Delta\lambda \approx 2500$. Our brown dwarf candidates were observed in either or both of the N3 and N5 configurations (see McLean et al. 2003) that cover part of the *J*-band window from 1.15 to 1.35 μm and part of the *H*-band window from 1.5 to 1.8 μm. Standard data acquisition and reduction techniques, as described in G. N. Mace et al. (in preparation), were used.

2.2.10. Magellan/FIRE

The Folded-port Infrared Echellette (FIRE; Simcoe et al. 2008, 2010) at the 6.5 m Walter Baade Telescope on Cerro Manqui at the Las Campanas Observatory, Chile, uses a 2048 × 2048 HAWAII-2RG array. In prism mode, it covers a wavelength range from 0.8 to 2.5 μm at a resolution ranging from $R = 500$ at *J* band to $R = 300$ at *K* band for a slit width of 0.″6. FIRE was used to confirm WISE 0734−7157 as a Y dwarf.[13] For standard data acquisition and reduction techniques for FIRE refer to the discussion in Kirkpatrick et al. (2011).

3. THE CLASSIFICATION OF Y DWARFS

3.1. Classifying the New Discoveries

Our new spectra, along with those from Cushing et al. (2011), are plotted in Figures 3–5. In Figures 3 and 4 we show all of the Y dwarfs except WISE 0535−7500 (which is plotted separately in Figure 5) and compare them to the T9.5 dwarf WISE 0148−7202 and other Y dwarfs. In Figure 5 we plot two versions of the spectrum of WISE 0535−7500. In the first, we show the contaminated spectrum as extracted by the *aXe* software from the *Hubble Space Telescope*. In the second, we plot our attempt at correcting the spectrum for the light of the contaminating object. This simplistic correction involves subtracting off a linear slope so that the mean level in the water absorption bands is zero. The resulting, quasi-corrected spectrum is sufficient to provide a crude classification despite the problems with data acquisition.

After examining these plots, several facts become apparent. (1) All seven of the new discoveries have *J*-band (∼1.27 μm) flux peaks as narrow or narrower than the Y0 standard, WISE 1738+2732, proposed by Cushing et al. (2011). The T9.5 dwarf, in contrast, has a wider *J*-band peak than any of these. This confirms that all are Y dwarfs, as defined by Cushing et al. (2011). (2) The spectra of WISE 1541−2250 and WISE 0350−5658 have distinctly narrower *J*-band peaks than the Y0 standard itself, meaning that both of these objects should be typed later than Y0. The plot shown in Figure 6 suggests that the *J*-band peak of WISE 0350−5658 is sufficiently narrower than WISE 1738+2732 that it should be typed a full subclass later. We therefore propose WISE 0350−5658 to be the tentative Y1 spectral standard, despite its southerly declination, until other Y1 dwarfs are identified. This also means that WISE 1541−2250, which has a slightly broader *J*-band peak, should be re-typed from Y0 to Y0.5. (3) The spectrum of WISE 1828+2650, though having a low signal-to-noise ratio, is still in a class by itself due to the near-equal heights of the *J*- and *H*-band (∼1.58 μm) peaks. Because it is so different from all of the other spectra, we re-classify it to be ⩾Y2.

3.2. Revisiting the Establishment of the Y Dwarf Class

Although Cushing et al. (2011) discussed in detail the establishment of the new Y dwarf spectral class, it is worth revisiting this based on the latest discoveries. We compare our set of observational Y dwarf spectra to theoretical expectations prior to the launch of *WISE*. Specifically, Burrows et al. (2003) used atmospheric models covering this temperature regime to cite five possible triggers that could lead to the introduction of

[13] Because of the faintness of this source at the *K* band, the FIRE spectrum beyond 1.65 μm is not plotted in the figures as it is very noisy.

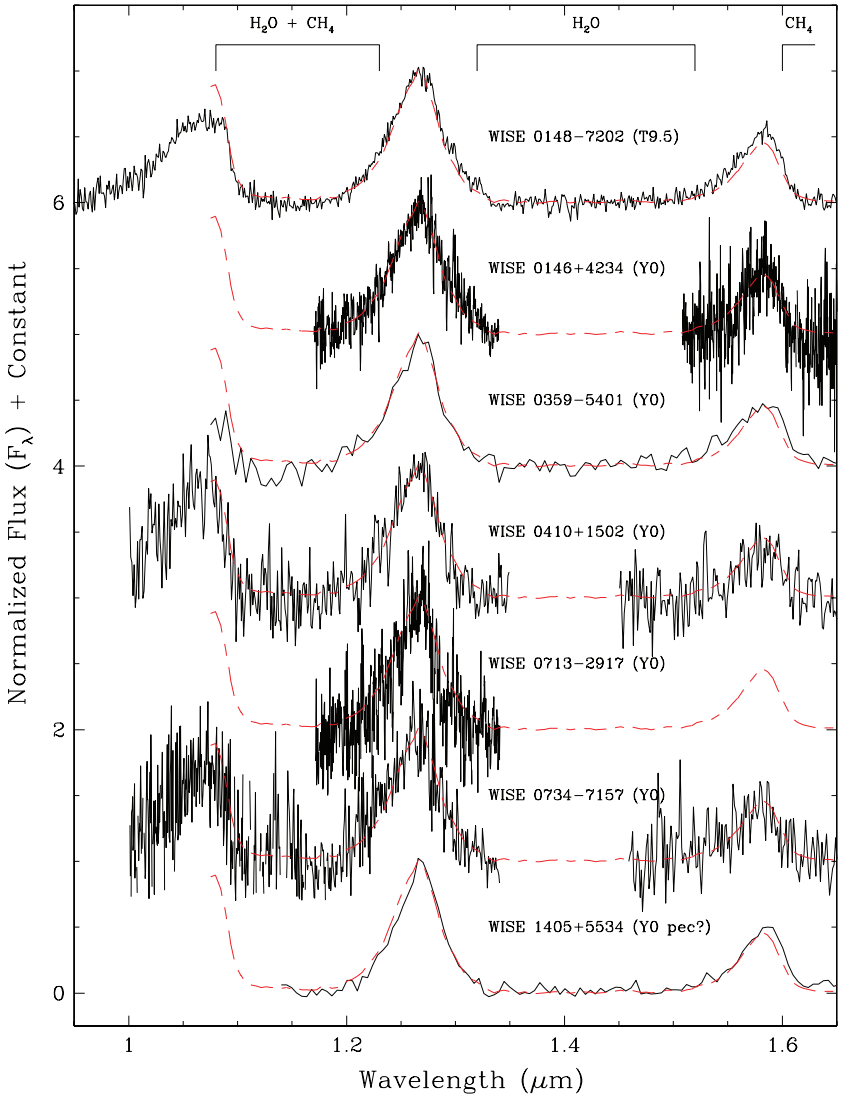

Figure 3. Along with Figures 4 and 5, the spectra of all known Y dwarfs together with a comparison spectrum of the T9.5 dwarf WISE 1048−7202. Each spectrum is normalized to one at its peak in the *J* band and integral offsets have been added to separate the spectra vertically. Overplotted on each spectrum is the Y0 dwarf spectral standard WISE 1738+2732 (dashed red curve). For NIRSPEC data taken in the N5 configuration (*H* band), the normalization has been set so that the *H*-band peak of the Y dwarf matches the *H*-band peak of the spectral standard.

(A color version of this figure is available in the online journal.)

a new class beyond the T dwarfs. We investigate each of these possibilities below.

1. *The disappearance of alkali resonance lines near 450 K.* The resonance lines of Na I and K I fall at optical wavelengths, where cold brown dwarfs have little flux, but the broad wings of these lines extend very far from the line cores and are believed to have an influence on the emergent flux as longward as 1 μm (Burrows & Volobuyev 2003). As discussed in Cushing et al. (2011), the *Y*-band ($\sim$1.07 μm) peaks for the Y dwarfs whose spectra cover that region generally appear to be as high or higher than the *J*-band peaks in units of F_λ. This effect is not seen in the spectra of late-T dwarfs (see, e.g., Kirkpatrick et al. 2011). A harbinger of this effect—seen as a blueward trend of *Y*-*J* color in the mid- to late-T dwarf regime—was noted by Leggett et al. (2010) and Burningham et al. (2010) and ascribed to a brightening of the *Y*-band peak due to reduced absorption by the wings of the K I as atomic potassium begins to form into KCl at cooler temperatures (Lodders 1999). Although indirect, this is evidence that we have pushed into the regime where these alkali lines have lost prominence. Further spectroscopic investigation at higher signal-to-noise levels is possible at the *Y* band using the G102 grism on board *HST*/WFC3.
2. *Water cloud formation below 400–500 K.* Although long predicted to be a possible trigger of a new spectral class at low temperatures, Burrows et al. (2003) found that the formation of these clouds has very little effect on the emergent spectra in their models. M. Marley (2012, private communication) also finds little effect shortward of 2 μm but finds that at longer wavelengths, for objects with $\lesssim$300 K, the effects are quite pronounced. The importance of these clouds should be re-investigated once newer atmospheric models are published for the coldest brown dwarfs.
3. *The emergence of ammonia absorption below 2.5 μm.* As shown in Figure 5 of Kirkpatrick (2008), the theoretical spectra of Burrows et al. (2003) indicate that absorption bands of NH_3, which first appear in the mid-infrared

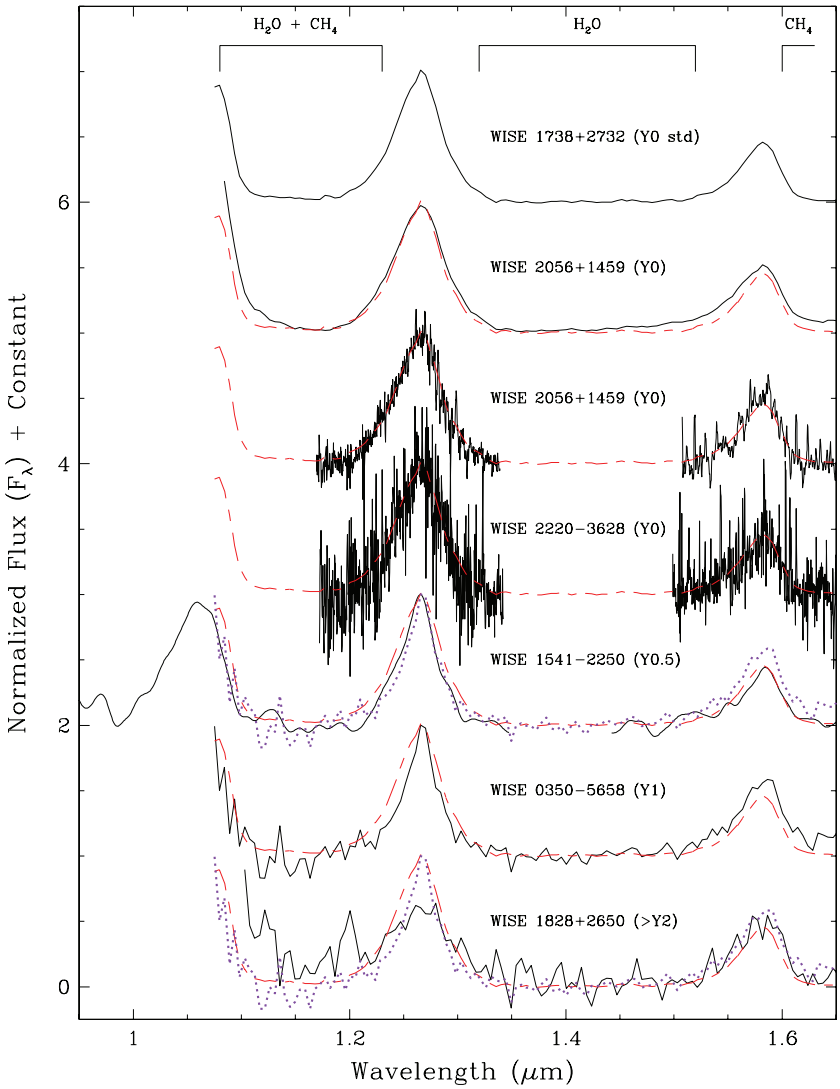

Figure 4. Spectra of Y dwarfs (continued). The spectrum of the Y1 standard, WISE 0350−5658, is shown by the purple dotted line and is normalized to one at the *J*-band peak. See the caption to Figure 3 for other details.

(A color version of this figure is available in the online journal.)

(10.5 μm) near the L/T transition (Cushing et al. 2006), finally appear at the *H* and *K* bands starting near 800 K and become prominent by 450 K. As shown in Figure 5 of Cushing et al. (2011), the *H*-band ammonia feature—the easier of these two to detect because the *K*-band feature falls within the telluric water band—is itself confused with overlying absorption by H_2O and CH_4 in the brown dwarf atmosphere. Nonetheless, signs of a possible NH_3 signature were noted by Cushing et al. (2011) in the 1.53–1.58 μm region of WISE 1738+2732. This region falls in an area of extremely low flux, so exquisite signal to noise is needed to detect it. Unfortunately, none of the spectra of our new objects has sufficient signal to investigate this feature further. Analyzing the near-infrared spectra of these objects for the presence of NH_3 bands will likely require higher resolution spectra than can be presently obtained.

4. *Collapse below 350 K of the optical and near-infrared fluxes, relative to those* $\gtrsim$*5 μm.* Burrows et al. (2003) state that this collapse in flux would manifest itself as a reversal of the blueward trend of $J-K$ (or $J-H$) colors. Figure 11 in Cushing et al. (2011) shows the $J-H$ color (on the MKO-NIR system) as a function of spectral type. That figure shows that the $J-H$ color stagnates near −0.4 mag for late-T dwarfs and then appears to turn to the red starting at Y0, although there are some blue outliers at Y0. With our new Y dwarf discoveries, new T dwarf discoveries from Mace (et al.), additional near-infrared photometry, and revised photometric reductions of previous Y dwarf discoveries (see footnotes to Table 2), we can revisit this plot. This new photometry, shown in Figure 7, more clearly shows the reversal of the $J-H$ color. After trending to the blue from early- to mid-T and stagnating for late-T types, the $J-H$ color turns to the red starting near Y0. Later Y dwarfs, such as the Y0.5 dwarf WISE 1541−2250 ($J-H>$ 0.54 mag) and the $\geqslant$Y2 dwarf WISE 1828+2650 ($J-H=$ 0.72 $\pm$ 0.42 mag), are roughly 1 mag redder than late-T dwarfs.

5. *The shift in position of the* ∼5 *μm peak.* As shown in Figures 7 and 8 of Kirkpatrick et al. (2011), the $J-$W2 and $H-$W2 colors continue to increase from mid-T to early-Y. Figure 11 from that paper shows an indication that the *Spitzer* ch1−ch2 color may reverse in the Y

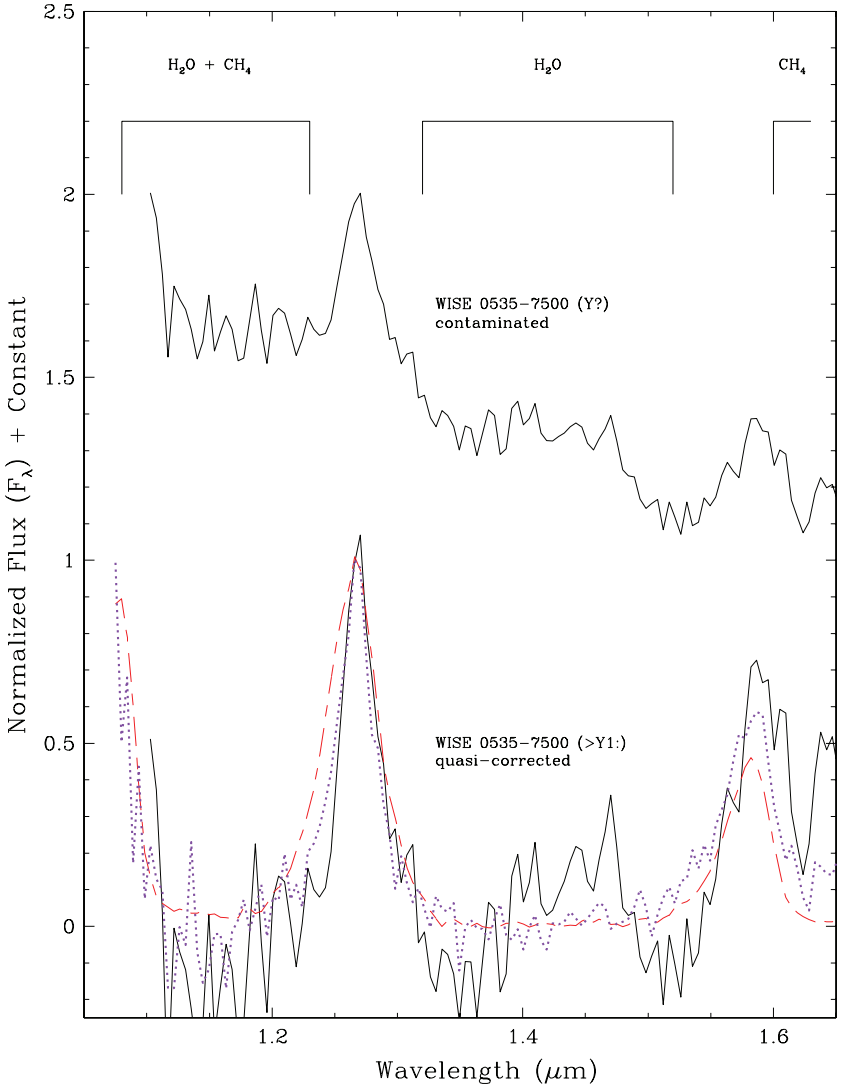

Figure 5. Spectra of Y dwarfs (continued). The spectrum of WISE 0535−7500 is shown in black both before (above) and after (below) subtraction of the overlapping field spectrum. Both spectra are normalized to one at the peak of *J* band, and the top spectrum is offset by one in the vertical direction to separate it from the lower spectrum. See the caption to Figures 3 and 4 for other details, and see the text for a description of the correction applied.

(A color version of this figure is available in the online journal.)

sequence, but this was based solely on the ch1−ch2 color of WISE 1828+2650. We can also revisit this trend using newly discovered Y dwarfs. Figure 8 shows the *J*−W2, F140W−W2, and *H*−W2 colors as a function of the ch1−ch2 color.[14] The ch1−ch2 color shows a broad range (of up to a magnitude) for Y0 dwarfs; similar scatter is seen in the ch1−ch2 colors of late-T dwarfs, which Leggett et al. (2010) attribute to gravity and/or metallicity effects. Dwarfs classified as Y1 or later are generally redder than these. It should be noted that the $\geqslant$Y2 dwarf, WISE 1828+2650, indicates a turn to the blue in ch1−ch2 color at later types. (The *J*−W2, F140W−W2, and *H*−W2 colors, nevertheless, still tend to run redder with advancing spectral type and may serve as a proxy for temperature for these early-Y dwarfs.)

WISE 1828+2650 satisfies the last two of the possible trigger conditions discussed above. The stark contrast between its spectral morphology and that of T dwarfs—namely, the near-equal heights of the *J* and *H* peaks that are manifested as a turn to the red in the $J-H$ color—satisfies the criteria needed to define a new spectral class. Moreover, Beichman et al. have recently measured the trigonometric parallax for this object, establishing it as an instrinsically dim source (see Section 4.3), and model fits by Cushing et al. (2011) suggest that its effective temperature is below 300 K. With more evidence now in hand, we still reach the same conclusion as Cushing et al. (2011) that WISE 1828+2650 should be considered as the archetypal Y dwarf.

Given that the ammonia absorption bands in the near-infrared are obscured by other strong absorption bands, we lack a clear signature that defines the exact onset of the Y class. A gradual change in spectral morphology is the norm, however, at the boundary between spectral classes. For example, there is very little change in the optical morphology of a late-K dwarf and an early-M dwarf, even though mid-K and mid-M spectra are markedly different, and the same is true at the boundary between

[14] Plots showing the *J*−ch2, F140W−ch2, and *H*−ch2 colors would look nearly identical. The W2 magnitudes listed in Table 1 are nearly identical to the ch2 magnitudes in Table 2, though the latter have errors generally two to three times smaller. However, the error in the color measurements is dominated by the *J*, F140W, or *H* terms anyway.

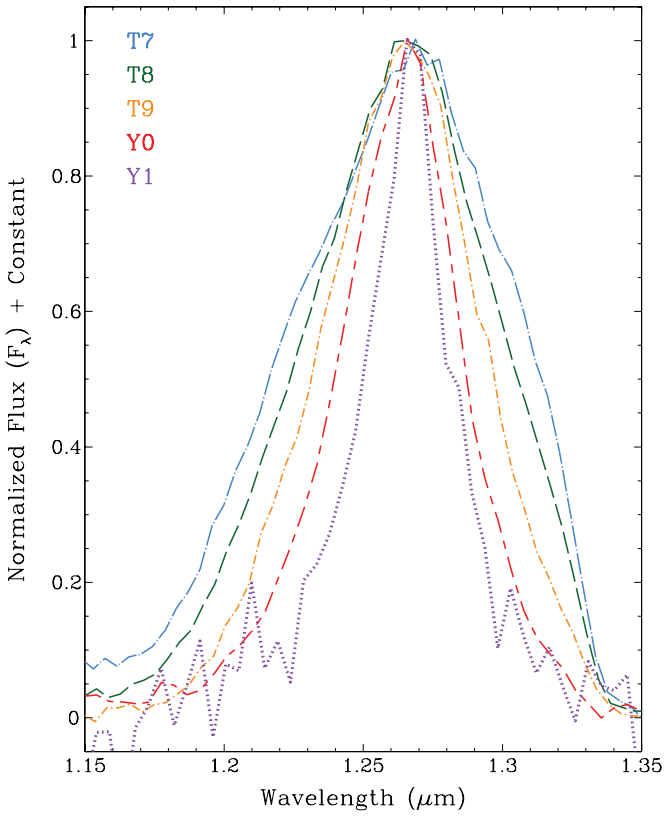

Figure 6. Overplots of the *J*-band spectra of the T7, T8, T9, and Y0 standards 2MASS 0727+1710 (light blue, dot/long-dash; Burgasser et al. 2002), 2MASS 0415−0935 (green, dash; Burgasser et al. 2002), UGPS 0722−0540 (gold, dot/short-dash; Lucas et al. 2010), and WISE 1732+2732 (red, long-dash/short-dash; Cushing et al. 2011), respectively, along with our proposed Y1 standard, WISE 0350−5658 (purple, dot). All spectra are normalized to one at their peak flux.

(A color version of this figure is available in the online journal.)

M and L classes. The L/T transition is unusual in its sudden appearance of a major absorption species that radically alters the appearance of the spectra (over what we now know is a very small temperature range; see Figure 8 of Kirkpatrick 2005). For Y dwarfs, we see a gradual change in the spectral morphology from late-T to early-Y, even though the spectra of a mid-T dwarf and that of WISE 1828+2650 are very different. We have further evidence that this gradual change continues down the Y sequence, as well: the spectrum of our new Y1 dwarf WISE 0350−5658 has as an *H*-band peak relative to that of the *J*-band peak that is higher than in the Y0 standard and this presages the effect of equal-peak heights seen in WISE 1828+2650. We therefore see no reason to deviate from the Y dwarf classification scheme presented in Cushing et al. (2011), which has so far been robust to new discoveries.

3.3. A New Spectral Index for Early-Y Dwarfs?

For early-Y dwarfs, we have based our classifications on the narrowness of the *J*-band peak using by-eye comparisons to our Y0 and Y1 spectral standards. Can a spectral index be created that distills this same information? A pre-existing index, dubbed W_J, was developed by Warren et al. (2007) to measure this narrowness of *J*-band for late-T dwarfs, but we find that it has problems in the Y dwarf regime. (See Figure 7 of Cushing et al. 2011 for a graphical representation of this index along with other indices measured for T dwarfs.) All of the Y dwarfs have a W_J index of ∼0.1, except for WISE 1828+2650, which is very noisy. Because the *J*-band peak is so narrow for Y dwarfs, the numerator of the W_J index (which is the flux integrated from 1.18 to 1.23 μm) is nearing 0. A better measure of the *J*-band peak can be obtained by moving this region of integration longward so that it still falls in a region with measurable flux nearer the peak. Also, the region used in the denominator of the index (1.26–1.285 μm), which measures the flux in the peak itself, as well as the region used in the numerator (to measure the blueward wing) can be narrowed to reflect the fact that the opacity hole in the spectrum has narrowed for the Y dwarfs.

Mace et al. define a new index, called *J*-narrow, which is the ratio of the median flux over the 1.245–1.260 μm region to the median flux over 1.260–1.275 μm. We show the results of measuring this index on our collection of *WISE*-discovered T and Y dwarfs in Figure 9. Note that for most of the T dwarfs, *J*-narrow has a value greater than 0.85. Y dwarfs have values less than this, the Y0 standard WISE 1728+2732 being the least narrow Y dwarf as measured by this index. (This is because our by-eye classification requires an object to have a *J*-band peak as least as narrow as that of the Y0 standard for it to be classified as a Y dwarf.) Whittling the wavelength region over which the index operates, though necessary, nonetheless comes at a price: high signal-to-noise spectra are required to make the index measurements robust. This is a difficult requirement to meet because Y dwarfs are notoriously hard to observe given their intrinsic faintness and the ones plotted in Figure 9 are among the closest, brightest Y dwarfs over the entire sky. Even though we present this new index for completeness, *we strongly recommend that researchers classify their spectra by overplotting the late-T and early-Y standards rather than resorting to the use of spectral indices, since the latter technique is far more prone to error when spectra have low signal to noise.*

4. Y DWARFS IN THE LARGER CONTEXT

As theorized, old brown dwarfs in the field population were expected to be very faint given the fact that they have no sustained source of energy in their interiors. The faintness of these objects as a function of time could be modeled based on interior physics (e.g., Figure 11 of Burrows et al. 1997), but the more difficult issue was predicting how frequently they might occur in nature, if at all. Using the Y dwarfs discovered by *WISE* and monitoring their astrometry to measure trigonometric parallaxes, we are able to demonstrate just how faint these objects are and can begin to put more solid limits on the Y dwarf space density and the shape of the mass function in the low-temperature, low-mass realm.

4.1. Absolute Magnitudes and the H-R Diagram

To understand the intrinsic faintness of Y dwarfs, we have constructed a Hertzsprung–Russell (H-R) diagram at the *H* band that contains a selection of main-sequence stars and brown dwarfs with spectral types running the gamut from O through Y. Objects were required to have high quality parallaxes and be free of complications such as being heavily reddened (which is mitigated by choosing only the most nearby examples) or belonging to a close multiple system. Our aim was to choose, if possible, at least 25 objects in each spectral class, spread evenly so that all integral subclasses were covered. All *H*-band magnitudes and errors were taken from 2MASS. Additional details are given below.

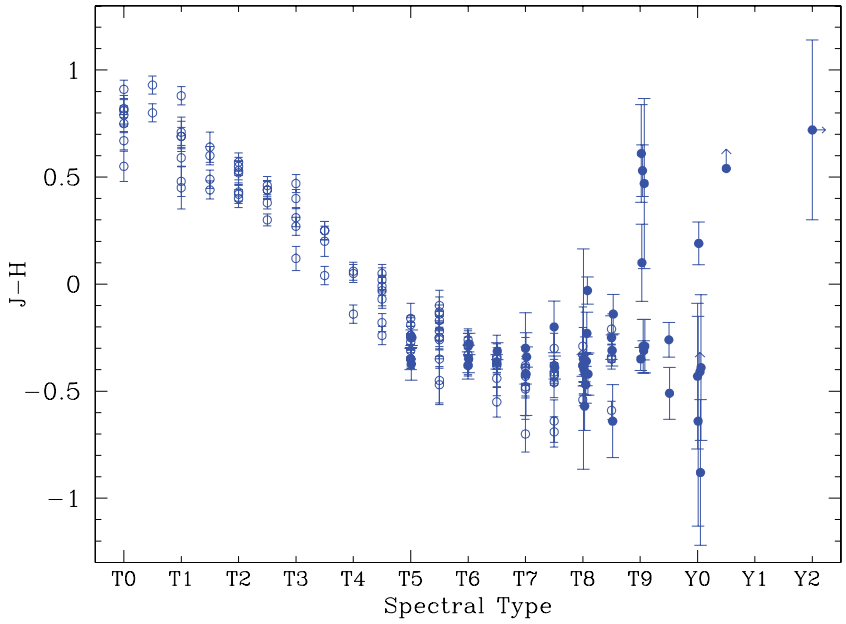

Figure 7. Plot of the $J-H$ color (on the MKO-NIR filter system) as a function of spectral type from T0 through Y2. Small offsets have been added to some of the spectral type values to ease visualization of individual data points. Colors for Y dwarfs from Table 2 and T dwarfs from Kirkpatrick et al. (2011) and G. N. Mace et al. (in preparation) are shown by solid blue points. Colors of other T dwarfs from Leggett et al. (2010) are shown by open blue points.

(A color version of this figure is available in the online journal.)

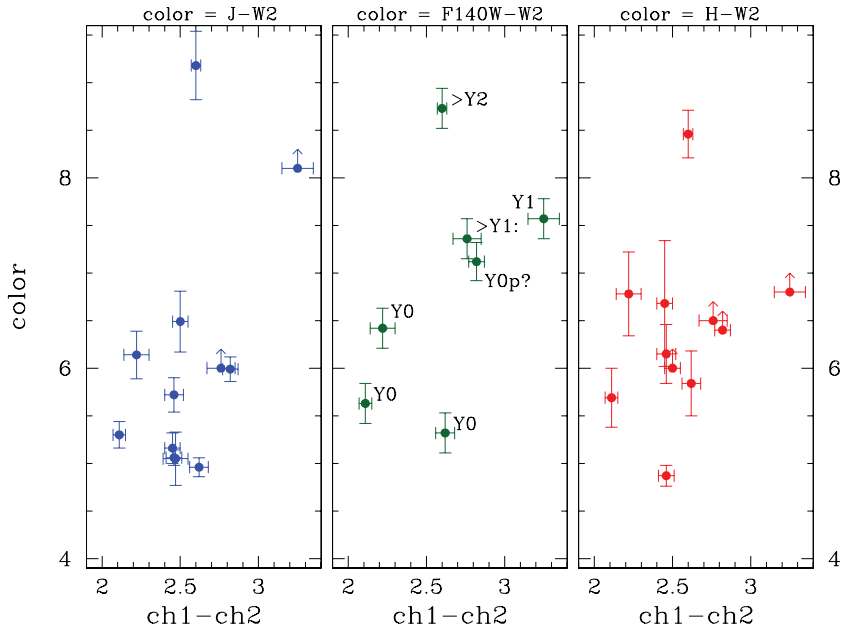

Figure 8. Various near-infrared/*WISE* colors plotted as a function of the *Spitzer* ch1–ch2 color. From left to right are shown the $J-$W2 color (blue), F140W$-$W2 color (green), and $H-$W2 color (red). All panels are shown with the same scales on the x and y axes. In the F140W$-$W2 panel, spectral types are shown next to each of the points.

(A color version of this figure is available in the online journal.)

O, B, and A dwarfs. Using Jim Kaler's "Stars" Web site,[15] we selected objects identified as O dwarfs and retained those having trigonometric parallaxes from *Hipparcos* (van Leeuwen 2007) that place them within 600 pc of the Sun and parallax errors less than 1 mas. Only 10 O dwarfs survived the cut, the earliest being the O7 V star 15 Monocerotis. Using the same Web site and *Hipparcos* parallaxes, we selected B dwarfs lying within 500 pc and A dwarfs lying within 100 pc. Retaining only those with parallax errors under ∼1 mas resulted in a sample of 26 B stars and 42 A stars.

F, G, and K dwarfs. Using SIMBAD, we selected F, G, and K stars whose *Hipparcos* parallaxes (van Leeuwen 2007) place them within 20.0, 18.2, and 13.4 pc of the Sun (i.e., parallax values exceeding 50, 55, and 75 mas), respectively. We retained those that Jim Kaler's "Stars" Web site confirms as having dwarf luminosity classes. Further requiring that the *Hipparcos* parallax errors are less than ∼0.5 mas resulted in a list of 35 F dwarfs, 53 G dwarfs, and 28 K dwarfs.

[15] See http://stars.astro.illinois.edu/sow/sowlist.html.

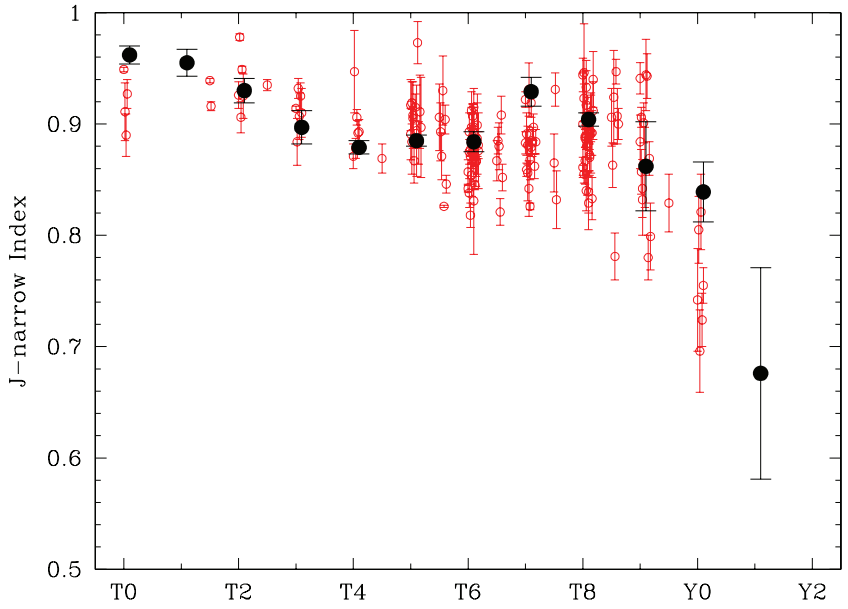

Figure 9. Values of our newly defined *J*-narrow index as a function of spectral type. Objects are taken from this paper, G. N. Mace et al. (in preparation), Cushing et al. (2011), and Kirkpatrick et al. (2011). See Mace et al. for details concerning these computations. Spectral standards are shown by solid black points and other objects are shown by open red points. Small toggles have been added to the spectral type values to reduce the amount of overlap in each spectral bin. With the exception of the Y1 standard, only those objects with *J*-narrow errors of less than 0.05 are plotted.

(A color version of this figure is available in the online journal.)

M dwarfs. We selected M dwarfs from the Research Consortium On Nearby Stars' (RECONS) Web page that lists the hundred nearest stellar systems to the Sun.[16] Dropping objects where the 2MASS *H*-band photometry or measured spectral type is a composite of multiple components resulted in a list of 72 M dwarfs.

L and T dwarfs. We selected from the literature those L and T dwarfs having measured trigonometric parallaxes. The list is available as Table 5 of Kirkpatrick et al. (2011). Retaining only those not known to be multiple systems and having well measured 2MASS *H*-band magnitudes results in 20 L dwarfs and 21 T dwarfs.

Y dwarfs. Due to the paucity of parallax data currently available for Y dwarfs, we retained all Y dwarfs from Marsh et al. (2012) and Beichman et al. (2012) having trigonometric parallax measurements at least five times the error. This selection yields four Y dwarfs.

The compiled list is illustrated in Figure 10. The trend of ever-dimming *H*-band magnitude as a function of later spectral type shows two well-known inflection points. The first of these occurs at early-M and is a result of hydrogen associating into H_2 at temperatures below ∼4000 K (Mould 1976; Mould & Hyland 1976). The other inflection point, at late-L to mid-T, is a flattening or brightening of the *H*-band flux over a range of spectral types near the L/T transition (see, e.g., Looper et al. 2008; Dahn et al. 2002; Vrba et al. 2004; Knapp et al. 2004; the brightening is even more dramatic in the *J* band). The physical cause for this brightening may be due to patchy clouds in the atmospheres of these objects (Marley et al. 2010). Below this second inflection point, the *H*-band magnitude plummets. By early-Y the absolute *H*-band magnitudes are ∼30 mag (or 12 orders of magnitude in flux) fainter than those of late-O dwarfs. As discussed later in this paper, the trend of absolute *H*-band flux may show another inflection point at early-Y, although more data are required to check this further.

[16] The list was consulted in late 2011 December. See http://www.recons.org/.

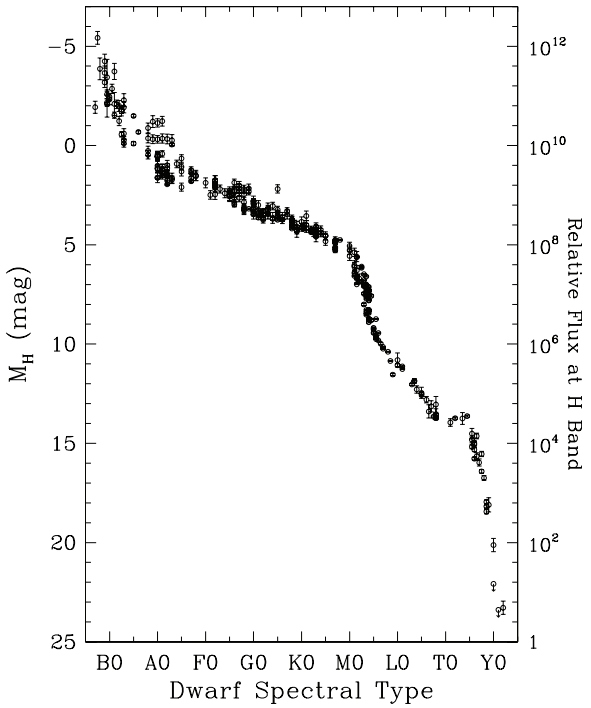

Figure 10. H-R diagram at *H* band showing the Y dwarfs in context with other field brown dwarfs and main-sequence stars. The intrinsically faintest Y dwarf so far recognized is roughly 12 orders of magnitude fainter than an O-type main-sequence star at this wavelength. See Section 4.1 for details about the sample plotted.

4.2. Y Dwarf Number Density and the 8 pc Census

To understand the importance of Y dwarfs in the Milky Way, we consider an all-sky, volume-limited sample of the solar neighborhood with which to compare the frequency of Y dwarfs relative to other spectral types. Previous authors have considered different volumes as defining the immediate solar neighborhood.

Building on earlier work[17] by Hertzsprung (1907, 1922), van de Kamp (1930, 1940, 1945, 1953, 1969, 1971) considered the sample out to ∼5 pc; Kuiper (1942) considered a volume out ∼10 pc; and Gliese (1956, 1969) and Gliese & Jahreiß (1979) considered a distance limit of ∼20 pc, although this was extended to 25 pc in Gliese & Jahreiß (1991). For our purposes, we will consider a distance limit of 8 pc because this bounds a volume with a sufficient number of objects (∼250) to provide adequate statistics across spectral classes.

Table 4 gives our update of all stars and brown dwarfs known or suspected to lie within 8 pc. This list relies heavily on previous work, most notably the list compiled by Reid & Gizis (1997) with updates in Reid et al. (2004) and I. N. Reid (2012, private communication) and the list of the hundred nearest stars compiled by RECONS at their Web site. The papers by Reid et al. consider only objects with decl. $> -30°$ and do not include several recently discovered, low-luminosity objects uncovered by surveys such as 2MASS, SDSS, DENIS, UKIDSS, and *WISE*; the RECONS list includes only objects with precisely determined trigonometric parallaxes and only objects within roughly 6.7 pc of the Sun. Therefore, we have combed the literature to uncover more newly discovered objects, suspects with unknown or poorly measured parallaxes, or objects near the outer limits of the 8 pc volume. Other updates in Table 4 include better characterization of previously known or newly identified multiple systems and consistent, MK-based spectral types for stars earlier than late-K (see Gray et al. 2003 and Gray et al. 2006). Further details on each column are given below.

Column 1 of Table 4 is intended to provide homage to the original discoverer or survey/mission responsible for first identifying the star as a nearby object. Exceptions are made in the case of stars with common names (e.g., Altair, Fomalhaut, and Vega), Bayer designations (e.g., α Cen A and B, p Eri AB), Flamsteed designations (e.g., 36 Oph ABC), or designations in old stellar catalogs (e.g., Lalande 21185, Lacaille 9352, AC+79 3888). In some cases, it is difficult to determine whether Willem Luyten or the Lowell Observatory group led by Henry Giclas was the first to discover an object because both groups were undergoing photographic proper motion surveys simultaneously. For such objects, the Luyten designation is used if the Lowell Observatory group lists one in its cross-references (Giclas et al. 1971, 1978), and the Giclas number is used if no Luyten designation is given.[18] Column 2 lists alternate names.

Column 3 of Table 4 gives the running number in Gliese (1956, 1969) or Gliese & Jahreiß (1979). SIMBAD has made it common practice to identify objects from any of these papers with a prefix of "GJ," but this was originally meant for objects only from Gliese & Jahreiß (1979). Moreover, for new objects (identified only by "NN") in Gliese & Jahreiß (1991), SIMBAD has created its own numbering scheme; identifiers with GJ numbers higher than GJ 2159 are solely a SIMBAD creation.[19] Gliese & Jahreiß (1991) do not provide catalog numbers for new objects nor are ones needed because all have published, well-recognized names. Such was not necessarily the case for earlier versions of the catalog—researchers in the early 1900's, notably Robert Innes, did not always affix numbers or names to their discoveries, and readers may not have had, as we do today, easy access to discovery papers. In deference to the intent of the original publications, we give a prefix of "Gl" to objects from Gliese (1956, 1969) and "GJ" only to those objects in Gliese & Jahreiß (1979). For other objects, the field in Column 3 is left blank.

Columns 4–6 of Table 4 give the measured trigonometric parallax, its error, and the reference for the measurement. If more than one group has measured the parallax, we list the published measurement with the smallest quoted error. For cases where the error in Column 5 is blank, the value in Column 4 is actually a spectrophotometric estimate based on the magnitude of the object and its spectral type. Columns 7 and 8 give the spectral type and its reference; cases where the spectral type is estimated are annotated as such. Column 9 provides an abbreviated sexagesimal J2000 position for the object in the form hhmm±ddss. Column 10 gives the rank of the system in distance from the Sun, and Column 11 gives the individual rank of each object; for example, Sirius A is in the fifth-closest stellar system to the Sun but is tied with its companion, Sirius B, as the seventh-closest star.

For reference, objects included in previous compilations of the 8 pc sample but now believed to lie beyond 8 pc are listed in Table 5. Among these is the intriguing multiple system ξ UMa (Alula Australis), in which Wright et al. (2012) have announced the discovery by *WISE* of a widely separated T8.5 companion.

Figure 11 graphically illustrates the 8 pc sample of Table 4 and shows that the solar neighborhood is dominated by M dwarfs. There are twice as many M dwarfs known as there are all other spectral types combined, although they comprise slightly less than half of the total stellar mass. Dwarfs of types L, T, and Y are much less common. L dwarfs are especially rare—only three examples are known within 8 pc—and represent a mix of old stars at the low-mass end of the stellar mass function and old brown dwarfs at the high-mass end of the substellar mass function.[20] The number of brown dwarfs then rises at later types—22 known T dwarfs and 8 known Y dwarfs are thought to lie within this 8 pc volume.

The statistics for T and Y dwarfs are still incomplete, however. For T dwarfs, a few late-type isolated objects may yet be found, and it is expected that T dwarf companions to some of the higher mass stars will continue to be uncovered. The number of Y dwarfs is incomplete because follow-up of Y dwarf candidates from *WISE* is still in its infancy and because the coldest Y dwarfs are likely beyond the detection threshold of all existing surveys. As discussed in the next section, distances to the Y dwarfs are only now being measured for the first time, so many of the Y dwarf distances in Table 4 are estimates only.

4.3. The Low-mass End of the Field Brown Dwarf Mass Function

We now concentrate on the low-mass tail of the field brown dwarf distribution in an updated attempt to determine the shape of the substellar mass function and its low-mass cutoff.

[17] Hertzsprung (1907) was the genesis of the H-R diagram; see Batten (1998) for more on the historical importance of this paper.

[18] Luyten did not usually provide cross-references to the Giclas numbers. The Lowell group aimed to acknowledge Luyten, however, when they rediscovered one of his proper motion objects. For more details, see the interview of Dr. Henry Giclas by Robert Smith on 1987 August 12, Niels Bohr Library & Archives, American Institute of Physics, College Park, MD, USA, http://www.aip.org/history/ohilist/5022.html.

[19] Likewise, we do not use LHS numbers (Luyten 1979) higher than LHS 5413 because these are also a SIMBAD creation.

[20] Using the Burgasser et al. (2004, 2007) luminosity function simulations, we find that an $\alpha = 0$ power law would suggest approximately 12 L dwarfs within this 8 pc volume. It is difficult to imagine that previous surveys have missed three quarters of all the nearby L dwarfs, so we conclude either that the appropriate value of α is less than zero and/or that a power law is a poor representation for the mass function of brown dwarfs. We return to this point in the next section.

Table 4
The Census of Stars and Brown Dwarfs within 8 pc of the Sun

Discovery Name	Other Name	Gliese Name	π_{trig}[a] (mas)	σ_π (mas)	π Ref.	Spec. Type	Spec. Ref.	J2000 Coords.	Sys. Rank	Indiv. Rank
(1)	(2)	(3)	(4)	(5)	(6)	(7)	(8)	(9)	(10)	(11)
Sun	Sol	...	...	...	...	G2 V	51	...	0	0
Proxima Cen[b]	α Cen C	Gl 551	769.91	0.54	16	M5.5 V	18	1429−6240	1	1
Rigel Kentaurus A	α Cen A	Gl 559 A	754.81	4.11	5	G2 V	50	1439−6050	1	2
Rigel Kentaurus B	α Cen B	Gl 559 B	...	...	...	K2 IV C2+1	50	1439−6050	1	2
Barnard's Star	...	Gl 699	545.4	0.3	16	M4 V	38	1757+0441	2	4
Wolf 359	...	Gl 406	419.1	2.1	6	M6 V	38	1056+0700	3	5
Lalande 21185	...	Gl 411	392.64	0.67	5	M2 V	38	1103+3558	4	6
Sirius A	α CMa A	Gl 244 A	379.21	1.58	5	A0mA1 Va	49	0645−1642	5	7
Sirius B	α CMa B	Gl 244 B	...	...	...	DA2	52	0645−1643	5	7
L 726-8 A	BL Cet	Gl 65 A	373.7	2.7	6	M5.5 V	38	0139−1757	6	9
L 726-8 B	UV Cet	Gl 65 B	...	...	...	M6 V	38	0139−1757	6	9
Ross 154	...	Gl 729	336.72	2.03	5	M3.5 V	21	1849−2350	7	11
Ross 248	...	Gl 905	316.0	1.1	6	M5.5 V	21	2341+4410	8	12
ϵ Eri	...	Gl 144	310.94	0.16	5	K2 V (k)	50	0332−0927	9	13
Lacaille 9352	...	Gl 887	305.26	0.70	5	M0.5 V	44	2305−3551	10	14
Ross 128	...	Gl 447	298.2	1.7	6	M4 V	21	1147+0048	11	15
L 789-6 A	...	Gl 866 A	289.5	4.4	6	M5[c] V	21	2238−1517	12	16
L 789-6 B	...	Gl 866 B	...	...	...	M5.5:[d] V	45	2238−1515	12	16
L 789-6 C	...	Gl 866 C	...	...	...	M6.5:[d] V	45	2238−1517	12	16
61 Cyg A	...	Gl 820 A	286.9	1.1	6	K5 V	38	2106+3844	13	19
61 Cyg B	...	Gl 820 B	...	...	...	K7 V	38	2106+3844	13	19
Procyon A	α CMi A	Gl 280 A	284.56	1.26	5	F5 IV-V	49	0739+0513	14	21
Procyon B	α CMi B	Gl 280 B	...	...	...	DA	52	0739+0515	14	21
Σ 2398 A	...	Gl 725 A	280.18	2.18	5	M3 V	41	1842+5937	15	23
Σ 2398 B	...	Gl 725 B	...	...	...	M3.5 V	41	1842+5937	15	23
Groombridge 34 A	...	Gl 15 A	278.76	0.77	5	M1.5 V	21	0018+4401	16	25
Groombridge 34 B	...	Gl 15 B	...	...	...	M3.5 V	21	0018+4401	16	25
ϵ Ind A	...	Gl 845 A	276.06	0.28	5	K4 V (k)	50	2203−5647	17	27
ϵ Ind Ba	...	Gl 845 Ba	...	...	...	T1	53	2204−5646	17	27
ϵ Ind Bb	...	Gl 845 Bb	...	...	...	T6	53	2204−5646	17	27
G 51-15	...	GJ 1111	275.8	3.0	6	M6.5 V	38	0829+2646	18	30
τ Cet	...	Gl 71	273.96	0.17	5	G8.5 V	50	0144−1556	19	31
L 372-58	...	GJ 1061	271.92	1.34	12	M5 V	12	0335−4430	20	32
L 725-32	...	Gl 54.1	268.8	3.2	6	M4.5 V	21	0112−1659	21	33
Luyten's Star	BD+05 1668	Gl 273	262.98	1.39	5	M3.5 V	38	0727+0513	22	34
SCR J1845−6357 A	...	...	259.45	1.11	12	M8.5 V	12	1845−6357	23	35
SCR J1845−6357 B	...	...	...	...	...	T6	54	1845−6357	23	35
Teegarden's Star	SO J025300.5+165258	...	259.25	0.94	74	M6 V	12	0253+1652	24	37
Kapteyn's Star	Z C 5h243[bb]	Gl 191	255.66	0.91	5	sdM1	44	0511−4501	25	38
Lacaille 8760	...	Gl 825	253.41	0.80	5	K7 V	44	2117−3852	26	39
Krüger 60 A	...	Gl 860 A	251.5	3.7	6	M3 V	39	2228+5741	27	40
Krüger 60 B	...	Gl 860 B	...	...	...	M4 V	39	2227+5741	27	40
DENIS-P J104814.7−395606.1	...	...	247.71	1.55	17	M8.5 V	20	1048−3956	28	42
UGPS J072227.51−054031.2	...	...	246	33	22	T9	4	0722−0540	29	43
Ross 614 A	...	Gl 234 A	242.32	3.12	5	M4-4.5 V	42	0629−0248	30	44
Ross 614 B	...	Gl 234 B	...	...	...	M4.5-6.5 V	42	0629−0248	30	44
WISE J035000.32−565830.2	...	...	238	38	2	Y1	1	0350−5658	31	46
WISEPA J154151.66−225025.2	...	...	238[rr]	...	1	Y0.5	1	1541−2250	32	47
BD−12 4523	Wolf 1061	Gl 628	232.98	1.60	5	M3 V	21	1630−1239	33	48
van Maanen's Star[e]	...	Gl 35	232.5	1.9	6	DZ8	52	0049+0523	34	49
Gou 32416[bb]	CD−37 15492	Gl 1	230.42	0.90	5	M1.5 V	44	0005−3721	35	50
Wolf 424 A	...	Gl 473 A	227.9	4.6	6	M5.5[c] V	40	1233+0901	36	51
Wolf 424 B	...	Gl 473 B	...	...	...	M5.5: V	46	1233+0901	36	51
L 1159-16	...	Gl 83.1	224.8	2.9	6	M4.5 V	38	0200+1303	37	53
Oe Arg 17415-6[bb]	BD+68 946	Gl 687	220.84	0.94	5	M3 V	21	1736+6820	38	54
LP 731-58	LHS 292	...	220.3	3.6	6	M6.5 V	40	1048−1120	39	55
Innes (unnumbered)[g]	CD−46 11540	Gl 674	220.24	1.42	5	M2.5 V	44	1728−4653	40	56
G 208-44 A	...	GJ 1245 A	220.2	1.0	6	M5.5[h] V	41	1953+4424	41	57
G 208-44 B	...	GJ 1245 C	...	...	...	M6.5:[i] V	1	1953+4424	41	57
G 208-45	...	GJ 1245 B	...	...	...	M5.5 V	41	1953+4424	41	57
Innes (unnumbered)[g]	Ci 20 658	Gl 440	215.80	1.25	8	DQ6	52	1145−6450	42	60
Ross 780	...	Gl 876	213.28	2.12	5	M3.5 V	21	2253−1415	43	61
G 158-27	...	GJ 1002	213.0	3.6	6	M5.5 V	21	0006−0732	44	62
L 143-23	LHS 288	...	208.95	2.73	12	M5 V	12	1044−6112	45	62
WISEPC J140518.40+553421.4	...	...	207	39	2	Y0p	4	1405+5534	46	62

Table 4
(Continued)

Discovery Name	Other Name	Gliese Name	π_{trig}[a] (mas)	σ_π (mas)	π Ref.	Spec. Type	Spec. Ref.	J2000 Coords.	Sys. Rank	Indiv. Rank
(1)	(2)	(3)	(4)	(5)	(6)	(7)	(8)	(9)	(10)	(11)
Lalande 21258 A	...	Gl 412 A	206.27	1.00	5	M1 V	21	1105+4331	47	65
Lalande 21258 B	...	Gl 412 B	...	...	...	M5.5 V	21	1105+4331	47	65
Groombridge 1618	...	Gl 380	205.21	0.54	5	K7 V	38	1011+4927	48	67
BD+20 2465	G 54-23	Gl 388	204.6	2.8	6	M3 V	21	1019+1952	49	68
DENIS J081730.0−615520	...	...	203	13	23	T6	23	0817−6155	50	69
CD−49 13515	L 354-89	Gl 832	201.87	1.01	5	M1.5 V	44	2133−4900	51	70
LP 944-20	...	...	201.4	4.2	27	M9 V	48	0339−3525	52	71
DENIS-P J025503.3−470049	...	...	201.37	3.89	13	L8	55	0255−4700	53	72
o^2 Eri A	...	Gl 166 A	200.62	0.23	5	K0.5 V	50	0415−0739	54	73
o^2 Eri B	...	Gl 166 B	...	...	...	DA4	52	0415−0739	54	73
o^2 Eri C	...	Gl 166 C	...	...	...	M4.5 V	38	0415−0739	54	73
Innes (unnumbered)[g]	CD−44 11909	Gl 682	196.90	2.15	5	M3.5 V	44	1737−4419	55	76
70 Oph A	...	Gl 702 A	196.72	0.83	5	K0- V	49	1805+0229	56	77
70 Oph B	...	Gl 702 B	...	0.83	5	K5 V	56	1805+0229	56	77
BD+43 4305	LFT 1737	Gl 873	195.22	1.87	5	M3.5 V	42	2246+4420	57	79
Altair	α Aql	Gl 768	194.95	0.57	5	A7 Vn	49	1950+0852	58	80
WISEPC J150649.97+702736.0	...	...	193	26	2	T6	3	1506+7027	59	81
WISEPC J205628.90+145953.3	...	...	192	...	1	Y0	4	2056+1459	60	82
G 9-38 A	...	GJ 1116 A	191.2	2.5	6	M5.5 V	57	0858+1945	61	83
G 9-38 B	...	GJ 1116 B	...	...	...	M5.5 V	57	0858+1945	61	83
G 99-49	...	...	190.93	1.89	12	M3.5 V	21	0600+0242	62	85
LP 656-38	LHS 1723	...	187.92	1.26	12	M4 V	12	0501−0656	63	86
2MASS J09393548−2448279	...	...	187.3	4.6	28	T8	53	0939−2448	64	87
AC+79 3888	LFT 849	Gl 445	186.86	1.70	5	M3.5 V	21	1147+7841	65	88
Lalande 25372	...	Gl 526	185.49	1.10	5	M1.5 V	21	1345+1453	66	89
Stein 2051 A	...	Gl 169.1A	180.6	0.8	6	M4 V	42	0431+5858	67	90
Stein 2051 B	...	Gl 169.1B	...	...	...	DC5	52	0431+5858	67	90
Wolf 294	...	Gl 251	179.01	1.60	5	M3 V	38	0654+3316	68	92
2MASSI J0415195−093506	...	...	177.3	2.2	76	T8	53	0415−0935	69	93
Strb. 1611[s]	Wolf 1453	Gl 205	176.77	1.18	5	M1.5 V	38	0531−0340	70	94
2MASSI J1835379+325954	LSR J1835+3259	...	176.5	0.5	31	M8.5 V	31	1835+3259	71	95
WISEPA J174124.26+255319.5	...	...	176	22	2	T9	3	1741+2553	72	96
LP 816-60	...	...	175.03	3.40	5	M4 V	50	2052−1658	73	97
L 449-1	...	...	175	...	14	M4 V	14	0517−3521	74	98
L 668-21 A	...	Gl 229 A	173.81	0.99	5	M1 V	38	0610−2151	75	99
L 668-21 B	...	Gl 229 B	...	...	...	T7 pec	53	0610−2152	75	99
σ Dra	...	Gl 764	173.77	0.18	5	G9 V	49	1932+6939	76	101
Ross 47	...	Gl 213	171.55	3.99	5	M4 V	38	0542+1229	77	102
Innes (unnumbered)[g]	...	Gl 693	171.48	2.31	5	M2 V	44	1746−5719	78	103
Lalande 27173 A	...	Gl 570 A	171.22	0.94	5	K4 V	50	1457−2124	79	104
Lalande 27173 B	...	Gl 570 B	...	...	...	M1[m] V	21	1457−2124	79	104
Lalande 27173 C	...	Gl 570 C	...	...	...	M3:[n] V	57	1457−2124	79	104
2MASSW J1457150−212148	...	Gl 570 D	...	...	...	T7.5	53	1457−2121	79	104
Wolf 1055	...	Gl 752 A	171.2	0.7	6	M3 V	38	1916+0510	80	108
van Biesbroeck 10	...	Gl 752 B	...	...	...	M8 V	41	1916+0509	80	108
WISE J053516.80−750024.9	...	...	170	44	2	$\geqslant$Y1:	1	0535−7500	81	110
L 347-14	...	Gl 754	169.03	1.55	17	M3 V	19	1920−4533	82	111
Innes (unnumbered)[g]	...	Gl 588	168.66	1.30	5	M2.5 V	44	1532−4116	83	112
36 Oph A	...	Gl 663 A	168.54	0.54	5	K0 V	59	1715−2636	84	113
36 Oph B	...	Gl 663 B	...	...	...	K1 V	59	1715−2636	84	113
36 Oph C[o]	...	Gl 664	...	...	...	K5 V (k)	50	1716−2632	84	113
η Cas A	...	Gl 34 A	167.98	0.48	5	F9 V	58	0049+5748	85	116
η Cas B	...	Gl 34 B	...	...	...	K7 V	21	0049+5749	85	116
Ross 882	...	Gl 285	167.88	2.31	5	M4 V	21	0744+0333	86	118
Lalande 46650	...	Gl 908	167.29	1.23	5	M1 V	21	2349+0224	87	119
2MASS J05332802−4257205	...	...	167	...	32	M4.5 V	32	0533−4257	88	120
2MASS J18450079−1409036[p]	...	...	167	...	32	M5 V	32	1845−1409	89	121
2MASS J18450097−1409053[p]	...	...	167	...	32	M5 V	32	1845−1409	89	121
2MASS J20360829−3607115	...	...	167	...	32	M4.5 V	32	2036−3607	90	123
L 722-22 A	...	GJ 1005 A	166.6	~2	24	M3.5 V	42	0015−1607	91	124
L 722-22 B	...	GJ 1005 B	...	...	...	M4.5-6.5 V	42	0015−1607	91	124
LPM 728 A	...	Gl 783 A	166.25	0.27	5	K2.5 V	50	2011−3606	92	126
LPM 728 B	...	Gl 783 B	...	...	...	M3.5 V[q]	56	2011−3606	92	126
WISEPA J025409.45+022359.1	...	...	166	26	2	T8	3	0254+0223	93	128
82 Eri	...	Gl 139	165.47	0.19	5	G8 V	50	0319−4304	94	129

Table 4
(Continued)

Discovery Name	Other Name	Gliese Name	π_{trig}[a] (mas)	σ_π (mas)	π Ref.	Spec. Type	Spec. Ref.	J2000 Coords.	Sys. Rank	Indiv. Rank
(1)	(2)	(3)	(4)	(5)	(6)	(7)	(8)	(9)	(10)	(11)
Ross 986 A	...	Gl 268 A	165.2	2.1	6	M4.5[c] V	38	0710+3831	95	130
Ross 986 B	...	Gl 268 B	...	...	...	M5: V	60	0710+3832	95	130
WISEPA J041022.71+150248.5	...	...	164	24	2	Y0	4	0410+1502	96	132
LP 44-113	...	GJ 1221	164.7	2.4	6	DXP9	52	1748+7052	97	133
δ Pav	...	Gl 780	163.71	0.17	5	G8 IV	50	2008−6610	98	134
2MASSI J0937347+293142	...	...	163.39	1.76	26	T6 pec	53	0937+2931	99	135
BD+53 1320	LFT 634	Gl 338 A	162.8	2.9	6	M0 V	38	0914+5241	100	136
BD+53 1321	LFT 635	Gl 338 B	...	...	...	K7 V	38	0914+5241	100	136
BD+19 5116 A	LFT 1799	Gl 896 A	161.76	1.66	5	M3.5 V	21	2331+1956	101	138
BD+19 5116 B	LFT 1800	Gl 896 B	...	...	...	M4.5 V	21	2331+1956	101	138
LPM 730	...	Gl 784	161.34	1.00	5	M0 V	56	2013−4509	102	140
WISE J014656.66+423410.0	...	...	159	...	1	Y0		0146+4234	103	141
Wolf 1481	...	Gl 555	158.46	2.62	17	M3.5 V	21	1434−1231	104	142
2MASS J15031961+2525196	...	...	157.2	2.2	76	T5	53	1503+2525	105	143
LP 368-128	LHS 2090	...	156.87	2.67	12	M6 V	12	0900+2150	106	144
L 471-42	LHS 337	...	156.78	1.99	12	M4 V	12	1238−3822	107	145
G 99-44	...	Gl 223.2	156.13	0.84	8	DZ9	52	0555−0410	108	146
G 180-60	...	...	156[r]	4	25	M5 V	65	1631+4051	109	147
SIMP J013656.5+093347	...	...	156	...	34	T2.5	34	0136+0933	110	148
Wolf 630 A	...	Gl 644 A	154.8	0.6	6	M2.5[t] V	21	1655−0819	111	149
Wolf 630 Ba	...	Gl 644 B	...	...	...	M3:[u] V	1	1655−0820	111	149
van Biesbroeck 8	...	Gl 644 C	... [v]	...	...	M7 V	41	1655−0823	111	149
Wolf 630 Bb	...	Gl 644 D	...	...	...	M3.5:[u] V	1	1655−0820	111	149
Wolf 629	...	Gl 643	... [w]	...	...	M3.5 V	38	1655−0819	111	149
Wolf 562	BD−7 4003	Gl 581	154.66	2.62	17	M2.5 V	21	1519−0743	112	154
BD+45 2505 A	LFT 1326	Gl 661 A	154.0	3.6	6	M3[c] V	39	1710+4542	113	155
BD+45 2505 B	LFT 1327	Gl 661 B	...	...	...	M3:[x] V	64	1712+4539	113	155
LP 71-82	...	...	154[f]	...	32,36	M5 V	32	1802+6415	114	157
G 202-48	...	Gl 625	153.46	0.99	5	M1.5 V	39	1625+5418	115	158
L 100-115	...	GJ 1128	153.05	2.41	17	M4.5 V	18	0942−6853	116	159
G 161-71	...	...	153[j]	...	35,72	M5 V	35	0944−1220	117	160
L 1190-34	...	GJ 1156	152.9	3.0	6	M5 V	21	1218+1107	118	161
BD+56 2966	LFT 1767	Gl 892	152.76	0.29	5	K3 V	49	2313+5710	119	162
2MASS J11145133−2618235	...	...	152	...	1	T7.5	53	1114−2618	120	163
Ross 104	...	Gl 408	150.10	1.70	5	M2.5 V	21	1100+2249	121	164
Ross 775 A	...	Gl 829 A	149.15	1.81	5	M3.5[c] V	39	2129+1738	122	165
Ross 775 B	...	Gl 829 B	...	...	...	M3.5:[y] V	1	2129+1738	122	165
SCR J1546−5534	...	...	149	...	11	late-M[z] V	1	1546−5534	123	167
ξ Boo A	...	Gl 566 A	148.98	0.48	5	G7 V	49	1451+1906	124	168
ξ Boo B	...	Gl 566 B	...	...	...	K4 V	67	1451+1906	124	168
Wolf 358	...	Gl 402	147.92	3.52	5	M4 V	38	1050+0648	125	170
G 41-14 A	...	...	147.66	1.98	12	M3.5[c] V	21	0858+0828	126	171
G 41-14 B	...	...	...	...	...	M3.5:[aa] V	1	0858+0828	126	171
G 41-14 C	...	...	...	...	...	M3.5:[aa] V	1	0858+0828	126	171
Ross 619	...	Gl 299	146.3	3.1	6	M4 V	21	0811+0846	127	174
Ross 671	...	Gl 880	146.09	1.00	5	M1.5 V	39	2256+1633	128	175
LP 914-54	LHS 3003	...	145.30	3.25	15	M7 V	66	1456−2809	129	176
LP 771-95[cc]	...	...	144.68	2.52	12	M2.5 V	12	0301−1635	130	177
LP 771-96 A	...	...	...	...	...	M3[dd] V	12	0301−1635	130	177
LP 771-96 B	...	...	...	...	...	M3.5:[ee] V	1	0301−1635	130	177
L 230-188	...	GJ 1068	143.42	1.92	17	M4.5[ff] V	44	0410−5336	131	180
WISE J192841.35+235604.9	...	...	143	...	1	T6	78	1928+2356	132	181
L 369-44[gg]	LP 993-116	...	143	...	32,72	M4 V	32	0245−4344	133	182
L 369-45[gg]	LP 993-115	...	143	...	32,72	M5:[hh] V	1	0245−4344	133	182
2MASS J18522528−3730363	...	...	143	...	32	M4.5 V	32	1852−3730	134	184
G 161-7 A	...	...	143[k]	...	35,72	M5[c] V	35	0915−1035	135	185
G 161-7 B	...	...	...	...	...	M5:[ll] V	1	0915−1035	135	185
BD+61 2068 A	LFT 1580 A	Gl 809 A	141.87	0.64	5	M0[c] V	39	2053+6209	136	187
BD+61 2068 B	LFT 1580 B	Gl 809 B	...	...	...	M?[ii] V	1	2053+6209	136	187
Ross 446	...	Gl 393	141.50	2.22	5	M2 V	21	1028+0050	137	189
WISE J071322.55−291751.9	...	...	141	...	1	Y0		0713−2917	138	190
WISE J000517.48+373720.5	...	...	141	...	1	T9	78	0005+3737	139	191
WISEPC J121756.91+162640.2	...	...	141	...	1	T9	3	1217+1626	140	192
2MASS J07290002−3954043	...	...	141	...	1	T8p	79	0729−3954	141	193
HR 6426 A	LFT 1336 A	Gl 667 A	139.5	6.3	6	K4- V	50	1718−3459	142	194

Table 4
(Continued)

Discovery Name	Other Name	Gliese Name	π_{trig}[a] (mas)	σ_π (mas)	π Ref.	Spec. Type	Spec. Ref.	J2000 Coords.	Sys. Rank	Indiv. Rank
(1)	(2)	(3)	(4)	(5)	(6)	(7)	(8)	(9)	(10)	(11)
HR 6426 B	LFT 1336 B	Gl 667 B	...	...	...	K4 V	56	1718−3459	142	194
HR 6426 C	LFT 1337	Gl 667 C	...	...	...	M1.5 V	44	1718−3459	142	194
HR 753 A	LFT 217 A	Gl 105 A	139.27	0.45	5	K3 V	49	0236+0653	143	197
HR 753 B	LFT 218	Gl 105 B	...	...	...	M3.5 V	21	0236+0652	143	197
HR 753 C	LFT 217 B	Gl 105 C	...	...	...	M7:[ii] V	68	0236+0653	143	197
SCR J0740−4257	LSR J07401−4257	...	139	...	7	M4.5 V	7	0740−4257	144	200
L 43-72	...	...	139	...	14	M4.5 V	14	1811−7859	145	201
G 157-77	...	GJ 1286	138.3	3.5	6	M5.5 V	21	2335−0223	146	202
LP 229-17[kk]	...	...	138	40	37	M3 V	37	1834+4007	147	203
LP 71-165	LHS 3376	...	137.5	5.3	6	M4.5 V	21	1818+6611	148	204
2MASSW J1507476−162738	...	...	136.4	0.6	30	L5	61	1507−1627	149	205
WISE J004945.61+215120.0	...	...	135	...	1	T8.5	78	0049+2151	150	206
L 788-34	LHS 3799	...	134.4	4.9	6	M4.5 V	21	2223−1736	151	207
G 203-47 A	...	...	134.31	1.99	5	M3.5 V[c]	21	1709+4340	152	208
G 203-47 B	...	...	134.31	1.99	5	D?[nn]	43	1709+4340	152	208
L 499-56	LHS 3746	...	134.29	1.31	12	M3 V	12	2202−3704	153	210
Lalande 1299	...	Gl 33	134.14	0.51	5	K2 V	49	0048+0516	154	211
β Hyi	...	Gl 19	134.07	0.11	5	G0 V	50	0025−7715	155	212
Ross 556	...	Gl 109	133.16	2.26	5	M3 V	21	0244+2531	156	213
107 Psc	...	Gl 68	132.76	0.50	5	K0 V	49	0142+2016	157	214
G 154-44	...	GJ 1224	132.6	3.7	6	M4.5 V	21	1807−1557	158	215
μ Cas A	...	Gl 53 A	132.38	0.82	5	K1 V Fe-2	49	0108+5455	159	216
μ Cas B	...	Gl 53 B	...	...	...	M3.5:[oo] V	9	0108+5455	159	216
LTT 9283[qq]	...	Gl 879	131.42	0.62	5	K4+ V k	50	2256−3133	160	218
Ross 490	...	Gl 514	130.62	1.05	5	M1 V	21	1329+1022	161	219
Vega	...	Gl 721	130.23	0.36	5	A0 Va	49	1836+3847	162	220
Wolf 718	...	Gl 673	129.86	0.73	5	K7 V	21	1725+0206	163	221
Fomalhaut[pp]	...	Gl 881	129.81	0.47	5	A4 V	50	2257−2937	164	222
LP 881-64 A[mm]	...	GJ 2005 A	129.47	2.48	15	M5.5 V	69	0024−2708	165	223
LP 881-64 B	...	GJ 2005 B	...	...	...	M8.5 V	69	0024−2708	165	223
LP 881-64 C	...	GJ 2005 C	...	...	...	M9 V	69	0024−2708	165	223
L 991-14	...	Gl 701	128.89	1.43	5	M0 V	21	1805−0301	166	226
G 109-35	...	GJ 1093	128.8	3.5	6	M5 V	21	0659+1920	167	227
Innes (unnumbered)[g]	...	Gl 480.1	128.52	3.90	5	M3 V	44	1240−4333	168	228
WISEP J060738.65+242953.4	...	...	128.2	...	71	L9	1	0607+2429	169	229
2MASS J03480772−602227	...	...	128	...	1	T7	53	0348−6022	170	230
p Eri A	...	Gl 66 A	127.84	2.19	5	K2 V	50	0139−5611	171	231
p Eri B	...	Gl 66 B	...	...	...	K2 V	50	0139−5611	171	231
BD−03 2870	LFT 3734	Gl 382	127.08	1.90	5	M2 V	38	1012−0344	172	233
L 97-12	...	Gl 293	126.25	1.34	8	DQ9	52	0753−6747	173	234
L 1813-21	LHS 1805	...	126.1	3.3	75	M3.5 V	21	0601+5935	174	235
LP 876-10	...	...	126[l]	...	35,70	M4 V	70	2248−2422	175	236
L 674-15	...	Gl 300	125.60	0.97	12	M3.5 V	21	0812−2133	176	237
AC+65 6955	LFT 1552	Gl 793	125.07	1.08	5	M2.5 V	44	2030+6526	177	238
G 99-47	...	GJ 1087	125.0	3.6	6	DAP9	52	0556+0521	178	239
LP 467-16	...	...	125	...	32,73	M5 V	3	0111+1526	179	240
2MASS J12140866−2345172	...	...	125	...	32	M4.5 V	32	1214−2345	180	241
2MASS J19513587−3510375	...	...	125	...	32	M4 V	32	1951−3510	181	242
SCR J0838−5855	...	...	125	...	7	M6 V	7	0838−5855	182	243

Notes. Code for references: (1) this paper, (2) Marsh et al. 2012; (3) Kirkpatrick et al. 2011; (4) Cushing et al. 2011; (5) van Leeuwen 2007; (6) van Altena et al. 1995; (7) Winters et al. 2011; (8) Subasavage et al. 2009; (9) Drummond et al. 1995; (10) Riedel et al. 2011; (11) Boyd et al. 2011; (12) Henry et al. 2006; (13) Costa et al. 2006; (14) Scholz et al. 2005a; (15) Costa et al. 2005; (16) Benedict et al. 1999; (17) Jao et al. 2005; (18) Henry et al. 2002; (19) Hawley et al. 1996; (20) Henry et al. 2004; (21) Henry et al. 1994; (22) Lucas et al. 2010; (23) Artigau et al. 2010; (24) Hershey & Taff 1998; (25) Ducourant et al. 1998; (26) Schilbach et al. 2009; (27) Tinney 1996; (28) Burgasser et al. 2008; (29) Vrba et al. 2004; (30) Dahn et al. 2002; (31) Reid et al. 2003; (32) Riaz et al. 2006; (33) Scholz 2010; (34) Artigau et al. 2006; (35) Scholz et al. 2005b; (36) Reid et al. 2007; (37) Jenkins et al. 2009; (38) Kirkpatrick et al. 1991; (39) Kirkpatrick 1992; (40) Henry et al. 1992; (41) Boeshaar & Tyson 1985; (42) Kirkpatrick & McCarthy 1994; (43) Delfosse et al. 1999; (44) Hawley et al. 1996; (45) Delfosse et al. 1999; (46) Torres et al. 1999; (47) McCarthy et al. 1988; (48) Kirkpatrick et al. 1999; (49) Gray et al. 2003; (50) Gray et al. 2006; (51) Garrison 1994; (52) McCook & Sion 2006; (53) Burgasser et al. 2006a; (54) Kasper et al. 2007; (55) Kirkpatrick et al. 2008; (56) Bidelman 1985; (57) Forveille et al. 1999; (58) Gray et al. 2001; (59) Irwin et al. 1996; (60) Tomkin & Pettersen 1986; (61) Kirkpatrick et al. 2000; (62) Burgasser et al. 2010; (63) Kirkpatrick et al. 2010; (64) Henry & McCarthy 1993; (65) Reid et al. 1995; (66) Kirkpatrick et al. 1995; (67) Wilson & Vainu Bappu 1957; (68) Golimowski et al. 2000; (69) Reiners et al. 2007; (70) Reid et al. 2004; (71) J. E. Gizis 2012, priviate communication; (72) Reid et al. 2002; (73) Reid & Cruz 2002; (74) Gatewood & Coban 2009; (75) Khrutskaya et al. 2010; (76) Dupuy & Liu 2012; (77) G. N. Mace et al., in preparation; (78) Looper et al. 2007.

Table 4
(Continued)

[a] Unless otherwise marked, the parallax for the primary (or for the combined system) is used for all components of the system.
[b] Proxima Centauri is the third member of the α Centauri system. The error bar quoted here for the parallax is the updated one used in Jao et al. (2005).
[c] The spectral type is a joint type including all objects in the system.
[d] These spectral types are estimates based on the M_V values for the B and C components as measured by Delfosse et al. (1999) and translated into spectral type using Table 3 of Kirkpatrick & McCarthy (1994).
[e] This object is sometimes referred to as van Maanen 2, although in the original discovery paper (van Maanen 1917) it is neither named nor numbered.
[f] We estimate a distance by averaging the 7.1 pc estimate of Reid et al. (2007) and the 6 pc estimate of Riaz et al. (2006).
[g] According to Luyten (1979), Innes discovered this object. However, Innes did not number his discoveries, so the discovery name is noted here simply as "Innes (unnumbered)."
[h] This is a composite type for G 208-44 AB (GJ 1245 AC).
[i] McCarthy et al. (1988) give delta(V) $\approx$ 2.0 mag for the G 208-44 AB pair, so we estimate the spectral type of G 208-44 B to be approximately one subclass later than G 208-44 A (assumed to have a type identical to the composite spectral type of M5.5 V).
[j] We estimate a distance by averaging the 6.9 pc estimate of Scholz et al. (2005b) and the 6.2 pc estimate of Reid et al. (2002).
[k] We estimate a distance by averaging the 7.3 pc estimate of Scholz et al. (2005b) and the 6.7 pc estimate of Reid et al. (2002).
[l] We estimate a distance by averaging the 7.2 pc estimate of Reid et al. (2004) and the 8.7 pc estimate of Scholz et al. (2005b).
[m] This spectral type is a composite type for the Lalande 27173 BC pair.
[n] This spectral type is estimated from the absolute J, H, K values measured by Forveille et al. (1999) and the absolute magnitudes vs. spectral type relation given in Table 3 of Kirkpatrick & McCarthy (1994).
[o] The parallax for 36 Oph A is assumed for 36 Oph C; an independent *Hipparcos* parallax for 36 Oph C is 167.49 $\pm$ 0.60 mas (van Leeuwen 2007).
[p] 2MASS J18450079−1409036 and 2MASS J18450097−1409053 appear to be a common proper motion pair based on Digitized Sky Survey R-band images taken in 1951 and again in 1988 (see http://irsa.ipac.caltech.edu/applications/FinderChart/).
[q] Hawley et al. (1997) say this is an M3 III but Luyten (1979) lists this pair as a common proper motion binary so the giant luminosity classification must be an error.
[r] Reid et al. (2004) state that they believe this parallax measurement may be in error because the result suggests a location on the H-R diagram significantly below the main sequence despite the fact that this M dwarf's spectrum shows no evidence of the low metallicity expected for such a location.
[s] Identification taken from van de Kamp (1930).
[t] This spectral type is the composite type for Wolf 630 ABaBb.
[u] The spectral type is estimated from the measured mass of this component (Ségransan et al. 2000) and a mapping of mass into spectral type using other objects in this table and their masses as measured in Henry & McCarthy (1993).
[v] Costa et al. (2005) measure an independent parallax of 155.43+/−1.33 mas for van Biesbroeck 8.
[w] van Leeuwen (2007) measures a parallax value of 148.92 $\pm$ 4.00 mas; an independent Yale parallax gives 169.84 $\pm$ 6.6 mas (van Altena et al. 1995).
[x] This spectral type is based on delta J, H, K values measured by Henry & McCarthy (1993) and using the absolute magnitude vs. spectral types tabulate in Table 3 of Kirkpatrick & McCarthy (1994).
[y] Given that the mass ratio is $\sim$1 (Delfosse et al. 1999), we assume equal spectral types for both components.
[z] SCR J1546−5534 has $J-Ks = 1.10$ mag from 2MASS; *WISE* photometry is corrupted by a brighter source immediately to the northwest (the Galactic latitude of this source is −0.8 deg) so we can only say that J-W2 < 3.65 and H-W2 < 2.99. The overall photometry from both 2MASS and *WISE* is consistent with a late-M dwarf.
[aa] Given that Delfosse et al. (1999) find nearly equal masses for components A and B and that component C is $\sim$0.5 mag fainter than the joint AB pair in adaptive optics imaging, we assume all components are roughly the same spectral type.
[bb] Identification taken from Hertzsprung (1922); Kapteyn's Star is also referred to as Cordoba 5h243 (van Maanen 1943).
[cc] The object LP 771-95 shares common proper motion with LP 771-96 AB. The parallax measured for LP 771-95 is assumed for LP 771-96 AB.
[dd] This is the composite spectral type for LP 771-96 AB.
[ee] This spectral type is estimated from the delta V, R, I values measured in Henry et al. (2006), the measured composite type for LP 771-96 AB, and spectral type vs. absolute magnitude relations given in Table 3 of Kirkpatrick & McCarthy (1994).
[ff] Rodgers & Eggen (1974) note peculiarities in the blue spectrum of this object.
[gg] These two objects share common proper motion.
[hh] Kuiper (1943) types this object one spectral subclass later than L 369-44; as Kuiper was probably typing on the Mt. Wilson system, we assign this object a type one subclass later than the type assigned for L 369-44 by Riaz et al. (2006).
[ii] BD+61 2068 is noted as a spectroscopic binary by Herbst & Layden (1987) (see also Heintz 1981). No other info is given, so an M spectral type is assumed for the secondary.
[jj] The spectral type is an estimate based on measured broadband colors.
[kk] The object LP 229-17 lies near on the sky and in distance to Vega.
[ll] Montagnier et al. (2006) show that this is a near equal-magnitude binary, so we estimate a spectral type identical to the joint spectrum.
[mm] GJ 2005 D, a fourth component reported elsewhere, may not exist according to Seifahrt et al. (2008).
[nn] This object is believed to be a white dwarf.
[oo] This spectral type is an estimate based on the measured absolute V magnitude.
[pp] Fomalhaut has common proper motion with LTT 9283 (Gl 879).
[qq] The object LTT 9283 has common proper motion with Fomalhaut but may lie slightly closer to the Sun than Fomalhaut itself.
[rr] Marsh et al. (2012) report a parallax of 0.″087 $\pm$ 0.″054 for this object, whereas Kirkpatrick et al. (2011) report 0.″351 $\pm$ 0.″108. Given the discrepancies in this measurements, we instead use our spectrophotometric distance estimate from Table 8.

As was done in Kirkpatrick et al. (2011), we focus on objects with spectral types of T6 or later. To sample a sufficiently large number of objects at these types, we consider distances larger than the 8 pc limit of the previous section, but we must keep in mind that samples should be reasonably complete (or completable) out to the distance limit we choose. Toward this end, we will use the depth of the *WISE* all-sky survey as the arbiter of the distance to which a complete census can be obtained, since it is the survey most capable of finding these coldest brown dwarfs. In Kirkpatrick et al. (2011) we

Table 5
Objects Once Listed as Falling Within 8 pc but Now Believed to Lie More Distant

Name	π_{trig} (mas)	σ_π (mas)	π Ref.	Spec. Type	Spec. Ref.	J2000 Coords.
(1)	(2)	(3)	(4)	(5)	(6)	(7)
Gl 915	122.27	1.13	3	DAP	10	0002−4309
2MASS J00155808−1636578[a]	123	...	12	M4 V	9, 11	0015−1636
Gl 54 AB	122.04	2.42	1	M2.5 V	13	0110−6726
Gl 102[b]	102.4	3.7	6	M4 V	14	0233+2455
Gl 143.1[c]	45.28	1.97	1	K7 V	15	0329−1140
Gl 178	123.94	0.17	1	F6 IV-V	16	0449+0657
Gl 185 AB	116.59	1.51	1	K7 V	17	0502−2115
Gl 190	107.85	2.10	1	M3.5 V	14	0508−1810
2MASS J05241914−1601153 AB[d]	<125	...	12	M4.5 V + M5 V	18	0524−1601
LP 949-15 = AP Col[e]	119.21	0.98	4	M5 V	19	0604−3433
SCR J0630−7643 AB[f]	114.16	1.85	2	M6 V	20	0630−7643
G 89-32 AB	116.60	0.97	2	M5 V	14	0736+0704
L 186-67 AB + L 186-66[g]	<125	...	12	M4.5 V + M6 V + >L0	18	0822−5726
NLTT 23956 + NLTT 23954[h]	81	...	1	M4.5 V + M6: V	11, 12	1018−2028
2MASS J10364483+1521394 ABC[i]	51	...	7	M3.5 V + M4.5 V + M4.5 V	7	1036+1521
2MASS J11102788−3731520 ABC[j]	24	...	21	M3 V	21	1110−3731
ξ UMa AaAbBaBb(Bc?)C[k]	113.20	4.60	5	F8.5 V + M3: V + G2 V + late-K: V + (K2-3 V) + T8.5	22, 23, 24, 25	1118+3131
LSPM J1206+7007S + LSPM J1206+7007N AB[l]	60	...	8	M3.5 + M4.5 V	26, 27	1206+7007
G 165-8 AB[m]	95	...	28	M4 V	29	1331+2916
LP 799-7[n]	92.86	0.89	4	M4.5 V	11	1359−1950
Gl 623 AB	124.12	1.16	1	M2.5 V	17	1624+4821
Gl 686	123.67	1.61	1	M0 V	17	1737+1835
WISEPA J173835.53+273258.9	111	36	30	Y0	31	1738+2732
χ Dra AB	124.11	0.87	1	F7 V (metal weak)	16	1821+7243
WISEPA J182831.08+265037.8	122	13	32	$\geqslant$Y2	12	1828+2650
Gl 831 AB	120.52	5.98	1	M4.5	17	2131−0947
WISE J222055.32−362817.5	123	...	12	Y0	12	2220−3628
Gl 884	121.69	0.69	1	K7+ V k	13	2300−2231

Notes. Code for references: (1) van Leeuwen 2007; (2) Henry et al. 2006; (3) Subasavage et al. 2009; (4) Riedel et al. 2011; (5) Perryman et al. 1997; (6) van Altena et al. 1995; (7) Daemgen et al. 2007; (8) Shkolnik et al. 2010; (9) Reid et al. 2007; (10) Koester et al. 2009; (11) Riaz et al. 2006; (12) this paper, (13) Gray et al. 2006; (14) Reid et al. 1995; (15) Hawley et al. 1997; (16) Gray et al. 2001; (17) Henry et al. 1994; (18) Bergfors et al. 2010; (19) Scholz et al. 2005a; (20) Henry et al. 2004; (21) Zuckerman & Song 2004; (22) Keenan & McNeil 1989; (23) Mason et al. 1995; (24) Griffin 1998; (25) Wright et al. 2012; (26) Reid et al. 2007; (27) Shkolnik et al. 2009; (28) Beuzit et al. 2004; (29) Reid et al. 2004; (30) Marsh et al. 2012; (31) Cushing et al. 2011 (32) Beichman et al. 2012.

[a] Reid et al. (2007) predicted a distance of 7.3 pc and Riaz et al. (2006) predicted 9 pc. We list the average of these two as the distance estimate.

[b] Riaz et al. (2006) predicted a distance of 8 pc.

[c] Riaz et al. (2006) predicted a distance of 4 pc based on what appears to be an erroneous measurement (M4.5 V) of this star's spectral type.

[d] Riaz et al. (2006) predicted a distance of 8 pc assuming this is a single star, but Bergfors et al. (2010) have shown this to be a near equal-mag double so the distance must be greater.

[e] Scholz et al. (2005a) predicted a distance of 6.1 pc.

[f] Winters et al. (2011) predicted a distance of 5.5 pc.

[g] Riaz et al. (2006) predicted a distance of 8 pc to L 186-67 (LHS 2005) assuming it is single. Bergfors et al. (2010) find that L 186-67 is a close double (M4.5 V + >L0) with a magnitude difference of 4.5 mag at z band. We assume that the binarity is enough to push this object outside of our 8 pc limit, but parallactic verification is warranted. Note that there is a common proper motion, third component (M6 V) named L 186-66 (LHS 2004).

[h] Riaz et al. (2006) predict a distance of 8 pc. However, their spectral type of M4.5 V for NLTT 23956 along with its 2MASS values of $J = 9.00$, $H = 8.42$, and $K_s = 8.15$ mag suggests, using Table 3 of Kirkpatrick & McCarthy (1994), a distance of 12.4, 12.3, and 12.2 pc in each band, respectively. Our estimate of 12.3 pc is assumed instead. We estimate a spectral type of M6 V for the fainter common proper motion companion, NLTT 23954, based on the fact that is it ∼1.5 mag fainter than NLTT 23956 in all 2MASS bands.

[i] Reid et al. (2007) predict a distance of 7.1 pc assuming it is single. Daemgen et al. (2007), however, have shown it to be a triple system.

[j] This object is also known as TWA 3 ABC, a member of the TW Hydrae Association, and believed to lie at a distance of 42 pc (Zuckerman & Song 2004), not 5 pc away as estimated by Riaz et al. (2006).

[k] An earlier parallax measurement, 127 ± 6 mas (Jenkins 1952), places this just inside the 8 pc volume. This is a remarkable quintuple or sextuple system. The speckle companion ξ UMa Bc (Mason et al. 1995) awaits independent verification, and a widely separated T8.5 companion (ξ UMa C) has recently been announced by Wright et al. (2012).

[l] Reid et al. (2007) predicted a distance of 5.1 pc for LSPM J1206+7007S. Shkolnik et al. (2010) find LSPM J1206+7007N to be a double-lined spectroscopic binary.

[m] Reid et al. (2004) predicted a distance of 7.9 pc assuming the star is single, but Beuzit et al. (2004) find it to be binary and adjust the distance estimate accordingly.

[n] Riaz et al. (2006) predicted a distance of 7 pc.

found that a distance limit of 20 pc worked well for integral T6–T6.5, T7–T7.5, and T8–T8.5 bins. At T9–T9.5, it was shown that *WISE* may only fully sample the entire sky out to ∼15 pc, so this limit was chosen for that spectral bin. The limit for Y dwarfs was chosen to be 10 pc, which we retain here and discuss in more detail in the discussion that follows.

Many of the objects will not have trigonometric parallax measurements, so distances must be estimated spectrophotometrically, i.e., each object's apparent magnitude will be compared to

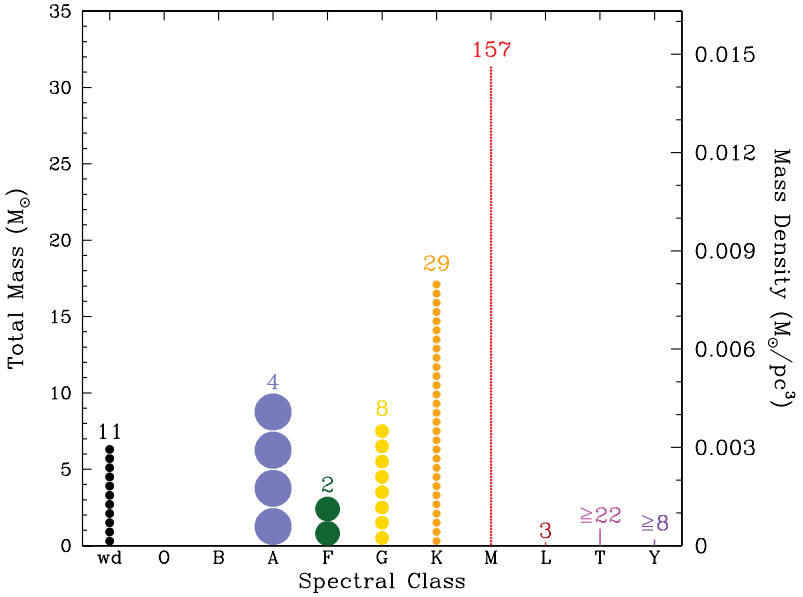

Figure 11. 8 pc sample as a function of spectral type plotted in three ways—as total mass (left axis), mass density (right axis), and histogram (numbers above each star stack). White dwarfs are shown in black, A stars in light blue, F stars in green, G stars in yellow, K stars in orange, M dwarfs in red, L dwarfs in firebrick, T dwarfs in magenta, and Y dwarfs in purple. The only bins believed to suffer from significant incompleteness are those of the T and Y dwarfs; it is likely that a small number of solivagant T dwarfs and a larger number of Y dwarfs have yet to be identified along with T and Y companions to higher-mass objects already known within the 8 pc volume.

(A color version of this figure is available in the online journal.)

the absolute magnitudes computed for similarly typed objects whose distances have been measured. Apparent magnitudes for these cold brown dwarfs are most easily measured from the ground in the *J* and *H* bands and from *WISE* at W2. Unfortunately, due to big differences in the *J*-band filters chosen for the two most popular filter systems (2MASS and the MKO-NIR system), fluxes can vary by several tenths of a magnitude for the same object (Stephens & Leggett 2004) because the spectral energy distributions of cold brown dwarfs are so complex at these same wavelengths. Fortunately, the *H*-band filters are very similar and as a result, *H*-band measurements show little variation between systems (Stephens & Leggett 2004). We will therefore use *H* and W2 photometry to estimate distances to objects lacking parallax information.

Table 6 presents a compilation of dwarfs that have measured trigonometric parallaxes, photometry at *H* and/or W2, and types later than T4. Trigonometric parallaxes for the Y dwarfs are taken from Marsh et al. (2012) and Beichman et al. (2012), although three objects from Marsh et al.—WISE 0359−5401, WISE 1541−2250, and WISE 2056+1459—are omitted here because their parallax values are roughly the size of the errors themselves. Unlike the other objects in these papers, these three objects lack measurements near the maximum parallax factor (or in the case of the *WISE* data points, have large astrometric uncertainties) and do not yet properly constrain the size of the parallactic motion.

Data in Table 6 are used to plot the absolute magnitude versus spectral type diagrams shown in Figures 12 and 13. Figure 12 shows a sharp drop in the absolute *H* magnitude near the T/Y transition. The absolute *H*-band magnitude for our latest object—the ⩾Y2 dwarf WISE 1828+2650—appears to indicate a stagnation or perhaps even a brightening in the *H* flux for later Y dwarfs relative to ones at Y0 and Y1. Figure 13 shows an even more surprising result: the absolute W2 magnitude plummets at Y0 and Y1 only to rebound appreciably for WISE 1828+2650 at ⩾Y2.

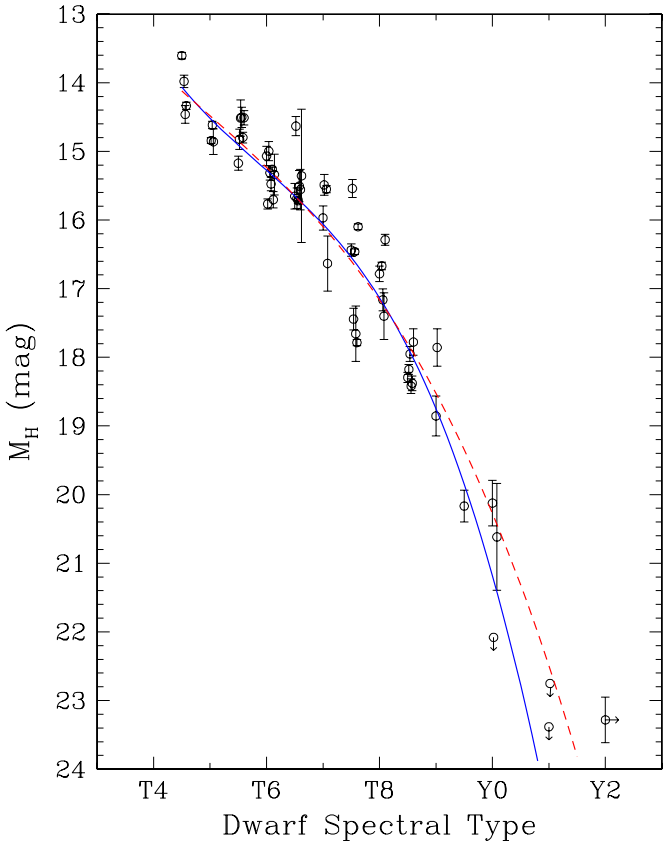

Figure 12. Plot of the absolute *H*-band magnitude of dwarfs with spectral types >T4 and measured trigonometric parallaxes, from Table 6. Third-order fits to the data are shown by the dashed red curve (which includes the point for WISE 1828+2650 at lower right) and the solid blue curve (which excludes WISE 1828+2650). See Section 4.3 for details.

(A color version of this figure is available in the online journal.)

Table 6
Late-T and Y Dwarfs with Measured Trigonometric Parallaxes

Discovery Name	Disc. Ref.	Spec. Type	Type Ref.	W1 (mag)	W2 (mag)	H (mag)	H Ref.	$\pi_{\rm trig}$ (arcsec)	$\pi_{\rm trig}$ Reference
(1)	(2)	(3)	(4)	(5)	(6)	(7)	(8)	(9)	(10)
SDSS J000013.54+255418.6	1	T4.5	52	...	...	14.73 ± 0.07	38	0.0708 ± 0.0019	39
ULAS J003402.77−005206.7	2	T8.5	32	17.47 ± 0.29	14.50 ± 0.08	18.49 ± 0.04	2	0.0780 ± 0.0036	40
HD 3651B (J0039+2115)	3	T7.5	3	...	...	16.68 ± 0.04	3	0.0904 ± 0.0003	41
CFBDS J005910.90−011401.3	4	T8.5	32	17.07 ± 0.15	13.68 ± 0.04	18.27 ± 0.05	4	0.1011 ± 0.0025	39
SDSS J020742.48+000056.2	5	T4.5	52	16.39 ± 0.08	15.07 ± 0.08	...	...	0.0293 ± 0.0040	40
2MASSI J0243137−245329	6	T6	52	14.67 ± 0.03	12.92 ± 0.03	15.14 ± 0.11	38	0.0936 ± 0.0036	42
WISEPA J025409.45+022359.1	7, 8	T8	7	15.76 ± 0.05	12.74 ± 0.03	16.30 ± 0.01	51	0.166 ± 0.026	43
WISE J035000.32−565830.2	51	Y1	51	>18.90	14.73 ± 0.06	>21.5	51	0.238 ± 0.038	43
WISEP J041022.71+150248.5	32	Y0	32	>18.33	14.18 ± 0.06	19.05 ± 0.09	51	0.164 ± 0.024	43
2MASSI J0415195−093506	6	T8	52	15.11 ± 0.04	12.26 ± 0.03	15.54 ± 0.11	38	0.1773 ± 0.0022	39
WISE J053516.80−750024.9	51	⩾Y1:	51	>18.92	15.06 ± 0.07	>21.6	51	0.170 ± 0.044	43
2MASS J05591914−1404488	9	T4.5	52	13.39 ± 0.03	11.90 ± 0.02	13.68 ± 0.04	38	0.0966 ± 0.0010	39
Gl 229B (J0610−2152)	10	T7p	52	...	...	14.35 ± 0.05	12	0.1738 ± 0.0010	41
UGPS J072227.51−054031.2	11	T9	32	15.19 ± 0.05	12.21 ± 0.03	16.90 ± 0.02	11	0.246 ±0.033	11
2MASSI J0727182+171001	6	T7	52	15.24 ± 0.05	12.96 ± 0.03	15.76 ± 0.17	38	0.1101 ± 0.0023	42
HIP 38939B (J0758−2539)	13	T4.5	13	15.92 ± 0.08	13.96 ± 0.05	15.80 ± 0.12	38	0.0540 ± 0.0011	41
DENIS J081730.0−615520	14	T6	14	12.96 ± 0.02	11.24 ± 0.02	13.53 ± 0.03	38	0.203 ±0.013	14
ULAS J082707.67−020408.2	15	T5.5	15	>17.77	15.26 ± 0.12	17.44 ± 0.05	15	0.0260 ± 0.0031	40
ULAS J090116.23−030635.0	15	T7.5	15	17.77 ± 0.31	14.60 ± 0.07	18.46 ± 0.13	15	0.0626 ± 0.0026	40
2MASSI J0937347+293142	6	T6p	52	14.07 ± 0.03	11.66 ± 0.02	14.70 ± 0.07	38	0.1634 ± 0.0018	44
2MASS J09393548−2448279	16	T8	52	15.03 ± 0.04	11.64 ± 0.02	15.80 ± 0.15	38	0.1873 ± 0.0046	45
ULAS J094806.06+064805.0	15	T7	15	...	...	19.46 ± 0.22	15	0.0272 ± 0.0042	40
ULAS J101821.78+072547.1	15	T5	15	17.78 ± 0.28	16.21 ± 0.27	17.87 ± 0.07	15	0.0250 ± 0.0020	40
SDSS J102109.69−030420.1 B	17	T5	39	...	...	16.59 ± 0.04	39	0.0307 ± 0.0013	39
2MASSI J1047538+212423	18	T6.5	52	15.43 ± 0.04	12.97 ± 0.03	15.80 ± 0.12	38	0.0947 ± 0.0038	42
SDSSp J111010.01+011613.1	5	T5.5	52	15.53 ± 0.05	13.92 ± 0.05	15.92 ± 0.14	38	0.0521 ± 0.0012	39
ξ UMa C (J1118+3125)	19	T8.5	19	16.16 ± 0.07	13.31 ± 0.03	18.15 ± 0.06	19	0.1132 ± 0.0046	57
ULAS J115038.79+094942.9	22	T6.5p	22	...	...	19.23 ± 0.06	22	0.0168 ± 0.0075	40
2MASS 12095613−1004008 B	17	T6.5:	39	...	...	18.12 ± 0.28	39	0.0307 ± 0.0013	39
2MASSI J1217110−031113	18	T7.5	52	15.29 ± 0.05	13.20 ± 0.04	15.75 ± 0.12	38	0.0908 ± 0.0022	47
2MASS J12255432−2739466 A	18	T5.5	39	...	...	15.42 ± 0.03	39	0.0751 ± 0.0025	47
2MASS J12255432−2739466 B	20	T8	39	...	...	16.91 ± 0.03	39	0.0751 ± 0.0025	47
2MASS J12373919+6526148	18	T6.5	52	15.48 ± 0.05	12.95 ± 0.03	15.74 ± 0.15	38	0.0961 ± 0.0048	42
Ross 458C (J1300+1221)	21	T8	32	16.01 ± 0.07	13.74 ± 0.04	17.01 ± 0.04	21	0.0855 ± 0.0015	41
ULAS J131508.42+082627.4	22	T7.5	22	...	...	19.50 ± 0.10	22	0.0428 ± 0.0077	40
ULAS J133553.45+113005.2	23	T8.5	32	16.88 ± 0.13	13.87 ± 0.04	18.25 ± 0.01	23	0.0967 ± 0.0032	40
SDSSp J134646.45−003150.4	24	T6.5	52	15.49 ± 0.05	13.57 ± 0.03	15.46 ± 0.12	38	0.0683 ± 0.0023	47
WISEPC J140518.40+553421.5	32	Y0	32	>18.82	14.10 ± 0.04	>20.5	51	0.207 ± 0.039	43
ULAS J141623.94+134836.3	25	T7.5	53	16.12 ± 0.20	12.79 ± 0.04	17.58 ± 0.03	25	0.1099 ± 0.0018	39
Gl 570D (J1457−2122)	26	T7.5	52	14.82 ± 0.03	12.11 ± 0.02	15.27 ± 0.09	38	0.1712 ± 0.0009	41
CFBDSIR J145829+101343 A	55	T8.5[d]	51	...	...	20.12 ± 0.10	56	0.0340 ± 0.0026	39
CFBDSIR J145829+101343 B	56	T9.5[d]	51	...	...	22.51 ± 0.16	56	0.0340 ± 0.0026	39
2MASS J15031961+2525196	27	T5	52	13.51 ± 0.02	11.72 ± 0.02	13.86 ± 0.03	38	0.1572 ± 0.0022	39
SDSS J150411.63+102718.4	28	T7	28	16.39 ± 0.07	14.06 ± 0.04	...	...	0.0461 ± 0.0015	39
HIP 73786 B (1504+0538)	54	T6:p	54	16.48 ± 0.08	14.23 ± 0.04	17.05 ± 0.04	54	0.0538 ± 0.0028	41
WISEPC J150649.97+702736.0	7	T6	7	13.39 ± 0.02	11.27 ± 0.02	13.91 ± 0.04	7	0.193 ± 0.026	43
SDSS J153417.05+161546.1 B	29	T5.5	39	...	...	17.53 ± 0.04	39	0.0249 ± 0.0011	39
2MASSI J1534498−295227 A	6	T4.5	39	...	...	15.36 ± 0.03	39	0.0624 ± 0.0013[c]	39
2MASSI J1534498−295227 B	20	T5	39	...	...	15.64 ± 0.03	39	0.0624 ± 0.0013[c]	39
2MASSI J1546291−332511	6	T5.5	52	15.30 ± 0.05	13.45 ± 0.04	15.45 ± 0.09	38	0.0880 ± 0.0019	47
2MASSI J1553022+153236 A	6	T6.5	39	...	...	16.34 ± 0.03	39	0.0751 ± 0.0009	39
2MASSI J1553022+153236 B	17	T7.5	39	...	...	16.72 ± 0.03	39	0.0751 ± 0.0009	39
SDSSp J162414.37+002915.6	30	T6	52	15.12 ± 0.04	13.09 ± 0.03	15.52 ± 0.10	38	0.0909 ± 0.0012	47
SDSS J162838.77+230821.1	28	T7	28	16.43 ± 0.09	13.96 ± 0.04	16.11 ± 0.15	38	0.0751 ± 0.0009	39
WISE J173835.53+273259.0	32	Y0	32	>18.41	14.55 ± 0.06	20.39 ± 0.33	51	0.111 ± 0.036	43
WISEPA J174124.26+255319.5	31, 7, 8	T9	7	15.38 ± 0.05	12.33 ± 0.03	16.63 ± 0.03	7	0.176 ± 0.022	43
SDSS J175805.46+463311.9[b]	1	T6.5	52	15.68 ± 0.04	13.82 ± 0.03	16.25 ± 0.22	38	0.0710 ± 0.0019	41
WISEPA J182831.08+265037.8	32	⩾Y2	51	>18.47	14.39 ± 0.06	22.85 ± 0.24	7, 32	0.122 ± 0.013	50
SCR 1845−6357 B	33	T6	34	...	...	13.19 ± 0.03	34	0.2595 ± 0.0011	48
Wolf 940 B (J2146−0010)	35	T8.5	32	16.72 ± 0.12	14.24 ± 0.05	18.77 ± 0.03	35	0.0835 ± 0.0039	49
eps Indi Bb (J2204−5646)	36, 37	T6	52	...	...	13.27 ± 0.10[a]	37	0.2761 ± 0.0003	41
2MASSI J2356547−155310	6	T5.5	52	15.58 ± 0.06	13.71 ± 0.04	15.63 ± 0.10	38	0.0690 ± 0.0034	42

Table 6
(Continued)

Notes. References: (1) Knapp et al. 2004; (2) Warren et al. 2007; (3) Luhman et al. 2007; (4) Delorme et al. 2008; (5) Geballe et al. 2002; (6) Burgasser et al. 2002; (7) Kirkpatrick et al. 2011; (8) Scholz et al. 2011; (9) Burgasser et al. 2000b; (10) Nakajima et al. 1995; (11) Lucas et al. 2010; (12) Leggett et al. 1999; (13) Deacon et al. 2011; (14) Artigau et al. 2010; (15) Lodieu et al. 2007; (16) Tinney et al. 2005; (17) Burgasser et al. 2006a; (18) Burgasser et al. 1999; (19) Wright et al. 2012; (20) Burgasser et al. 2003b; (21) Goldman et al. 2010; (22) Pinfield et al. 2008; (23) Burningham et al. 2008; (24) Tsvetanov et al. 2000; (25) Scholz 2010; (26) Burgasser et al. 2000a; (27) Burgasser et al. 2003a; (28) Chiu et al. 2006; (29) Liu et al. 2006; (30) Strauss et al. 1999; (31) Gelino et al. 2011; (32) Cushing et al. 2011; (33) Biller et al. 2006; (34) Kasper et al. 2007; (35) Burningham et al. 2009; (36) Volk et al. 2003; (37) McCaughrean et al. 2004; (38) 2MASS, (39) Dupuy & Liu 2012; (40) Marocco et al. 2010; (41) van Leeuwen 2007; (42) Vrba et al. 2004; (43) Marsh et al. 2012; (44) Schilbach et al. 2009; (45) Burgasser et al. 2008; (46) Perryman et al. 1997; (47) Tinney et al. 2003; (48) Henry et al. 2006; (49) van Altena et al. 1995; (50) Beichman et al. 2012; (51) this paper, (52) Burgasser et al. 2006a; (53) Burgasser et al. 2010; (54) Murray et al. 2011; (55) Delorme et al. 2010; (56) Liu et al. 2011; (57) Karataş et al. 2004.

[a] An *H*-band magnitude error of 0.1 mag is assigned here since its value is not specified in McCaughrean et al. (2004).

[b] The association of SDSS J175805.46+463311.9 to G 204-39—the latter of which has a measured parallax—was made by Faherty et al. (2010).

[c] See discussion in Dupuy & Liu (2012) regarding the discrepancy between the parallax value quoted here and that determined by Tinney et al. (2003).

[d] Cushing et al. (2011) assign this binary a composite type of T9 on the revised late-T dwarf classification scheme. Given the Dupuy & Liu (2012) measurements of the parallax and the Liu et al. (2011) *H*-band measurements of the individual components, we infer spectral types of T8.5 and T9.5 based on absolute *H* magnitudes of 17.8 and 20.2 mag.

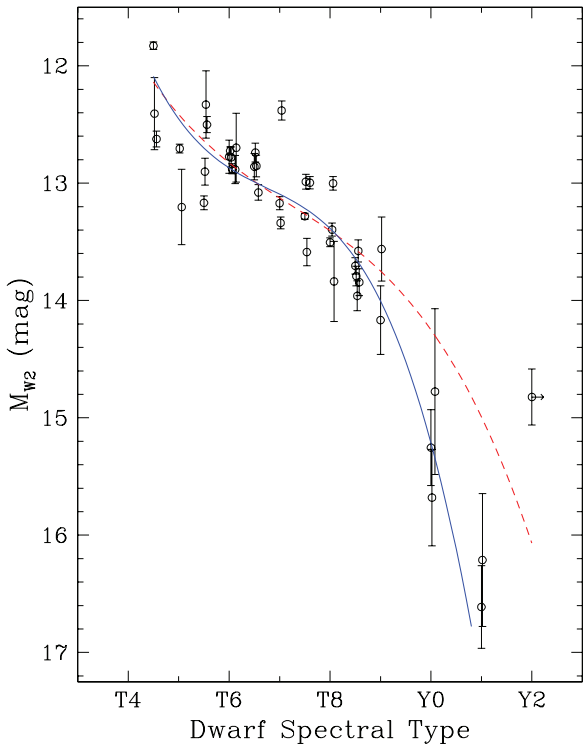

Figure 13. Plot of the absolute W2-band magnitude of dwarfs with spectral types >T4 and measured trigonometric parallaxes, from Table 6. Third-order fits to the data are shown by the dashed red curve (which includes the point for WISE 1828+2650 near the right edge) and the solid blue curve (which excludes WISE 1828+2650). See Section 4.3 for details.

(A color version of this figure is available in the online journal.)

We suggest three possible scenarios to explain this observed behavior. (1) The parallax value for WISE 1828+2650 is the only one of the Y dwarf parallax measures robust enough to trust. In this case, the plummeting absolute magnitudes and Y0 and Y1 can be discounted until longer timeline astrometric monitoring of these objects has produced results with smaller measurement errors. (2) Despite their large errors, the Y0 and Y1 points indicate a pronounced dimming of the *H* and, more notably, W2 fluxes; the discrepant point for WISE 1828+2650 merely demonstrates that it (and not the other Y dwarfs) is the oddball, its weirdness being attributable to an unknown physical cause or misclassification due to a peculiar spectral morphology.[21] (3) All trigonometric parallaxes are credible, and the observed behavior represents a real brightening of the fluxes for later Y dwarfs relative to ones at Y0–Y1.

It is clear that continued astrometric monitoring programs targeting Y dwarfs at improved precisions are critical in determining which of these scenarios is the correct one. For now, we perform weighted least-squares fits to the absolute magnitude versus spectral type diagrams with the caveat that they represent our best determinations at this time and will certainly have to be revised as future data become available. Third-order polynomials were fit to data in these diagrams both with and without WISE 1828+2650; for fits that included WISE 1828+2650, a spectral type of exactly Y2 was assumed for the object. For Figure 12, fits included the two upper limit M_H values by assuming that the limits measured in *H* band were actual detections with errors equal to the error in the *H*-band measurement of WISE 1828 (0.24 mag). Although this is an ad hoc assumption, we feel that it is better to fit (conservatively) to available data in that region rather than to drop the information entirely.

The resulting least-square fits to the data are given by the following equations:

$$M_H = 20.272231 + 1.9695993(\text{type}) + 0.23810003(\text{type})^2 + 0.015161356(\text{type})^3,$$

which includes WISE 1828+2650 (red dashed curve in Figure 12) or

$$M_H = 21.179419 + 2.9205146(\text{type}) + 0.53564210(\text{type})^2 + 0.043616246(\text{type})^3,$$

which excludes it (blue solid curve in Figure 12). Also,

$$M_{W2} = 14.249389 + 0.60675032(\text{type}) + 0.12183371(\text{type})^2 + 0.014785180(\text{type})^3,$$

which includes WISE 1828+2650 (red dashed curve in Figure 13) or

$$M_{W2} = 15.213242 + 1.5891486(\text{type}) + 0.42455282(\text{type})^2 + 0.043434368(\text{type})^3,$$

[21] Note that invoking unresolved binarity for this object would account for only 0.75 mag of brightening, far below what is required to account for the W2 discrepancy.

which excludes it (blue solid curve in Figure 13). In each equation, the spectral type is given by type = 0 for Y0, 1 for Y1, −1 for T9, −2 for T8, etc. These relations are considered valid only over the range from T7 to Y1.

For subsequent analyses we have used only the fits that exclude WISE 1828+2650 because these relations are needed solely to estimate distances to objects of earlier type than WISE 1828+2650 itself. In this case, we are explicitly assuming that scenario (1) above is incorrect and that either (2) or (3) is a more credible hypothesis. If we instead discover later that this assumption is incorrect, it will have the effect of increasing the distances to the Y0 and Y1 dwarfs, which will result in a reduction of the computed space density for objects at those types.

Using these fits, we have estimated distances for each of the objects identified in our all-sky census of brown dwarfs with types ⩾T6 (Table 7) using their measured (or assumed) spectral types and measured H and/or W2 magnitudes. These distance estimates are shown in Table 8.

We have checked the distance distribution of objects in each spectral type bin by performing the $V/V_{\rm max}$ test (Schmidt 1968), which checks the uniformity of a distribution of objects in space. The quantity V is the volume of space interior to object i at distance d_i, and $V_{\rm max}$ is the full volume of space contained within the distance limit, $d_{\rm max}$, of the sample. For a uniform sample, the average value, $\langle V/V_{\rm max}\rangle$, should be 0.5 because half of the sample should lie in the nearer half of the volume and the rest should lie in the farther half. If this number is not near 0.5, then the sample is either non-homogeneous or incomplete. $V/V_{\rm max}$ values are given in Column 8 of Table 8 for each object falling within $d_{\rm max}$. The average value of $V/V_{\rm max}$ in each integral spectral type bin is listed in Table 9.

For our sample we find that the T dwarf bins have $\langle V/V_{\rm max}\rangle$ values less than 0.5. This indicates that objects near the $d_{\rm max}$ limit have yet to be identified, meaning that the sample is still slightly incomplete at larger distances. For Y dwarfs (except for the Y2 bin with only a single object), the $\langle V/V_{\rm max}\rangle$ values are even further below 0.5. This indicates larger incompleteness at the furthest reaches of the volume, which is not surprising given that follow-up has so far concentrated on only the closest, brightest examples. Concentrated work on the discovery of additional Y dwarfs is still badly needed.

Table 9 lists the final number of objects in each bin along with the measured space density for each. For the mid- to late-T dwarfs, whose mapping from spectral type to absolute magnitude is reasonably well established, our two biggest sources of error are sample incompleteness and the effects of binarity (Kirkpatrick et al. 2011). For the former, we can use the $\langle V/V_{\rm max}\rangle$ values above to estimate the extent of the incompleteness per bin. If we assume that the incompleteness lies solely in the third of the volume furthest from the Sun, then we can estimate the number of objects needed to give a value of $\langle V/V_{\rm max}\rangle = 0.5$. If we arbitrarily place all such missing objects at the midpoint of that incomplete shell, each object would have $\langle V/V_{\rm max}\rangle = 0.84$, which corresponds to a distance of 18.9, 14.2, and 9.4 pc, respectively, for $d_{\rm max}$ values of 20, 15, and 10 pc. Under these assumptions, we find that a total of 10, 12, 20, and 4 additional objects are needed to fill out the T6–6.5, T7–7.5, T8–8.5, and T9–9.5 bins, respectively.

This complete sample, however, will still suffer from the effects of unresolved binarity, the brighter magnitude of the composite system leading to a nearer distance estimate than is actually the case. This will cause a few of the nearest objects

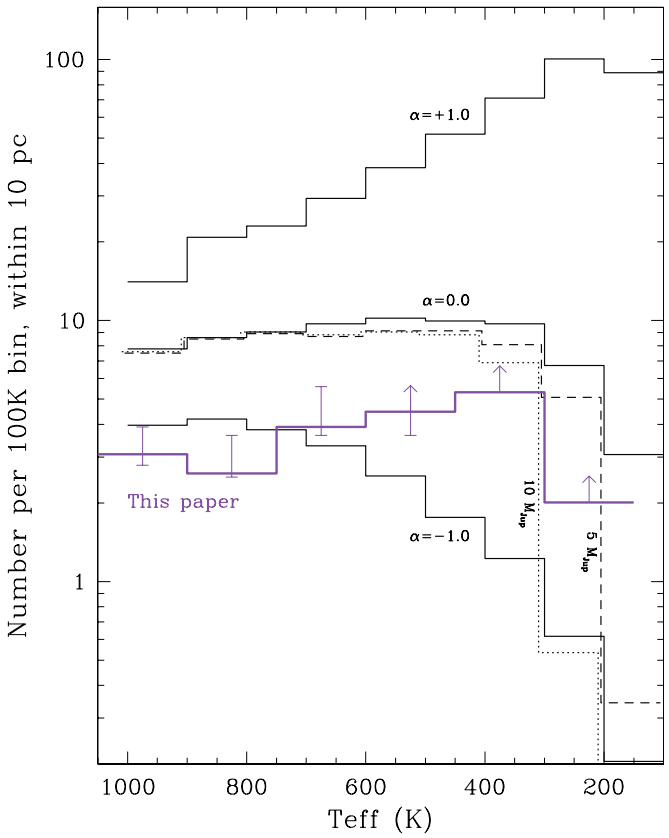

Figure 14. Predicted number of brown dwarfs within 10 pc for three different power-law mass functions ($dN/dM \propto M^{-\alpha}$) with $\alpha = -1$, 0, and +1 (solid black) having a minimum formation mass of 1 $M_{\rm Jup}$. Also shown for the $\alpha = 0$ model is the predicted number of brown dwarfs if a minimum formation mass of 5 $M_{\rm Jup}$ (dashed black) or 10 $M_{\rm Jup}$ (dotted black) is assumed. These simulations are from Burgasser et al. (2004, 2007). Space densities using our full accounting of objects in the immediate solar neighborhood (Tables 8 and 9) are shown by the heavy purple line.

(A color version of this figure is available in the online journal.)

to be pushed to larger distances that still fall within $d_{\rm max}$, but the bigger effect will be in eliminating objects entirely from the sample that were just within the $d_{\rm max}$ limit before correction. Burgasser et al. (2007) summarize the results of high-resolution imaging and radial velocity surveys for very low mass objects in the field along with high-resolution imaging surveys of very low mass objects in young clusters and conclude that as many as 30% (or more) of these objects could be binary. As a worst-case scenario, we assume that 30% of our systems are eliminated as having distances beyond $d_{\rm max}$ once binarity is taken into account. We then find that the sample numbers previously corrected for incompleteness should now be reduced by 14, 13, 17, and 8 objects in the T6–6.5, T7–7.5, T8–8.5, and T9–9.5 bins, respectively.

For the Y dwarf bins, the uncertain mapping from spectral type to absolute magnitude along with known incompleteness of the sample are likely the biggest contributors to the uncertainty in the space density estimates. We consider the sample incompleteness to be the dominant effect, and hence we believe that our measured space density estimates for the Y dwarfs should be considered lower limits.

Results are plotted in Figure 14. Also plotted are the results of luminosity function simulations by Burgasser (2007; based on earlier work by Burgasser et al. 2004) that show the

Table 7
Photometry for Objects in the All-sky Late-T and Y Dwarf Census

Discovery Name	Disc. Ref.	*WISE* Designation[a]	Spec. Type	Type Ref.	*H* (mag)	*H* ref.	W2 (mag)	W1–W2 (mag)	*H*–W2 (mag)
(1)	(2)	(3)	(4)	(5)	(6)	(7)	(8)	(9)	(10)
T6–T6.5 dwarfs									
WISEPC J000849.76−173922.6	1	WISE J000849.75−173922.9	T6	1	17.77 ± 0.13	1	14.56 ± 0.07	1.86 ± 0.12	3.22 ± 0.15
2MASS J00345157+0523050	4	WISE J003452.02+052307.0	T6.5	5	15.44 ± 0.08	57	12.52 ± 0.03	2.54 ± 0.05	2.92 ± 0.09
WISE J003830.54+840517.7	2	WISE J003830.54+840517.7	T6	2	...	-	15.34 ± 0.09	2.19 ± 0.20	...
WISE J013525.64+171503.4	2	WISE J013525.64+171503.4	T6	2	...	-	14.74 ± 0.07	2.45 ± 0.17	...
WISEPA J022105.94+384202.9	1	WISE J022105.97+384203.2	T6.5	1	17.45 ± 0.15	1	14.70 ± 0.08	2.18 ± 0.17	2.76 ± 0.17
CFBDS J022638−072831	56	Not detected	T6.5	56	18.65 ± 0.02	56	...	...	...
2MASSI J0243137−245329	6	WISE J024313.47−245331.9	T6	5	15.14 ± 0.11	57	12.92 ± 0.03	1.75 ± 0.04	2.21 ± 0.11
CFBDS J025401−182529	46	WISE J025401.70−182528. 8	T6.5	46	18.49 ± 0.05	56	15.72 ± 0.12	>2.64	2.77 ± 0.13
UGCS J030013.86+490142.5	7	WISE J030013.76+490141.7	T6.5	7	18.37 ± 0.16	58	15.91 ± 0.20	>2.28	2.46 ± 0.26
CFBDS J030130−104504	46	WISE J030130.46−104504.1	T6	46	...	-	15.32 ± 0.11	1.72 ± 0.16	...
CFBDS J030225−144125	56	Not detected	T6	56	17.97 ± 0.04	56	...	...	...
WISEPA J030533.54+395434.4	1	WISE J030533.51+395434.6	T6	1	17.08 ± 0.12	1	14.69 ± 0.07	2.69 ± 0.25	2.39 ± 0.14
WISEPA J030724.57+290447.6	1	WISE J030724.59+290447.4	T6.5	1	17.70 ± 0.14	1	14.99 ± 0.11	2.23 ± 0.24	2.71 ± 0.18
CFHT J0344+3206[b]	55	Not detected	(T6:)	55	21.65 ± 0.08	55	...	...	...
WISEPA J041054.48+141131.6	1	WISE J041054.48+141131.1	T6	1	17.26 ± 0.12	1	15.08 ± 0.10	1.95 ± 0.19	2.19 ± 0.16
WISEPA J051317.28+060814.7	1	WISE J051317.27+060814.7	T6.5	1	16.13 ± 0.08	1	13.86 ± 0.05	1.97 ± 0.08	2.28 ± 0.09
WISEPA J052536.33+673952.3	1	WISE J052536.35+673952.6	T6p	1	17.87 ± 0.05	1	15.04 ± 0.09	>2.94	2.83 ± 0.11
SOri70 (J0538−0236)	8	Not detected	T6:	5	20.42 ± 0.11	8	...	...	...
WISEPA J054231.26−162829.1	1	WISE J054231.27−162829.1	T6.5	1	16.57 ± 0.10	1	13.98 ± 0.05	2.41 ± 0.10	2.59 ± 0.11
WISEPA J061213.93−303612.7	1	WISE J061213.85−303612. 5	T6	1	17.06 ± 0.11	1	14.03 ± 0.04	2.32 ± 0.08	3.03 ± 0.12
WISEPA J061407.49+391236.4	1	WISE J061407.49+391235.9	T6	1	16.36 ± 0.25	1	13.65 ± 0.04	2.83 ± 0.12	2.71 ± 0.25
WISEPA J062542.21+564625.5	1	WISE J062542.22+564625.4	T6	1	16.90 ± 0.10	1	14.38 ± 0.06	1.95 ± 0.10	2.52 ± 0.12
WISEPA J062720.07−111428.8	1	WISE J062720.07−111428.0	T6	1	15.44 ± 0.08	1	13.26 ± 0.03	1.74 ± 0.05	2.18 ± 0.08
WISE J073347.94+754439.2	2	WISE J073347.94+754439.2	T6	2	...	-	14.77 ± 0.07	2.39 ± 0.16	...
DENIS J081730.0−615520	9	WISE J081729.74−615504.0	T6	9	13.53 ± 0.03	57	11.24 ± 0.02	1.72 ± 0.03	2.29 ± 0.04
ULAS J081948.09+073323.3	10	Not detected	T6p	10	18.36 ± 0.03	10	...	...	...
ULAS J085342.94+000651.8	10	WISE J085342.83+000650.8	T6p	10	19.21 ± 0.06	58	15.79 ± 0.19	2.23 ± 0.42	3.42 ± 0.20
ULAS J085715.96+091325.3	10	not detected	T6	10	18.89 ± 0.10	10	...	...	...
WISEPC J092906.77+040957.9	1	WISE J092906.77+040957.9	T6.5	1	17.37 ± 0.07	1	14.23 ± 0.06	2.40 ± 0.13	3.14 ± 0.09
2MASSI J0937347+293142	6	WISE J093735.61+293127.7	T6p	5	14.70 ± 0.07	57	11.66 ± 0.02	2.42 ± 0.04	3.05 ± 0.07
WISEPC J095259.29+195507.3	1	WISE J095259.29+195508.1	T6	1	17.22 ± 0.10	1	14.34 ± 0.06	2.53 ± 0.17	2.88 ± 0.12
WISEPA J101905.63+652954.2	1	WISE J101905.62+652954.2	T6	1	16.52 ± 0.12	1	14.03 ± 0.04	2.39 ± 0.08	2.49 ± 0.12
ULAS J103434.52−001553.0	10	Not detected	T6.5p	10	19.00 ± 0.03	10	...	...	...
CFBDS J104209+580856	46	WISE J104209.85+580856.0	T6.5	46	18.21 ± 0.05	56	15.30 ± 0.10	1.95 ± 0.18	2.91 ± 0.11
2MASSI J1047538+212423	11	WISE J104752.37+212417.5	T6.5	5	15.80 ± 0.12	57	12.97 ± 0.03	2.46 ± 0.05	2.83 ± 0.12
WISEPC J112254.73+255021.5	1	WISE J112254.72+255022.2	T6	1	16.64 ± 0.11	1	13.97 ± 0.05	2.22 ± 0.10	2.67 ± 0.12
ULAS J115038.79+094942.9	12	Not detected	T6.5p	12	19.23 ± 0.06	12	...	...	...
ULAS J115338.74−014724.1	10	Not detected	T6	10	17.97 ± 0.02	10	...	...	...
NTTDF1205−0744	13	Not detected	T6:	5	...		...	...	...
ULAS J120744.65+133902.7	10	WISE J120744.63+133903.8	T6	10	18.52 ± 0.05	58	15.79 ± 0.18	>2.08	2.73 ± 0.18
2MASS J12095613−1004008B	52	Not detected	T6.5:	65	18.08 ± 0.26	52	...	...	...
SDSS J121440.95+631643.4B	47	Blended w/component A	(T6)	47	...	-	...	...	...
WISE J122558.86−101345.0	2	WISE J122558.86−101345.0	T6	2	16.46 ± 0.15	2	13.99 ± 0.05	2.35 ± 0.10	...
2MASS J12373919+6526148	11	WISE J123737.38+652608.4	T6.5	5	15.74 ± 0.15	57	12.95 ± 0.03	2.54 ± 0.05	2.79 ± 0.15
WISEPC J132004.16+603426.2	1	WISE J132004.16+603426.3	T6.5	1	16.56 ± 0.13	1	14.41 ± 0.05	2.52 ± 0.12	2.15 ± 0.14
ULAS J132605.18+120009.9	10	WISE J132605.25+120010.2	T6p	10	17.93 ± 0.09	58	15.38 ± 0.10	1.59 ± 0.16	2.55 ± 0.14
SDSSp J134646.45−003150.4	14	WISE J134646.07−003151.4	T6.5	5	15.46 ± 0.12	57	13.57 ± 0.03	1.92 ± 0.06	1.89 ± 0.12
ULAS J144555.24+125735.1	10	Not detected	T6.5	10	19.10 ± 0.05	10	...	...	...
ULAS J150457.66+053800.8[c]	51	WISE J150457.57+053759.8	T6:p	51	17.05 ± 0.03	51	14.23 ± 0.04	2.25 ± 0.09	2.32 ± 0.05
WISEPC J150649.97+702736.0	1	WISE J150649.98+702736.1	T6	1	13.91 ± 0.04	1	11.27 ± 0.02	2.12 ± 0.03	2.64 ± 0.04
ULAS J152526.25+095814.3	10	WISE J152526.19+095814.9	T6.5	10	19.17 ± 0.03	58	16.44 ± 0.22	>2.50	2.73 ± 0.22
ULAS J152912.23+092228.5	10	Not detected	T6	10	19.13 ± 0.05	10	...	...	...
2MASSI J1553022+153236A	6	WISE J155301.95+153238.8	T6.5	65	16.34 ± 0.03	65	13.02 ± 0.03[g]	2.28 ± 0.06[g]	...
WISEPA J161215.94−342027.1	1	WISE J161215.93−342028.5	T6.5	1	16.96 ± 0.03	45	13.96 ± 0.05	>4.23	3.00 ± 0.06
2MASS J16150413+1340079	15	WISE J161504.36+134004.2	T6	15	16.49 ± 0.25	57	14.19 ± 0.05	2.08 ± 0.10	2.30 ± 0.26
WISEPA J162208.94−095934.6	1	WISE J162208.94−095934.4	T6	1	16.05 ± 0.05	1	14.17 ± 0.06	2.34 ± 0.15	1.88 ± 0.08
SDSSp J162414.37+002915.6	16	WISE J162414.09+002915.6	T6	5	15.52 ± 0.10	57	13.09 ± 0.03	2.04 ± 0.05	2.44 ± 0.11
WISEPA J162725.64+325525.5	1,3	WISE J162725.65+325524.6	T6	1	16.40 ± 0.05	1	13.60 ± 0.04	2.65 ± 0.08	2.80 ± 0.06
WISE J172134.46+111739.4	2	WISE J172134.46+111739.4	T6	2	...	-	14.28 ± 0.06	1.62 ± 0.09	...
WISEPA J172844.93+571643.6	1	WISE J172844.93+571642.7	T6	1	17.88 ± 0.07	1	15.01 ± 0.05	2.94 ± 0.19	2.87 ± 0.09
WISE J174640.78−033818.0	2	WISE J174640.78−033818.0	T6	2	17.45 ± 0.04	2	14.79 ± 0.10	>3.23	2.66 ± 0.11
SDSS J175805.46+463311.9[d]	17	WISE J175805.47+463316.8	T6.5	5	16.25 ± 0.22	57	13.82 ± 0.03	1.86 ± 0.05	2.43 ± 0.22
SCR J1845−6357B	18	Blended w/SCR J1845−6357A	T6	19	...	-	...	...	...
WISEPA J190624.75+450808.2	1	WISE J190624.74+450807.1	T6	1	16.32 ± 0.09	1	13.82 ± 0.04	2.27 ± 0.07	2.51 ± 0.10

Table 7
(Continued)

Discovery Name	Disc. Ref.	*WISE* Designation[a]	Spec. Type	Type Ref.	*H* (mag)	*H* ref.	W2 (mag)	W1–W2 (mag)	*H*–W2 (mag)
(1)	(2)	(3)	(4)	(5)	(6)	(7)	(8)	(9)	(10)
WISE J192841.35+235604.9	2	WISE J192841.35+235604.9	T6	2	...	-	12.11 ± 0.03	1.83 ± 0.04	...
2MASS J21543318+5942187	15	WISE J215432.95+594213.8	T6	15	15.77 ± 0.17	57	13.51 ± 0.03	2.14 ± 0.08	2.26 ± 0.17
ϵ Ind Bb (J2204−5646)	20	Blended w/ϵ Ind Ba	T6	5	...	-	...	...	...
UDXS J221903.10+002418.2	54	Not detected	(T6:)	54	...	-	...	...	...
2MASS J22282889−4310262	21	WISE J222829.00−431029.5	T6	5	15.36 ± 0.12	57	13.33 ± 0.04	1.94 ± 0.06	2.04 ± 0.12
WISE J223720.39+722833.8	2	WISE J223720.39+722833.8	T6	2	...	-	13.61 ± 0.04	2.06 ± 0.07	...
WISE J230133.32+021635.1	2	WISE J230133.32+021635.1	T6.5	2	...	-	14.34 ± 0.06	1.96 ± 0.10	...
ULAS J230601.02+130225.0	10	WISE J230601.02+130225.3	T6.5	10	18.00 ± 0.02	58	15.07 ± 0.10	3.33 ± 0.51	2.94 ± 0.10
ULAS J231557.61+132256.2	10	WISE J231557.66+132255.5	T6.5	10	18.16 ± 0.05	58	15.47 ± 0.13	2.36 ± 0.34	2.69 ± 0.14
CFBDS J232304−015232	56	WISE J232304.41−015233.8	T6	56	17.46 ± 0.04	56	15.07 ± 0.11	1.61 ± 0.17	2.39 ± 0.12
WISE J234228.98+085620.2	2	WISE J234228.98+085620.2	T6.5	2	...	-	13.97 ± 0.05	2.10 ± 0.09	...
WISEPA J234351.20−741847.0	1	WISE J234351.20−741846.9	T6	1	>16.14	1	13.73 ± 0.04	2.01 ± 0.06	>2.41
WISE J235716.49+122741.8	2	WISE J235716.49+122741.8	T6	2	...	-	13.99 ± 0.05	1.85 ± 0.08	...
			T7–T7.5 dwarfs						
HD 3651B (J0039−2115)	22,23	Blended w/HD 3651A	T7.5	23	16.75 ± 0.16	22	...	...	...
WISE J004024.88+090054.8	2	WISE J004024.88+090054.8	T7	2	...	-	13.92 ± 0.07	2.14 ± 0.11	...
2MASS J00501994−3322402	24	WISE J005021.03−332228.9	T7	5	15.84 ± 0.19	57	13.55 ± 0.04	1.99 ± 0.06	2.29 ± 0.19
WISEPA J012333.21+414203.9	1	WISE J012333.23+414203.8	T7	1	17.20 ± 0.13	1	15.03 ± 0.07	2.01 ± 0.14	2.18 ± 0.15
ULAS J013939.77+004813.8	25	Not detected	T7.5	25	19.12 ± 0.05	25	...	...	...
ULAS J015024.37+135924.0	10	WISE J015024.39+135923.8	T7.5	10	18.11 ± 0.02	58	15.24 ± 0.09	2.75 ± 0.30	2.87 ± 0.10
WISEPC J022322.39−293258.1	1	WISE J022322.36−293257.1	T7.5	1	17.30 ± 0.11	1	14.03 ± 0.04	3.11 ± 0.13	3.27 ± 0.12
WISEPA J022623.98−021142.8	1	WISE J022623.98−021142.8	T7	1	18.84 ± 0.24	45	14.59 ± 0.06	3.01 ± 0.20	...
WISE J024124.73−365328.0	2	WISE J024124.73−365328.0	T7	2	16.98 ± 0.09	45	14.34 ± 0.04	2.55 ± 0.11	...
CFBDS J030135−161418	56	WISE J030135.16−161417.8	T7	56	18.99 ± 0.10	56	15.59 ± 0.10	3.07 ± 0.41	3.40 ± 0.14
WISE J032547.72+083118.2	2	WISE J032547.72+083118.2	T7	2	16.15 ± 0.08	45	13.49 ± 0.04	1.95 ± 0.07	2.66 ± 0.09
2MASS J03480772−602227	21	WISE J034807.33−602234.9	T7	5	15.56 ± 0.14	57	12.54 ± 0.02	2.47 ± 0.04	3.02 ± 0.15
WISEPA J052844.51−330823.9	1	WISE J052844.51−330823.9	T7p	1	16.97 ± 0.14	1	14.60 ± 0.06	3.13 ± 0.24	2.37 ± 0.15
UGCS J053022.52−052447.4	7	Not detected	T7:	7	19.13 ± 0.29	7	...	...	...
Gl229B (J0610−2152)	27	Blended w/Gl 229A	T7p	5	∼14.3	63	...	...	...
WISE J061437.73+095135.0	2	WISE J061437.73+095135.0	T7	2	16.82 ± 0.10	45	14.29 ± 0.07	2.63 ± 0.20	2.53 ± 0.12
2MASSI J0727182+171001	6	WISE J072719.13+170951.6	T7	5	15.76 ± 0.17	57	12.96 ± 0.03	2.28 ± 0.06	2.79 ± 0.17
ULAS J085910.69+101017.1	12	WISE J085910.63+101014.8	T7	12	18.58 ± 0.06	58	15.28 ± 0.14	2.44 ± 0.35	3.30 ± 0.15
ULAS J090116.23−030635.0	28	WISE J090116.21−030636.0	T7.5	28	18.46 ± 0.13	58	14.60 ± 0.07	3.17 ± 0.32	3.86 ± 0.15
CFBDS J092250+152741	46	Not detected	T7	46	18.81 ± 0.10	56	...	...	...
ULAS J094806.06+064805.0	28	Not detected	T7	28	19.46 ± 0.22	28	...	...	...
WISE J103907.73−160002.9	2	WISE J103907.73−160002.9	T7.5	2	17.19 ± 0.20	45	14.16 ± 0.05	2.49 ± 0.12	3.03 ± 0.21
2MASS J11145133−2618235	24	WISE J111448.79−261827.7	T7.5	5	15.73 ± 0.12	57	12.24 ± 0.03	3.13 ± 0.06	3.50 ± 0.13
WISE J112438.12−042149.7	2	WISE J112438.12−042149.7	T7	2	...	-	14.05 ± 0.05	2.51 ± 0.13	...
2MASSI J1217110−031113	11	WISE J121710.30−031112.1	T7.5	5	15.75 ± 0.12	57	13.20 ± 0.04	2.09 ± 0.06	2.55 ± 0.12
WISP J1232−0033	68	Not detected	T7	68	...	-	...	...	...
ULAS J124804.56+075904.0	10	WISE J124804.49+075903.5	T7	10	18.15 ± 0.08	58	15.37 ± 0.13	1.91 ± 0.24	2.78 ± 0.15
Kelu-1 Ab[h] (J1305−2541)	60	Blended w/ components Aa,B	(T7.5)	60	...	-	...	...	...
ULAS J131508.42+082627.4	12	Not detected	T7.5	12	19.50 ± 0.10	12	...	...	...
ULAS J134940.81+091833.3	10	Not detected	T7	10	19.43 ± 0.03	10	...	...	...
ULAS J141623.94+134836.3	29	WISE J141623.94+134836.0	T7.5	30	17.58 ± 0.03	58	12.79 ± 0.04	3.33 ± 0.20	4.79 ± 0.05
WISEPC J145715.03+581510.2	1	WISE J145715.03+581510.2	T7	1	16.64 ± 0.29	1	14.47 ± 0.04	2.36 ± 0.09	2.17 ± 0.29
Gl570D (J1457−2122)	31	WISE J145715.84−212207.9	T7.5	5	15.27 ± 0.09	57	12.11 ± 0.02	2.71 ± 0.04	3.15 ± 0.09
SDSS J150411.63+102718.4	32	WISE J150411.80+102715.7	T7	32	...	-	14.06 ± 0.04	2.33 ± 0.08	...
WISE J152305.10+312537.6	2	WISE J152305.10+312537.6	T7 p	2	18.69 ± 0.18	45	14.39 ± 0.04	3.52 ± 0.22	4.30 ± 0.18
WISE J154459.27+584204.5	2	WISE J154459.27+584204.5	T7.5	2	18.34 ± 0.29	45	15.03 ± 0.06	3.36 ± 0.31	3.31 ± 0.30
2MASSI J1553022+153236B	5	Blended w/component A	T7.5	65	16.72 ± 0.03	65	...	...	...
SDSS J162838.77+230821.1	32	WISE J162839.00+230818.0	T7	32	16.11 ± 0.15	57	13.96 ± 0.04	2.47 ± 0.10	2.15 ± 0.16
WISEPA J185215.78+353716.3	1	WISE J185215.76+353716.7	T7	1	>17.41	1	14.24 ± 0.05	2.31 ± 0.11	>3.17
WISE J201404.13+042408.5	2	WISE J201404.13+042408.5	T7 p	2	18.66 ± 0.30	45	15.16 ± 0.12	>2.78	3.50 ± 0.32
WISEPA J201824.96−742325.9	26	WISE J201824.97−742327.5	T7	26	17.17 ± 0.04	-	13.62 ± 0.04	2.92 ± 0.11	3.55 ± 0.06
WISEPC J215751.38+265931.4	1	WISE J215751.35+265931.4	T7	1	17.45 ± 0.04	1	14.48 ± 0.06	2.65 ± 0.16	2.97 ± 0.07
WISEPC J220922.10−273439.5	1	WISE J220922.11−273439.6	T7	1	>16.41	1	13.84 ± 0.05	2.66 ± 0.12	>2.57
WISEPC J221354.69+091139.4	1	WISE J221354.68+091139.4	T7	1	17.09 ± 0.11	1	14.60 ± 0.07	2.10 ± 0.13	2.49 ± 0.13
UDXS J221611.51+003308.1	54	Not detected	(T7.5:)	54	...	-	...	...	...
WISEPC J231939.13−184404.3	1	WISE J231939.14−184404.4	T7.5	1	17.95 ± 0.05	1	13.76 ± 0.05	3.39 ± 0.17	4.19 ± 0.07
ULAS J232123.79+135454.9	33	WISE J232123.83+135453.5	T7.5	10	17.15 ± 0.03	58	14.10 ± 0.06	3.21 ± 0.22	3.05 ± 0.06
ULAS J232802.03+134544.8	10	WISE J232802.12+134545.3	T7	10	18.17 ± 0.02	58	15.39 ± 0.13	2.61 ± 0.40	2.78 ± 0.13
WISE J233543.79+422255.2	2	WISE J233543.79+422255.2	T7	2	...	-	15.31 ± 0.10	3.24 ± 0.52	...
WISEPC J234026.62−074507.2	1	WISE J234026.62−074508.1	T7	1	16.19 ± 0.06	1	13.58 ± 0.04	2.37 ± 0.09	2.61 ± 0.07
WISEPC J234841.10−102844.4	1	WISE J234841.10−102844.1	T7	1	16.93 ± 0.12	1	14.40 ± 0.06	2.49 ± 0.16	2.53 ± 0.14

Table 7
(Continued)

Discovery Name	Disc. Ref.	*WISE* Designation[a]	Spec. Type	Type Ref.	*H* (mag)	*H* ref.	W2 (mag)	W1–W2 (mag)	*H*–W2 (mag)
(1)	(2)	(3)	(4)	(5)	(6)	(7)	(8)	(9)	(10)
T8–T8.5 dwarfs									
WISE J001505.87−461517.6	2	WISE J001505.87−461517.6	T8	2	...	-	14.25 ± 0.06	2.77 ± 0.16	...
WISE J003231.09−494651.4	2	WISE J003231.09−494651.4	T8.5	2	...	-	15.07 ± 0.09	3.01 ± 0.35	...
ULAS J003402.77−005206.7	35	WISE J003402.78−005208.1	T8.5	36	18.49 ± 0.04	58	14.50 ± 0.08	2.97 ± 0.30	3.99 ± 0.09
WISE J004945.61+215120.0	2	WISE J004945.61+215120.0	T8.5	2	...	-	12.97 ± 0.03	2.50 ± 0.05	...
CFBDS J005910.90−011401.3	37	WISE J005911.08−011400.9	T8.5	36	18.27 ± 0.05	59	13.68 ± 0.04	3.39 ± 0.16	4.59 ± 0.07
CFBDS J013302+023128	56	WISE J013302.44+023128.9	T8.5	56	18.62 ± 0.10	56	15.10 ± 0.09	2.69 ± 0.28	3.52 ± 0.14
WISE J024512.62−345047.8	2	WISE J024512.62−345047.8	T8	2	...	-	14.56 ± 0.06	3.36 ± 0.32	...
WISE J024714.52+372523.5	2	WISE J024714.52+372523.5	T8	2	18.24 ± 0.19	2	14.70 ± 0.08	>3.67	3.54 ± 0.21
WISEPA J025409.45+022359.1	1,42	WISE J025409.51+022358.6	T8	1	16.29 ± 0.04	1	12.74 ± 0.03	3.02 ± 0.06	3.55 ± 0.05
WISEPA J031325.96+780744.2	1	WISE J031325.94+780744.3	T8.5	1	17.63 ± 0.06	1	13.19 ± 0.03	2.69 ± 0.07	4.45 ± 0.07
WISE J031624.35+430709.1	2	WISE J031624.35+430709.1	T8	2	19.70 ± 0.09	45	14.56 ± 0.07[j]	>3.30[j]	5.14 ± 0.11[j]
WISE J032120.91−734758.8	2	WISE J032120.91−734758.8	T8	2	19.06 ± 0.12	2	15.60 ± 0.08	>3.59	...
WISEPC J032337.53−602554.9	1	WISE J032337.53−602554.5	T8.5	1	18.40 ± 0.02	1	14.50 ± 0.05	3.61 ± 0.33	3.90 ± 0.06
WISE J033605.05−014350.4	2	WISE J033605.05−014350.4	T8::	2	...	-	14.54 ± 0.07	>3.423	...
2MASSW J0337036−175807B	53	Blended w/component A	(T8??)	53	...	-	...	...	...
2MASSI J0415195−093506	6	WISE J041521.21−093500.6	T8	5	15.54 ± 0.11	57	12.26 ± 0.03	2.85 ± 0.05	3.28 ± 0.12
WISEPA J045853.89+643452.9A	34	WISE J045853.89+643452.5	T8.5	61	17.41 ± 0.06[g]	1	13.03 ± 0.03[g]	3.64 ± 0.12[g]	4.38 ± 0.07[g]
WISEPA J050003.05−122343.2	1	WISE J050003.04−122343.2	T8	1	18.13 ± 0.12	1	13.94 ± 0.04	3.72 ± 0.25	4.19 ± 0.13
WISEPA J062309.94−045624.6	1	WISE J062309.94−045624.6	T8	1	17.31 ± 0.11	1	13.82 ± 0.04	3.52 ± 0.20	3.50 ± 0.12
2MASS J07290002−3954043	15	WISE J072859.49−395345.7	T8p	15	15.98 ± 0.18	57	12.96 ± 0.03	2.29 ± 0.05	3.02 ± 0.19
WISEPA J074457.15+562821.8	1	WISE J074457.25+562821.0	T8	1	17.59 ± 0.12	1	14.49 ± 0.06	2.59 ± 0.16	3.10 ± 0.13
WISEPA J075003.84+272544.8	1	WISE J075003.78+272545.4	T8.5	1	19.00 ± 0.06	1	14.46 ± 0.07	>3.65	4.54 ± 0.09
WISEPC J075946.98−490454.0	1	WISE J075946.98−490454.0	T8	1	17.41 ± 0.04	45	13.86 ± 0.04	>4.05	3.55 ± 0.05
WISE J081220.04+402106.2	2	WISE J081220.04+402106.2	T8	2	18.30 ± 0.20	2	15.08 ± 0.10	3.16 ± 0.48	3.22 ± 0.22
WISEPC J083641.12−185947.2	1	WISE J083641.10−185947.0	T8p	1	18.79 ± 0.26	45	15.18 ± 0.10	>3.23	3.61 ± 0.28
WISEPA J085716.25+560407.6	1	WISE J085716.24+560407.6	T8	1	17.49 ± 0.14	1	14.11 ± 0.05	3.37 ± 0.22	3.38 ± 0.15
WISEPA J090649.36+473538.6	1	WISE J090649.35+473538.5	T8	1	17.81 ± 0.16	1	14.65 ± 0.08	2.83 ± 0.24	3.17 ± 0.18
2MASS J09393548−2448279	24	WISE J093935.91−244838.5	T8	5	15.78 ± 0.15	57	11.64 ± 0.02	3.39 ± 0.05	4.16 ± 0.15
ULAS J101721.40+011817.9	38	Not detected	T8p	38	19.07 ± 0.02	38	...	...	...
WISEPC J101808.05−244557.7	1	WISE J101808.04−244557.9	T8	1	18.00 ± 0.23	45	14.17 ± 0.05	3.21 ± 0.22	3.83 ± 0.24
CFBDS J102841+565401[e]	46	Not detected	T8	46	18.38 ± 0.08	56	...	...	...
WISEPC J104245.23−384238.3	1	WISE J104245.23−384238.3	T8.5	1	19.08 ± 0.11	45	14.52 ± 0.06	>4.06	4.56 ± 0.13
ξ UMa C (J1118+3125)	67	WISE J111838.70+312537.9	T8.5	67	18.15 ± 0.06	67	13.31 ± 0.03	2.85 ± 0.08	2.28 ± 0.06
WISEPC J115013.88+630240.7	1	WISE J115013.85+630241.5	T8	1	>18.01	1	13.40 ± 0.03	3.59 ± 0.11	>4.61
2MASS J12255432−2739466B	64	Blended w/component A	T8	64,65	16.91 ± 0.03	65	...	...	...
ULAS J123828.51+095351.3	38	WISE J123828.38+095352.1	T8	36	19.20 ± 0.02	58	15.22 ± 0.12	>2.79	3.98 ± 0.12
Ross458C (J1300+1221)	39	WISE J130041.65+122114.6	T8	36	17.01 ± 0.04	58	13.74 ± 0.04	2.27 ± 0.08	3.27 ± 0.06
ULAS J130217.21+130851.2	10	WISE J130217.08+130851.0	T8	36	18.60 ± 0.06	58	14.95 ± 0.10	>2.66	3.65 ± 0.11
WISEPA J132233.66−234017.1	1,3	WISE J132233.64−234016.8	T8	1	16.61 ± 0.14	1	13.93 ± 0.04	3.06 ± 0.14	2.68 ± 0.15
ULAS J133553.45+113005.2	38	WISE J133553.41+113004.8	T8.5	36	18.25 ± 0.01	58	13.87 ± 0.04	3.01 ± 0.13	4.39 ± 0.04
WISE J143311.42−083736.4	2	WISE J143311.42−083736.4	T8::	2	19.42 ± 0.21	2	15.23 ± 0.10	>3.51	4.19 ± 0.23
WISEPA J143602.19−181421.8	1	WISE J143602.20−181421.9	T8p	1	>17.62	45	14.71 ± 0.06	2.50 ± 0.16	>2.91
CFBDSIR J145829+101343A	44	WISE J145829.40+101341.7	T8.5	45[i]	20.18 ± 0.10	66	15.66 ± 0.12[g]	>3.15[g]	...
WISE J151721.13+052929.3	2	WISE J151721.13+052929.3	T8	2	18.85 ± 0.15	58	15.13 ± 0.08	>2.97	3.72 ± 0.17
WISEPC J151906.64+700931.5	1	WISE J151906.63+700931.4	T8	1	18.28 ± 0.07	1	14.14 ± 0.03	3.03 ± 0.10	4.15 ± 0.08
WISEPA J161705.75+180714.3	26	WISE J161705.74+180714.2	T8	26	18.23 ± 0.08	1	14.16 ± 0.05	2.96 ± 0.16	4.08 ± 0.09
WISEPA J165311.05+444423.9	1,3	WISE J165311.05+444422.8	T8	1	17.53 ± 0.05	1	13.81 ± 0.04	2.68 ± 0.08	3.72 ± 0.06
WISEPA J171104.60+350036.8	1	WISE J171104.60+350036.8	T8	1	>18.12	1	14.72 ± 0.06	>3.43	>3.40
WISEPA J171717.02+612859.3	1	WISE J171717.02+612859.3	T8	1	18.91 ± 0.09	1	15.09 ± 0.05	3.33 ± 0.20	3.83 ± 0.10
WISE J180901.07+383805.4	2	WISE J180901.07+383805.4	T8	2	...	-	15.18 ± 0.08	>2.84	...
WISEPA J181210.85+272144.3	26	WISE J181210.85+272144.3	T8.5:	1	18.83 ± 0.16	1	14.23 ± 0.05	3.58 ± 0.29	4.60 ± 0.17
WISEPA J195905.66−333833.7	1	WISE J195905.65−333833.5	T8	1	17.18 ± 0.05	1	13.88 ± 0.05	2.56 ± 0.11	3.30 ± 0.07
WISEPC J201546.27+664645.1[f]	2	Blended w/nearby source	T8	2	17.66 ± 0.23	2	14.68 ± 0.06	2.02 ± 0.11	1.82 ± 0.11
WISE J201920.76−114807.6	2	WISE J201920.76−114807.6	T8.5:	2	18.32 ± 0.11	2	14.32 ± 0.06	2.96 ± 0.22	3.89 ± 0.11
Wolf 940B (J2146−0010)	40	WISE J214638.99−001039.6	T8.5	36	18.77 ± 0.03	58	14.24 ± 0.05	2.49 ± 0.13	4.53 ± 0.06
WISEPC J222623.05+044003.9	1	WISE J222623.05+044004.0	T8	1	16.95 ± 0.17	45	14.71 ± 0.09	2.58 ± 0.24	2.24 ± 0.19
WISEPC J225540.74−311841.8	1	WISE J225540.75−311842.0	T8	1	17.70 ± 0.11	1	14.18 ± 0.06	2.74 ± 0.18	3.52 ± 0.12
WISEPA J231336.40−803700.3	26	WISE J231336.38−803700.2	T8	26	17.28 ± 0.14	45	13.64 ± 0.03	2.65 ± 0.07	3.64 ± 0.14
T9–T9.5 dwarfs									
WISE J000517.48+373720.5	2	WISE J000517.48+373720.5	T9	2	...	-	13.27 ± 0.03	3.61 ± 0.12	...
WISE J003829.05+275852.1	2	WISE J003829.05+275852.1	T9	2	18.92 ± 0.04	45	14.38 ± 0.05	3.67 ± 0.29	4.54 ± 0.06
WISEPC J014807.25−720258.7	1,36	WISE J014807.25−720258.7	T9.5	1	19.22 ± 0.04	1	14.69 ± 0.05	>4.25	4.53 ± 0.07
WISE J032517.69−385454.1	2	WISE J032517.69−385454.1	T9	2	...	-	14.98 ± 0.06	3.47 ± 0.31	...
WISE J033515.01+431045.1	2	WISE J033515.01+431045.1	T9::	2	19.60 ± 0.26	45	14.60 ± 0.08	>3.55	5.00 ± 0.27

Table 7
(Continued)

Discovery Name	Disc. Ref.	*WISE* Designation[a]	Spec. Type	Type Ref.	*H* (mag)	*H* ref.	W2 (mag)	W1–W2 (mag)	*H*–W2 (mag)
(1)	(2)	(3)	(4)	(5)	(6)	(7)	(8)	(9)	(10)
WISE J041358.14−475039.3	2	WISE J041358.14−475039.3	T9	2	20.12 ± 0.20	2	15.69 ± 0.08	>3.70	...
WISEPA J045853.89+643452.9B	3	Blended w/component A	T9.5	61	...	-	...	...	...
UGPS J072227.51−054031.2	43	WISE J072227.27−054029.9	T9	36	16.15 ± 0.21	57	12.21 ± 0.03	2.97 ± 0.06	3.93 ± 0.21
WISE J072312.44+340313.5	2	WISE J072312.44+340313.5	T9:	2	>18.47	2	14.73 ± 0.08	>3.54	>3.74
WISEPA J075108.79−763449.6	1	WISE J075108.80−763449.5	T9	1	>19.02	1	14.52 ± 0.04	3.01 ± 0.14	>4.50
WISE J081117.81−805141.3	2	WISE J081117.81−805141.3	T9.5:	2	19.88 ± 0.21	2	14.38 ± 0.04	2.91 ± 0.13	...
WISE J105130.01−213859.7	2	WISE J105130.01−213859.7	T9:	2	19.19 ± 0.39	2	14.54 ± 0.06	2.63 ± 0.18	...
WISEPC J121756.91+162640.2	1	WISE J121756.90+162640.8	T9	1	18.18 ± 0.05	1	13.09 ± 0.03	3.71 ± 0.14	5.09 ± 0.06
WISP J1305−2538	68	Not detected	T9.5+	68	...	-	...	...	...
WISEPC J131106.24+012252.4	1	WISE J131106.20+012254.3	T9:	1	19.32 ± 0.23	45	14.76 ± 0.09	3.50 ± 0.47	4.56 ± 0.25
WISE J131833.98−175826.5	2	WISE J131833.98−175826.5	T9:	2	17.71 ± 0.23	2	14.75 ± 0.07	3.35 ± 0.35	2.96 ± 0.24
CFBDSIR J145829+101343B	50	Blended w/A component	T9.5	45	22.51 ± 0.16	66	...	...	...
WISE J154214.00+223005.2	2	WISE J154214.00+223005.2	T9.5	2	21.80 ± 0.80	2	15.02 ± 0.06	>3.86	6.78 ± 0.80
WISEPA J161441.45+173936.7	1,3	WISE J161441.46+173935.5	T9	1	18.47 ± 0.22	1	14.25 ± 0.05	>3.65	4.22 ± 0.22
WISEPA J174124.26+255319.5	1,3,42	WISE J174124.25+255319.6	T9	1,42	16.63 ± 0.03	1	12.33 ± 0.03	3.05 ± 0.06	4.30 ± 0.04
WISEPA J180435.40+311706.1	1	WISE J180435.37+311706.4	T9.5:	1	19.21 ± 0.11	1	14.70 ± 0.06	>3.94	4.51 ± 0.13
WISE J210200.15−442919.5	41	WISE J210200.15−442919.5	T9	41	18.39 ± 0.12	45	14.12 ± 0.05	2.83 ± 0.18	4.26 ± 0.09
WISEPA J213456.73−713743.6	1	WISE J213456.73−713744.5	T9p	1	19.81 ± 0.12	45	13.99 ± 0.05	>3.75	5.82 ± 0.13
WISEPC J232519.54−410534.9	1	WISE J232519.53−410535.0	T9p	1	19.22 ± 0.11	1	14.13 ± 0.05	3.47 ± 0.25	5.09 ± 0.12
WISE J233226.49−432510.6	41	WISE J233226.49−432510.6	T9:	41	19.40 ± 0.18	45	14.99 ± 0.09	>2.89	4.41 ± 0.20
WISEPC J234446.25+103415.8	1	WISE J234446.23+103415.6	T9	1	19.07 ± 0.11	1	15.11 ± 0.12	>2.92	3.96 ± 0.16
Y dwarfs									
WISE J014656.66+423410.0	2	WISE J014656.66+423410.0	Y0	2	18.71 ± 0.24	45	15.08 ± 0.07	>3.91	3.63 ± 0.25
WISE J035000.32−565830.2	45	WISE J035000.32−565830.2	Y1	45	>21.5	45	14.73 ± 0.06	>4.17	>6.8
WISE J035934.06−540154.6	45	WISE J035934.06−540154.6	Y0	45	22.20 ± 0.43	45	15.42 ± 0.07	>3.87	6.78 ± 0.44
WISEPA J041022.71+150248.5	1,36	WISE J041022.71+150248.4	Y0	36	19.05 ± 0.09	1	14.18 ± 0.06	>4.15	4.87 ± 0.11
WISE J053516.80−750024.9	45	WISE J053516.80−750024.9	⩾Y1	45	>21.6	45	15.06 ± 0.07	>3.86	>6.5
WISE J071322.55−291751.9	45	WISE J071322.55−291751.9	Y0	45	>19.3	-	14.48 ± 0.06	>3.87	>4.8
WISE J073444.02−715744.0	45	WISE J073444.02−715744.0	Y0	45	...	-	15.36 ± 0.06	>4.06	...
WD 0806−661B	48	Not detected	(Y?)	49	...	-	...	...	...
WISEPC J140518.40+553421.4	1,36	WISE J140518.39+553421.3	Y0p	36	>20.5	1	14.10 ± 0.04	>4.72	>6.4
WISEPA J154151.66−225025.2	1,36	WISE J154151.65−225024.9	Y0.5	36	>20.2	1	14.25 ± 0.06	2.49 ± 0.18	>6.0
WISEPA J173835.53+273258.9	1,36	WISE J173835.53+273259.0	Y0	36	20.39 ± 0.33	1	14.55 ± 0.06	>3.86	5.84 ± 0.34
WISEPA J182831.08+265037.8	1,36	WISE J182831.08+265037.7	⩾Y2	45	22.85 ± 0.24	1	14.39 ± 0.06	>4.08	8.46 ± 0.25
WISEPC J205628.90+145953.3	1,36	WISE J205628.91+145953.2	Y0	36	19.62 ± 0.31	1	13.93 ± 0.05	>4.33	5.69 ± 0.31
WISE J222055.31−362817.4	45	WISE J222055.31−362817.4	Y0	45	20.81 ± 0.30	45	14.66 ± 0.06	>3.99	...

Notes. Code for references: (1) Kirkpatrick et al. 2011; (2) G. N. Mace et al., in preparation; (3) Gelino et al. 2011; (4) Burgasser et al. 2004; (5) Burgasser et al. 2006a; (6) Burgasser et al. 2002; (7) Lodieu et al. 2009; (8) Zapatero Osorio et al. 2002; (9) Artigau et al. 2010; (10) Burningham et al. 2010; (11) Burgasser et al. 1999; (12) Pinfield et al. 2008; (13) Cuby et al. 1999; (14) Tsvetanov et al. 2000; (15) Looper et al. 2007; (16) Strauss et al. 1999; (17) Knapp et al. 2004; (18) Biller et al. 2006; (19) Kasper et al. 2007; (20) Scholz et al. 2003; (21) Burgasser et al. 2003c; (22) Mugrauer et al. 2006; (23) Luhman et al. 2007; (24) Tinney et al. 2005; (25) Chiu et al. 2008; (26) Burgasser et al. 2011; (27) Nakajima et al. 1995; (28) Lodieu et al. 2007; (29) Scholz 2010; (30) Burgasser et al. 2010; (31) Burgasser et al. 2000a; (32) Chiu et al. 2006; (33) Scholz 2010; (34) Mainzer et al. 2011; (35) Warren et al. 2007; (36) Cushing et al. 2011; (37) Delorme et al. 2008; (38) Burningham et al. 2008; (39) Goldman et al. 2010; (40) Burningham et al. 2009; (41) C. G. Tinney et al., in preparation; (42) Scholz et al. 2011; (43) Lucas et al. 2010; (44) Delorme et al. 2010; (45) This paper, (46) Reylé et al. 2010; (47) Geißler et al. 2011; (48) Luhman et al. 2011; (49) Luhman et al. 2012; (50) Liu et al. 2011; (51) Murray et al. 2011; (52) Liu et al. 2010; (53) Stumpf et al. 2010; (54) Lodieu et al. 2009; (55) Burgess et al. 2009; (56) Albert et al. 2011; (57) 2MASS, (58) UKIDSS, (59) CFBDS, (60) Stumpf et al. 2008; (61) Burgasser et al. 2012; (62) Burgasser et al. 2006b; (63) Matthews et al. 1996; (64) Burgasser et al. 2003b; (65) Dupuy & Liu 2012; (66) Liu et al. 2011; (67) Wright et al. 2012; (68) Masters et al. 2012.

[a] *WISE* sources are given designations as follows. The prefix is "WISE" for sources taken from the four-band cryogenic atlas source catalog, "WISER" for sources taken from the four-band cryogenic atlas source reject table, "WISEPC" for sources taken from the first-pass processing operations co-add Source Working Database, or "WISEPA" for objects drawn from the preliminary release Atlas Tile Source Working Database. The suffix is the J2000 position of the source in the format Jhhmmss.ss±ddmmss.s.

[b] Also known as IC348 CH4 2 034449.52+320635.4.

[c] Also known as HIP 73786B or Gl 576B.

[d] This is a companion to G 204-39 from Faherty et al. (2010), $d = 13.6$ pc.

[e] Object is seen on the *WISE* images but is not successfully extracted.

[f] Object is not detected by *WISE* Pass2 processing, so the quoted *WISE* photometry comes from Pass1.

[g] These values represent the combined light of the composite system.

[h] This object may not exist.

[i] Cushing et al. (2011) assigns this binary a composite type of T9 on the revised late-T dwarf classification scheme. Given the Dupuy & Liu (2012) measurements of the parallax and the Liu et al. (2011) *H*-band measurements of the individual components, we infer spectral types of T8.5 and T9.5 based on absolute *H* magnitudes of 17.8 and 20.2 mag.

[j] *Spitzer*/IRAC follow-up of this sources shows that the *WISE* photometry is blended with a bright, nearby source.

Table 8
Distances for Objects in Table 7

Discovery Name	Spec. Type	$\pi_{\rm trig}$ (pc)	$\pi_{\rm trig}$ ref.	D_H (pc)	D_{W2} (pc)	$D_{\rm adopted}$ (pc)	$\frac{V}{V_{\rm max}}$
(1)	(2)	(3)	(4)	(5)	(6)	(7)	(8)
T6–T6.5 dwarfs (distance limit = 20 pc, $\langle \frac{V}{V_{\rm max}} \rangle = 0.41$)							
WISEPC J000849.76−173922.6	T6	...	...	31.5	21.8	26.7	...
2MASS J00345157+0523050	T6.5	...	...	9.1	8.1	8.6	0.08
WISE J003830.54+840517.7	T6	...	...	...	31.2	31.2	...
WISE J013525.64+171503.4	T6	...	...	...	23.7	23.7	...
WISEPA J022105.94+384202.9	T6.5	...	...	22.9	22.0	22.4	...
CFBDS J022638−072831	T6.5	...	...	39.8	...	39.8	...
2MASSI J0243137−245329	T6	0.0936 ± 0.0036	5	9.4	10.2	10.7	0.15
CFBDS J025401−182529	T6.5	...	...	37.0	35.2	36.1	...
UGCS J030013.86+490142.5	T6.5	...	...	35.0	38.4	36.7	...
CFBDS J030130−104504	T6	...	...	...	30.9	30.9	...
CFBDS J030225−144125	T6	...	...	34.6	...	34.6	...
WISEPA J030533.54+395434.4	T6	...	...	22.9	23.1	23.0	...
WISEPA J030724.57+290447.6	T6.5	...	...	25.7	25.1	25.4	...
CFHT J0344+3206	(T6:)	...	...	188.3	...	188.3	...
WISEPA J041054.48+141131.6	T6	...	...	24.9	27.7	26.3	...
WISEPA J051317.28+060814.7	T6.5	...	...	12.5	14.9	13.7	0.32
WISEPA J052536.33+673952.3	T6p	...	...	33.0	27.2	30.1	...
SOri70 (J0538−0236)	T6:	...	...	106.8	...	106.8	...
WISEPA J054231.26−162829.1	T6.5	...	...	15.3	15.8	15.5	0.47
WISEPA J061213.93−303612.7	T6	...	...	22.7	17.1	19.9	0.99
WISEPA J061407.49+391236.4	T6	...	...	16.5	14.3	15.4	0.46
WISEPA J062542.21+564625.5	T6	...	...	21.1	20.0	20.6	...
WISEPA J062720.07−111428.8	T6	...	...	10.8	12.0	11.4	0.19
WISE J073347.94+754439.2	T6	...	...	...	24.0	24.0	...
DENIS J081730.0−615520	T6	0.203 ± 0.013	3	4.5	4.7	4.9	0.01
ULAS J081948.09+073323.3	T6p	...	...	41.4	...	41.4	...
ULAS J085342.94+000651.8	T6p	...	...	61.2	38.4	49.8	...
ULAS J085715.96+091325.3	T6	...	...	52.8	...	52.8	...
WISEPC J092906.77+040957.9	T6.5	...	...	22.1	17.7	19.9	0.99
2MASSI J0937347+293142	T6p	0.1634 ± 0.0018	7	7.7	5.7	6.1	0.03
WISEPC J095259.29+195507.3	T6	...	...	24.5	19.7	22.1	...
WISEPA J101905.63+652954.2	T6	...	...	17.7	17.1	17.4	0.66
ULAS J103434.52−001553.0	T6.5p	...	...	46.8	...	46.8	...
CFBDS J104209+580856	T6.5	...	...	32.5	29.0	30.7	...
2MASSI J1047538+212423	T6.5	0.0947 ± 0.0038	5	10.7	9.9	10.6	0.15
WISEPC J112254.73+255021.5	T6	...	...	18.7	16.6	17.7	0.69
ULAS J115038.79+094942.9	T6.5p	0.0168 ± 0.0075	1	52.0	...	59.5	...
ULAS J115338.74−014724.1	T6	...	...	34.6	...	34.6	...
NTTDF1205−0744	T6:	...	...	...	...	∼90[b]	...
ULAS J120744.65+133902.7	T6	...	...	44.5	38.4	41.5	...
2MASS J12095613−1004008B	T6.5:	0.0307 ± 0.013	11	30.6	...	32.6	...
SDSS J121440.95+631643.4B	(T6)	...	...	...	...	>20.9[c]	...
WISE J122558.86−101345.0	T6	...	...	17.2	16.8	17.0	0.61
2MASS J12373919+6526148	T6.5	0.0961 ± 0.0048	5	10.4	9.8	10.4	0.14
WISEPC J132004.16+603426.2	T6.5	...	...	15.1	19.2	17.2	0.64
ULAS J132605.18+120009.9	T6p	...	...	33.9	31.8	32.9	...
SDSSp J134646.45−003150.4	T6.5	0.0683 ± 0.0023	9	9.2	13.1	14.6	0.39
ULAS J144555.24+125735.1	T6.5	...	...	49.0	...	49.0	...
HIP 73786B (J1504+0538)	T6:p	0.0538 ± 0.0028	6	22.6	18.7	18.6	0.80
WISEPC J150649.97+702736.0	T6	0.193 ± 0.026	14	5.3	4.8	5.2	0.02
ULAS J152526.25+095814.3	T6.5	...	...	50.6	49.0	49.8	...
ULAS J152912.23+092228.5	T6	...	...	59.0	...	59.0	...
2MASSI J1553022+153236A	T6.5	0.0751 ± 0.0009	11	13.7	>10.1	13.3	0.29
WISEPA J161215.94−342027.1	T6.5	...	...	18.3	15.6	17.0	0.61
2MASS J16150413+1340079	T6	...	...	17.5	18.4	17.9	0.72
WISEPA J162208.94−095934.6	T6	...	...	14.3	18.2	16.2	0.53
SDSSp J162414.37+002915.6	T6	0.0909 ± 0.0012	9	11.2	11.1	11.0	0.17
WISEPA J162725.64+325525.5	T6	...	...	16.8	14.0	15.4	0.46
WISE J172134.46+111739.4	T6	...	...	...	19.1	19.1	0.87
WISEPA J172844.93+571643.6	T6	...	...	33.2	26.8	30.0	...
WISE J174640.78−033818.0	T6	...	...	27.2	24.2	25.7	...
SDSS J175805.46+463311.9	T6.5	0.0710 ± 0.0019	6	13.2	14.7	13.9	0.34

Table 8
(Continued)

Discovery Name	Spec. Type	$\pi_{\rm trig}$ (pc)	$\pi_{\rm trig}$ ref.	D_H (pc)	D_{W2} (pc)	$D_{\rm adopted}$ (pc)	$\frac{V}{V_{\rm max}}$
(1)	(2)	(3)	(4)	(5)	(6)	(7)	(8)
SCR J1845−6357B	T6	0.2595 ± 0.0011	10	...	...	3.9	0.01
WISEPA J190624.75+450808.2	T6	...	...	16.2	15.5	15.8	0.49
WISE J192841.35+235604.9	T6	...	...	...	7.0	7.0	0.04
2MASS J21543318+5942187	T6	...	...	12.6	13.4	13.0	0.27
ϵ Ind Bb (J2204−5646)	T6	0.2761 ± 0.0003	6	...	...	3.6	0.01
UDXS J221903.10+002418.2	(T6:)	...	...	...	...	∼60[d]	...
2MASS J22282889−4310262	T6	...	...	10.4	12.4	11.4	0.19
WISE J223720.39+722833.8	T6	...	...	...	14.1	14.1	0.35
WISE J230133.32+021635.1	T6	...	...	...	18.6	18.6	0.80
ULAS J230601.02+130225.0	T6.5	...	...	29.5	26.1	27.8	...
ULAS J231557.61+132256.2	T6.5	...	...	31.8	31.3	31.6	...
CFBDS J232304−015232	T6	...	...	27.3	27.5	27.4	...
WISE J234228.98+085620.2	T6.5	...	...	...	15.7	15.7	0.48
WISEPA J234351.20−741847.0	T6	...	...	>14.9	14.9	14.9	0.41
WISE J235716.49+122741.8	T6	...	...	...	16.8	16.8	0.59
	T7–T7.5 dwarfs (distance limit = 20 pc, $\langle \frac{V}{V_{\rm max}} \rangle = 0.37$)						
HD 3651B (J0039+2115)	T7.5	0.0904 ± 0.0003	6	11.0	...	11.1	0.17
WISE J004024.88+090054.8	T7	...	...	...	14.6	14.6	0.39
2MASS J00501994−3322402	T7	...	...	9.0	12.3	10.7	0.15
WISEPA J012333.21+414203.9	T7	...	...	16.9	24.4	20.6	...
ULAS J013939.77+004813.8	T7.5	...	...	32.7	...	32.7	...
ULAS J015024.37+135924.0	T7.5	...	...	20.6	25.4	23.0	...
WISEPC J022322.39−293258.1	T7.5	...	...	14.2	14.6	14.4	0.37
WISEPA J022623.98−021142.8	T7	...	...	36.0	19.9	27.9	...
WISE J024124.73−365328.0	T7	...	...	15.3	17.7	16.5	0.56
CFBDS J030135−161418	T7	...	...	38.5	31.6	35.0	...
WISE J032547.72+083118.2	T7	...	...	10.4	12.0	11.2	0.18
2MASS J03480772−602227	T7	...	...	7.9	7.7	7.8	0.06
WISEPA J052844.51−330823.9	T7p	...	...	15.2	20.0	17.6	0.68
UGCS J053022.52−052447.4	T7:	...	...	41.1	...	41.1	...
Gl229B (J0610−2152)	T7p	0.1738 ± 0.0010	6	4.4	...	5.8	0.02
WISE J061437.73+095135.0	T7	...	...	14.2	17.3	15.8	0.49
2MASSI J0727182+171001	T7	0.1101 ± 0.0023	5	8.7	9.4	9.1	0.09
ULAS J085910.69+101017.1	T7	...	...	31.9	27.4	29.6	...
ULAS J090116.23−030635.0	T7.5	0.0626 ± 0.0026	1	24.2	18.9	16.0	0.51
CFBDS J092250+152741	T7	...	...	35.5	...	35.5	...
ULAS J094806.06+064805.0	T7	0.0272 ± 0.0042	1	47.8	...	36.8	...
WISE J103907.73−160002.9	T7.5	...	...	13.5	15.5	14.5	0.38
2MASS J11145133−2618235	T7.5	...	...	6.9	6.4	6.6	0.04
WISE J112438.12−042149.7	T7	...	...	...	15.5	15.5	0.47
2MASSI J1217110−031113	T7.5	0.0908 ± 0.0022	9	6.9	9.9	11.0	0.17
WISP J1232−0033	T7	...	...	...	...	∼270[i]	...
ULAS J124804.56+075904.0	T7	...	...	26.2	28.5	27.3	...
Kelu-1 Ab[a] (J1305−2544)	(T7.5)	0.0536 ± 0.0020	8	...	...	18.7	0.82
ULAS J131508.42+082627.4	T7.5	0.0428 ± 0.0077	1	39.0	...	23.4	...
ULAS J134940.81+091833.3	T7	...	...	47.2	...	47.2	...
ULAS J141623.94+134836.3	T7.5	0.1099 ± 0.0018	11	16.1	8.2	9.1	0.09
WISEPC J145715.03+581510.2	T7	...	...	13.1	18.8	16.0	0.51
Gl570D (J1457−2122)	T7.5	0.1712 ± 0.0009	6	5.6	6.0	5.8	0.02
SDSS J150411.63+102718.4	T7	0.0461 ± 0.0015	11	...	15.6	21.7	...
WISE J152305.10+312537.6	T7 p	...	...	33.6	18.2	25.9	...
WISE J154459.27+584204.5	T7.5	...	...	22.9	23.1	23.0	...
2MASSI J1553022+153236B	T7.5	0.0751 ± 0.0009	11	10.8	...	13.3	0.29
SDSS J162838.77+230821.1	T7	0.0751 ± 0.0009	11	10.2	14.9	13.3	0.29
WISEPA J185215.78+353716.3	T7	...	...	>18.6	17.0	17.0	0.61
WISE J201404.13+042408.5	T7 p	...	...	33.1	25.9	29.5	...
WISEPA J201824.96−742325.9	T7	...	...	16.7	12.7	14.7	0.40
WISEPC J215751.38+265931.4	T7	...	...	19.0	18.9	18.9	0.84
WISEPC J220922.10−273439.5	T7	...	...	>11.7	14.1	14.1	0.35
WISEPC J221354.69+091139.4	T7	...	...	16.1	20.1	18.0	0.73
UDXS J221611.51+003308.1	(T7.5:)	...	...	...	...	∼81[d]	...
WISEPC J231939.13−184404.3	T7.5	...	...	19.1	12.9	16.0	0.51
ULAS J232123.79+135454.9	T7.5	...	...	13.2	15.0	14.1	0.35

Table 8
(Continued)

Discovery Name	Spec. Type	$\pi_{\rm trig}$ (pc)	$\pi_{\rm trig}$ ref.	D_H (pc)	D_{W2} (pc)	$D_{\rm adopted}$ (pc)	$\frac{V}{V_{\rm max}}$
(1)	(2)	(3)	(4)	(5)	(6)	(7)	(8)
ULAS J232802.03+134544.8	T7	...	...	26.4	28.8	27.6	...
WISE J233543.79+422255.2	T7	...	...	...	27.7	27.7	...
WISEPC J234026.62−074507.2	T7	...	...	10.6	12.5	11.6	0.20
WISEPC J234841.10−102844.4	T7	...	...	14.9	18.2	16.6	0.57
T8–T8.5 dwarfs (distance limit = 20 pc, $\langle \frac{V}{V_{\rm max}} \rangle = 0.35$)							
WISE J001505.87−461517.6	T8	...	...	...	14.9	14.9	0.41
WISE J003231.09−494651.4	T8.5	...	...	...	19.3	19.3	0.90
ULAS J003402.77−005206.7	T8.5	0.0780 ± 0.0036	1	13.4	14.9	12.8	0.26
WISE J004945.61+215120.0	T8.5	...	...	...	7.4	7.4	0.05
CFBDS J005910.90−011401.3	T8.5	0.1011 ± 0.0025	11	12.1	10.2	9.9	0.12
CFBDS J013302+023128	T8.5	...	...	14.2	19.6	16.9	0.60
WISE J024512.62−345047.8	T8	...	...	...	17.2	17.2	0.64
WISE J024714.52+372523.5	T8	...	...	16.7	18.3	17.5	0.67
WISEPA J025409.45+022359.1	T8	0.166 ± 0.026	14	6.8	7.4	6.0	0.03
WISEPA J031325.96+780744.2	T8.5	...	...	9.0	8.1	8.6	0.08
WISE J031624.35+430709.1	T8	...	...	32.6	17.2	32.6[h]	...
WISE J032120.91−734758.8	T8	...	...	24.3	27.7	26.0	...
WISEPC J032337.53−602554.9	T8.5	...	...	12.8	14.9	13.9	0.34
WISE J033605.05−014350.4	T8::	...	...	...	17.0	17.0	0.61
2MASSW J0337036−175807B	(T8??)	...	...	...	...	∼29[e]	...
2MASSI J0415195−093506	T8	0.1773 ± 0.0022	11	4.8	6.0	5.6	0.02
WISEPA J045853.89+643452.9A	T8.5	...	...	>8.1	>7.6	∼11[f]	0.17
WISEPA J050003.05−122343.2	T8	...	...	15.8	12.9	14.4	0.37
WISEPA J062309.94−045624.6	T8	...	...	10.9	12.2	11.5	0.19
2MASS J07290002−3954043	T8p	...	...	5.9	8.2	7.1	0.04
WISEPA J074457.15+562821.8	T8	...	...	12.3	16.6	14.5	0.38
WISEPA J075003.84+272544.8	T8.5	...	...	16.9	14.6	15.8	0.49
WISEPC J075946.98−490454.0	T8	...	...	11.4	12.4	11.9	0.21
WISE J081220.04+402106.2	T8	...	...	17.1	21.8	19.5	0.93
WISEPC J083641.12−185947.2	T8p	...	...	21.5	22.8	22.2	...
WISEPA J085716.25+560407.6	T8	...	...	11.8	14.0	12.9	0.27
WISEPA J090649.36+473538.6	T8	...	...	13.7	17.9	15.8	0.49
2MASS J09393548−2448279	T8	0.1873 ± 0.0046	15	5.4	4.5	5.3	0.02
ULAS J101721.40+011817.9	T8p	...	...	24.4	...	24.4	...
WISEPC J101808.05−244557.7	T8	...	...	14.9	14.4	14.6	0.39
CFBDS J102841+565401	T8	...	...	17.8	...	17.8	0.70
WISEPC J104245.23−384238.3	T8.5	...	...	17.6	15.0	16.3	0.54
ξ UMa C (J1118+3125)	T8.5	0.1132 ± 0.0046	18	11.4	8.6	8.8	0.09
WISEPC J115013.88+630240.7	T8	...	...	>15.0	10.1	10.1	0.13
2MASS J12255432−2739466B	T8	0.0751 ± 0.0025	9	9.0	...	13.3	0.29
ULAS J123828.51+095351.3	T8	...	...	25.9	23.3	24.6	...
Ross458C (J1300+1221)	T8	0.0855 ± 0.0015	6	9.5	11.8	11.7	0.20
ULAS J130217.21+130851.2	T8	...	...	19.7	20.6	20.1	...
WISEPA J132233.66−234017.1	T8	...	...	7.9	12.8	10.4	0.14
ULAS J133553.45+113005.2	T8.5	0.0967 ± 0.0032	1	12.0	11.1	10.3	0.14
WISE J143311.42−083736.4	T8::	...	...	28.7	23.4	26.0	...
WISEPA J143602.19−181421.8	T8p	...	...	>12.5	18.4	18.4	0.78
CFBDSIR J145829+101343A	T8.5	0.0340 ± 0.0026	11	29.2	>25.4	29.4	...
WISE J151721.13+052929.3	T8	...	...	22.1	22.3	22.2	...
WISEPC J151906.64+700931.5	T8	...	...	17.0	14.2	15.6	0.47
WISEPA J161705.75+180714.3	T8	...	...	16.6	14.3	15.4	0.46
WISEPA J165311.05+444423.9	T8	...	...	12.0	12.2	12.1	0.22
WISEPA J171104.60+350036.8	T8	...	...	>15.8	18.5	18.5	0.79
WISEPA J171717.02+612859.3	T8	...	...	22.7	21.9	22.3	...
WISE J180901.07+383805.4	T8	...	...	...	22.8	22.8	...
WISEPA J181210.85+272144.3	T8.5:	...	...	15.7	13.1	14.4	0.37
WISEPA J195905.66−333833.7	T8	...	...	10.2	12.6	11.4	0.19
WISEPC J201546.27+664645.1	T8	...	...	12.8	18.1	15.5	0.47
WISE J201920.76−114807.6	T8.5:	...	...	12.4	13.7	13.0	0.27
Wolf 940B (J2146−0010)	T8.5	0.0835 ± 0.0039	17	15.2	13.2	12.0	0.22
WISEPC J222623.05+044003.9	T8	...	...	9.2	18.4	13.8	0.33
WISEPC J225540.74−311841.8	T8	...	...	13.0	14.4	13.7	0.32
WISEPA J231336.40−803700.3	T8	...	...	10.7	11.2	11.0	0.17

Table 8
(Continued)

Discovery Name	Spec. Type	$\pi_{\rm trig}$ (pc)	$\pi_{\rm trig}$ ref.	D_H (pc)	D_{W2} (pc)	$D_{\rm adopted}$ (pc)	$\frac{V}{V_{\rm max}}$
(1)	(2)	(3)	(4)	(5)	(6)	(7)	(8)
T9–T9.5 dwarfs (distance limit = 15 pc, $\langle \frac{V}{V_{\rm max}} \rangle = 0.44$)							
WISE J000517.48+373720.5	T9	...	...	...	7.1	7.1	0.11
WISE J003829.05+275852.1	T9	...	...	10.8	11.9	11.3	0.43
WISEPC J014807.25−720258.7	T9.5	...	...	7.5	10.8	9.2	0.23
WISE J032517.69−385454.1	T9	...	...	...	15.7	15.7	...
WISE J033515.01+431045.1	T9::	...	...	14.8	13.2	14.0	0.81
WISE J041358.14−475039.3	T9	...	...	18.8	21.7	20.3	...
WISEPA J045853.89+643452.9B	T9.5	...	...	...	...	∼11[f]	0.39
UGPS J072227.51−054031.2	T9	0.246 ± 0.033	2	3.0	4.4	4.1	0.02
WISE J072312.44+340313.5	T9:	...	...	>8.8	14.0	14.0	0.81
WISEPA J075108.79−763449.6	T9	...	...	>11.3	12.7	12.0	0.51
WISE J081117.81−805141.3	T9.5:	...	...	10.2	9.4	9.8	0.28
WISE J105130.01−213859.7	T9:	...	...	12.2	12.8	12.5	0.58
WISEPC J121756.91+162640.2	T9	...	...	7.7	6.6	7.1	0.11
WISP J1305−2538	T9.5+	...	...	...	...	∼50[i]	...
WISEPC J131106.24+012252.4	T9:	...	...	13.0	14.2	13.6	0.75
WISE J131833.98−175826.5	T9:	...	...	6.2	14.1	10.1	0.31
CFBDSIR J145829+101343B	T9.5	0.0340 ± 0.0026	11	34.1	...	29.4	...
WISE J154214.00+223005.2	T9.5	...	...	24.6:	12.6	12.6[g]	0.59
WISEPA J161441.45+173936.7	T9	...	...	8.8	11.2	10.0	0.30
WISEPA J174124.26+255319.5	T9	0.176 ± 0.022	14	3.8	4.6	5.7	0.05
WISEPA J180435.40+311706.1	T9.5:	...	...	7.5	10.9	9.2	0.23
WISE J210200.15−442919.5	T9	...	...	8.5	10.5	9.5	0.25
WISEPA J213456.73−713743.6	T9p	...	...	16.3	9.9	13.1	0.67
WISEPC J232519.54−410534.9	T9p	...	...	12.4	10.6	11.5	0.45
WISE J233226.49−432510.6	T9:	...	...	13.5	15.7	14.6	0.92
WISEPC J234446.25+103415.8	T9	...	...	11.6	16.6	14.1	0.83
Y0–0.5 dwarfs (distance limit = 10 pc, $\langle \frac{V}{V_{\rm max}} \rangle = 0.30$)							
WISE J014656.66+423410.0	Y0	...	...	3.2	9.4	6.3	0.25
WISE J035934.06−540154.6	Y0	...	...	16.0	11.0	13.5	...
WISEPA J041022.71+150248.5	Y0	0.164 ± 0.024	14	3.8	6.2	6.1	0.23
WISE J071322.55−291751.9	Y0	...	...	>4.2	7.1	7.1	0.36
WISE J073444.02−715744.0	Y0	...	...	...	10.7	10.7	...
WISEPC J140518.40+553421.4	Y0p?	0.207 ± 0.039	14	>7.3	6.0	4.8	0.11
WISEPA J154151.66−225025.2	Y0.5	...	...	>3.0	4.2	4.2	0.07
WISEPA J173835.53+273258.9	Y0	0.111 ± 0.036	14	7.0	7.4	9.0	0.73
WISEPC J205628.90+145953.3	Y0	...	...	4.9	5.5	5.2	0.14
WISE J222055.32−362817.5	Y0	...	...	8.4	7.8	8.1	0.53
Y1–1.5 dwarfs (distance limit = 10 pc, $\langle \frac{V}{V_{\rm max}} \rangle = 0.14$)							
WISE J035000.32−565830.2	Y1	0.238 ± 0.038	14	2.3	3.1	4.2	0.07
WISE J053516.80−750024.9	⩾Y1:	0.170 ± 0.044	14	2.4	3.6	5.9	0.21
Y2–2.5 dwarfs (distance limit = 10 pc, $\langle \frac{V}{V_{\rm max}} \rangle = 0.55$)							
WD 0806−661B	(Y?)	0.0522 ± 0.0017	16	...	...	19.2	...
WISEPA J182831.08+265037.8	⩾Y2	0.122 ± 0.013	13	...	...	8.2	0.55

Notes. Parallax references: (1) Marocco et al. 2010; (2) Lucas et al. 2010; (3) Artigau et al. 2010; (4) Perryman et al. 1997; (5) Vrba et al. 2004; (6) van Leeuwen 2007; (7) Schilbach et al. 2009; (8) Dahn et al. 2002; (9) Tinney et al. 2003; (10) Henry et al. 2006; (11) Dupuy & Liu 2012; (12) Kirkpatrick et al. 2011; (13) Beichman et al. 2012; (14) Marsh et al. 2012; (15) Burgasser et al. 2008; (16) Subasavage et al. 2009 (17) van Altena et al. 1995; (18) Karataş et al. 2004.

[a] This object may not exist.

[b] Distance estimate from Cuby et al. (1999).

[c] Geißler et al. (2011) estimate that the primary (if this is a true binary) has a type of T2. The *J* band combined light of the system is 16.05 mag from Chiu et al. (2006). The *J*-band absolute magnitude relation from Looper et al. (2008) gives $M_J = 14.45$ mag for a T2 dwarf, meaning that this system is no closer than 20.9 pc.

[d] Distance estimate from Lodieu et al. (2009).

[e] Distance estimate from Stumpf et al. (2010).

[f] Distance estimate from Burgasser et al. (2012).

[g] Assumed distance is that derived from the W2 estimate only because the *H*-band measurement is very uncertain.

[h] Assumed distance is that derived from the *H* estimate only because the W2 measurement is blended with a nearby source.

[i] Distance estimate from Masters et al. (2012).

Table 9
Updated Space Densities for the All-sky, Volume-limited Sample of Late-T and Y Dwarfs

Spectral Type Range (1)	Approx. $T_{\rm eff}$ Range (K) (2)	$d_{\rm max}$ (pc) (3)	Total No. of Objects (4)	Obs. Space Density (#/pc^3) (5)	$\langle V/V_{\rm max}\rangle$ (6)	# per 100 K Bin w/in 10 pc (7)
T6–T6.5	900–1050	20	38	1.1e-3	0.41	3.1
T7–T7.5	750–900	20	31	9.3e-4	0.37	2.6
T8–T8.5	600–750	20	46	1.4e-3	0.35	3.9
T9–T9.5	450–600	15	22[a]	1.6e-3[a]	0.44	4.5[a]
Y0–Y0.5	300–450	10	8[a]	1.9e-3[a]	0.30	5.3[a]
$\geqslant$Y1	150–300	10	3[a]	7.2e-4[a]	0.28	2.0[a]

Note. [a] These values should be taken as lower limits only, given that follow-up of $\geqslant$T9 dwarf discoveries within this volume is still incomplete.

expected distribution of objects for power-law mass functions with various slopes of α, the functional form of which is given by $dN/dM \propto M^{-\alpha}$, where N is number of objects and M is the mass. A nominal low-mass cutoff of 1 $M_{\rm Jupiter}$, a constant birthrate over 0.1–10 Gyr, and evolutionary models of Baraffe et al. (2003) are assumed for the simulations, as well as an overall normalization of 0.0037 objects pc^{-3} for stars with 0.09–0.1 $M_\odot$, based on Reid et al. (1999). We show results for $\alpha = -1, 0, +1$ as well as the effect of increasing the low-mass cutoff to 5 $M_{\rm Jupiter}$ or to 10 $M_{\rm Jupiter}$ for the $\alpha = 0$ model. Our measurements, shown by the purple line, are overplotted on the simulations for comparison.

It is obvious from this diagram that the density of late-T dwarfs falls most closely along the $\alpha = -1.0$ model. For these results to match more closely to the $\alpha = 0.0$ model would require that our current census of these objects be deficient by a factor of two to three which does not seem plausible given that the follow-up presented in Kirkpatrick et al. (2011) and G. N. Mace et al. (in preparation) has already completed a large portion of the follow-up needed for the brightest *WISE* T dwarf candidates over the entire sky. Although densities as large as those predicted by an intermediate $\alpha = -0.5$ model are still possible, these brown dwarfs appear to be rarer than the $\alpha = 0.0$ simulation predicts.

Turning to the Y dwarfs, we find that the number density climbs relative to the T dwarfs. This would ordinarily suggest a steeper slope ($\alpha > 0.0$), if these fits were done independently of results at higher masses. The simulations of Burgasser et al. (2004, 2007) are normalized so that the space density for low-mass stars matches observational measures, so the space densities in Figure 14 are what would be expected if the same power law applied from low-mass stars to low-mass brown dwarfs. It may simply be that the power-law approximation is not ideal at lower masses or it may be that our space densities for Y dwarfs are overestimates if our trigonometric parallaxes for the Y0 and Y1 dwarfs are systematically too large. If we use the red curves from Figures 12 and 13 (i.e., the relations including WISE 1828+2650 in the fits), we find that the number densities in the Y dwarf bins drop by a factor of three. At face value this would result in space densities that more closely favor a slope of $\alpha = 0.0$ (but not its normalization). However, it must be kept in mind that the coldest bins in Figure 14 are based on only a handful of discoveries identified so far. Other Y dwarfs are certain to be added as other candidate objects from *WISE* are more fully characterized and as Y dwarf companions to higher mass objects are uncovered. Thus, we expect that these pessimistic values of the Y dwarf space density themselves represent only lower limits.

Models by Burrows et al. (2003) show that a brown dwarf of mass 5 $M_{\rm Jupiter}$ takes ~5 Gyr to cool to 200 K; a brown dwarf of mass 10 $M_{\rm Jupiter}$, even if formed at the same time as the Milky Way itself, has not yet had enough time to cool to 200 K. Our preliminary results suggest that the low-mass cutoff for star formation is below 10 and possibly even below 5 $M_{\rm Jupiter}$ (see Figure 14). Old brown dwarfs with masses below 5 $M_{\rm Jupiter}$ fall into a temperature regime ($T_{\rm eff} < 200$ K) that is too faint for *WISE* to sample a sufficient volume. As such, we may not be able to place stronger constraints on the low-mass cutoff using *WISE* discoveries alone.

It is possible to produce a larger number of cold Y dwarfs relative to L and T dwarfs—and therefore provide a better match to our results—if we drop the assumption that the star formation rate has been constant over the last 10 Gyr and instead use an exponentially declining star formation rate over time or a scenario whereby all star formation took place in the first 1 Gyr of the Milky Way's lifetime. Burgasser et al. (2004) confirm that the numbers of cold brown dwarfs is markedly higher than that of warmer brown dwarfs under both of these assumptions, but they caution that there is little other physical evidence supporting star formation rates like these. There are other possibilities, too. The Burgasser et al. (2004) simulations do not account for relative differences in the dynamical "heating" of low-mass versus high-mass brown dwarfs over time. That is, the scale height of the lower mass objects is expected to be larger than that of the higher mass group, due to the greater influence on boosting the velocities of the lower mass brown dwarfs during encounters with other objects as they orbit the Galaxy. However, this would tend to make the low-mass brown dwarfs somewhat rarer in the solar neighborhood, making the mismatch between our results and the simulations even more striking.

With these caveats in mind, we compare these preliminary results to other work in the literature that has attempted to measure the substellar mass function. We select four such avenues of exploration to use as comparison: earlier wide-field surveys for field brown dwarfs, a deep search using the *Spitzer Space Telescope*, studies in young clusters and star formation regions, and the results of field objects indirectly detected by microlensing surveys.

4.3.1. Comparison to Results from Other Field Brown Dwarf Studies

A few other wide-field searches have earlier attempted to determine the slope of the field mass function for objects later than spectral type T6. Metchev et al. (2008) used a cross-correlation of 2MASS with SDSS Data Release 1 to determine a space density of $4.7^{+3.1}_{-2.8} \times 10^{-3}$ objects pc^{-3} over the range T6–T8. Their results favor $\alpha \approx 0$. Reylé et al. (2010) used

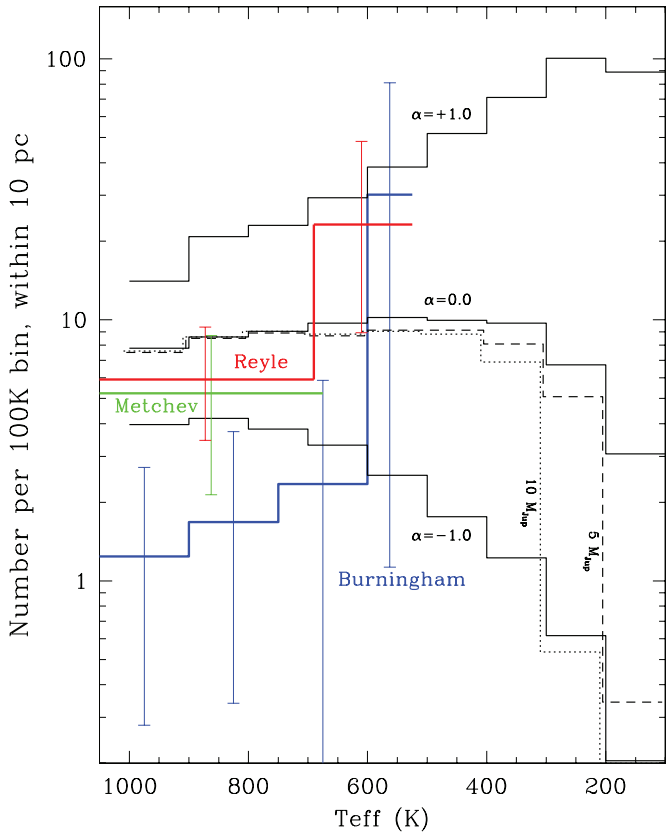

Figure 15. Previous measurements of the space density of mid- to late-T dwarfs from Metchev et al. (2008) (green), Reylé et al. (2010) (red), and Burningham et al. (2010) (blue) overplotted on the same simulations from Figure 14.

(A color version of this figure is available in the online journal.)

data from the Canada–France Brown Dwarf Survey to determine space densities of $5.3^{+3.1}_{-2.2} \times 10^{-3}$ objects pc^{-3} for T6–T8 and $8.3^{+9.0}_{-5.1} \times 10^{-3}$ objects pc^{-3} for T8.5–T9. Their results favor $\alpha \lesssim 0$. Burningham et al. (2010) used data from UKIDSS to determine space densities in the range $(0.30 \pm 0.20) \times 10^{-3}$ to $(0.59 \pm 0.39) \times 10^{-3}$ objects pc^{-3} for T6–T6.5, $(0.40 \pm 0.28) \times 10^{-3}$ to $(0.79 \pm 0.55) \times 10^{-3}$ objects pc^{-3} for T7–T7.5, $(0.58 \pm 0.51) \times 10^{-3}$ to $(1.1 \pm 1.0) \times 10^{-3}$ objects pc^{-3} for T8–T8.5, and $(3.1 \pm 2.9) \times 10^{-3}$ to $(7.6 \pm 6.9) \times 10^{-3}$ objects pc^{-3} for T9. These results favor $\alpha < 0$, confirming the earlier UKIDSS analysis by Pinfield et al. (2008). Figure 15 summarizes these results for direct comparison to our results in Figure 14.

It should be noted that results from each of these studies were derived using a relatively small number of sources—4 objects with types of T6 or later for Metchev et al. (2008), 13 objects with types ⩾T6 for Reylé et al. (2010), and 25 objects with types ⩾T6 for Burningham et al. (2010). Our new *WISE* study uses a sample of 148 objects (Table 9) with types ⩾T6, almost six times the number in the most data-rich of these previous surveys. It should be noted that the average distance to the Reylé et al. (2010) and Burningham et al. (2010) samples are much larger than for the sample we present in Tables 7 and 8. Our *WISE*-enabled sample is the nearest sample possible, and thus the one for which parallaxes and info on unresolved binarity will be most readily obtained, allowing for refinements of our space density numbers to unequalled precisions in the future. Nevertheless, despite the sparseness of the earlier data, those results are in general agreement with our space density results for objects earlier than T9.

4.3.2. Comparison to Results from the Spitzer Deep, Wide-field Survey

Eisenhardt et al. (2010) identified a sample of 14 cool brown dwarf candidates (spectral types >T7) using data from the 10 deg^2 *Spitzer* Deep, Wide-field Survey (SDWFS). The coldest of these candidates, SDWFS J143356.62+351949.2, has colors of ch1−ch2 = 2.24 ± 0.46 mag and H−ch2>5.73 mag. Using Figures 11 and 14 of Kirkpatrick et al. (2011) we find that the ch1−ch2 color is typical of a T9 dwarf and the H−ch2 color suggests that its type is ⩾T8. This survey, therefore, was probing down as far as late-T but probably not to early-Y.

Eisenhardt et al. (2010) found that the assumed space density and measured color distribution of the 14 brown dwarf candidates most closely matched a Chabrier (2003) log-normal mass function, or a power-law mass function with $\alpha = 1.3$, as long as the 4.5 μm flux of the Burrows et al. (2003) models was adjusted downward.[22] This value of α, however, is very high compared to the one we deduce from our measurements of field, late-T dwarfs in the all-sky sample ($-0.5 < \alpha < 0.0$).

New data have become available that shed additional light on these results. SDWFS J143356.62+351949.2 was imaged with *HST*/WFC3 in 8 exposures of 1400 s duration on 2009 December 3, and in 12 exposures of 700 s duration on 2009 December 16, as part of program 12044. Assuming a magnitude of W2 ≈ ch2 = 18.47 mag, the marginal F140W detection at 26.2 mag is fainter than the ∼25 mag expected for a T9 dwarf (see Figure 8). The F127M filter covers 1.239–1.308 μm, and from Figures 4 and 6 should include at least half the light seen in the 1.193–1.592 μm F140W filter. With <20% of the F140W bandpass, the F127M filter should thus produce a noticeably brighter magnitude if the object were a cold brown dwarf. However, the source is completely undetected in F127M, with a 2σ limit of 26.2 mag. We consider it more likely that this object is an extremely red extragalactic source. The SDWFS results, because of their depth, may have been more heavily contaminated by extragalactic objects than previously believed, leading to the higher value of α.

4.3.3. Comparison to the Initial Mass Function in Open Clusters and Star-forming Regions

Because of its proximity, relatively young age, and compactness on the sky, the Pleiades has been one of the most popular open clusters in which to hunt for brown dwarfs. Many studies have attempted to measure the slope of the substellar initial mass function in this cluster, with a sampling of results suggesting $\alpha = 0 - 1$ (Festin 1998), $\alpha = 0.6$ (Bouvier et al. 1998), and $\alpha = 0.62 \pm 0.14$ (Casewell et al. 2007). Other open clusters are found to have initial mass functions that are similar to that of the Pleiades (Bastian et al. 2010). These values of α are slightly larger than the one we derive.

Studies of the brown dwarf population in star formation regions are hampered by the larger distances to these areas and to complications with survey completeness, which is impacted by variable extinction across the field. However, low-mass brown dwarfs are still in a young, warm state and are easier to detect than in older clusters. Luhman (2007) compare results in Taurus, Chamaeleon I, IC 348, and the Trapezium Cluster to conclude that an initial mass function with slope $\alpha \lesssim 0$ is consistent with the ratio of the number of stars to brown dwarfs seen in those regions. Although doubts about the universality of the

[22] Such flux suppression is expected if non-equilibrium chemistry is altering the predicted depths of the CO fundamental band at 4.7 μm (Golimowski et al. 2004; Saumon et al. 2007).

initial mass function persist, Andersen et al. (2008) found that this assumption is credible and, having combined observational results in seven star formation regions and open clusters in the mass range 0.03–1.0 $M_{\odot}$—including the Pleiades, the Orion Nebula Cluster, and Taurus—conclude that $\alpha < 0$. These studies are in good agreement with our results using field brown dwarfs.

4.3.4. Comparison to the Number Density of Solivagant Objects Found by Microlensing Surveys

Sumi et al. (2011) have used the collection of observed microlensing events detected in the Microlensing Observations in Astrophysics and Optical Gravitational Lensing Experiment surveys to study the random stellar and substellar populations of the Milky Way. These populations are indirectly observed as lensing sources that temporarily brighten background sources in the Galactic Bulge as they pass through the line of sight between the Earth and the Bulge source. The duration of the magnification event depends upon the mass, distance, and transverse speed of the lens, and can be related back to mass using assumptions about the kinematic and space distribution of the lenses. Sumi et al. (2011) identify 474 well-characterized events with which they study the field mass function of the lensing sources. They fit these results with a tripartite power-law function that, in the brown dwarf regime ($0.01 \leqslant M/M_{\odot} \leqslant 0.08$), has an exponent of $\alpha = 0.49^{+0.24}_{-0.27}$. This value of α is similar to that found for brown dwarfs in the Pleiades but is somewhat larger than what we find in the field.

Sumi et al. (2011) also find that another population—rogue planets—may be needed to explain results at very low masses. However, this population is detectable over the low-mass tail of the brown dwarf population only at masses below $\sim 4\ M_{\rm Jupiter}$ (Einstein radius crossing times of less than two days). Models from Burrows et al. (2003) predict that an old (5 Gyr) solar metallicity brown dwarf with mass of 5 $M_{\rm Jupiter}$ would have an effective temperature of only 200 K and would be too dim to be imaged by *WISE* beyond ∼1 pc. Given that these objects would be much rarer than low-mass brown dwarfs (see Figure 2 of Sumi et al. 2011), they will not have any impact on the *WISE* results presented here.

5. CONCLUSIONS

We have presented 7 new Y dwarf discoveries from *WISE*, bringing the total number of Y dwarf discovered by *WISE* to 13. Using these Y dwarf discoveries along with *WISE* T dwarf discoveries from Kirkpatrick et al. (2011) and G. N. Mace et al. (in preparation) and discoveries from previous searches for field brown dwarfs, we compute space densities for late-T and early-Y dwarfs and find that stars outnumber brown dwarfs in the solar neighborhood by a factor of roughly six. However, this factor is certain to shrink in the future for two reasons: (1) the census of stars within a few parsecs of the Sun is well known, whereas that for late-T and Y dwarfs is still incomplete, so the ratio of stars to brown dwarfs is expected to decrease in the future; (2) the field sample does not yet show any clear signature that we have probed beyond star formation's low-mass cutoff, meaning that colder, very low mass objects likely exist and are too faint for even *WISE* to detect. This having been said, however, we expect the total number of Y dwarfs identified by *WISE* to be only a few dozen when follow-up is largely complete. Unless there is a *vast* reservoir of cold brown dwarfs invisible to *WISE*, the space density of stars is still expected to greatly outnumber that of brown dwarfs.

Because of the extreme faintness of these Y dwarfs, we have so far only been able to tease out a few hints regarding their distances, their atmospheric details, and their variety. Future work is needed to identify more examples and to characterize more fully the physical properties of ones already recognized. The study of Y-type brown dwarfs is still in its infancy but the glimpses caught so far promise tantalizing results ahead.

We thank the referee, Sandy Leggett, for constructive comments that helped to improve the paper. This publication makes use of data products from the *Wide-field Infrared Survey Explorer*, which is a joint project of the University of California, Los Angeles, and the Jet Propulsion Laboratory/California Institute of Technology, funded by the National Aeronautics and Space Administration. This publication also makes use of data products from 2MASS, SDSS, and DSS. 2MASS is a joint project of the University of Massachusetts and the Infrared Processing and Analysis Center/California Institute of Technology, funded by the National Aeronautics and Space Administration and the National Science Foundation. SDSS is funded by the Alfred P. Sloan Foundation, the Participating Institutions, the National Science Foundation, the U.S. Department of Energy, the National Aeronautics and Space Administration, the Japanese Monbukagakusho, the Max Planck Society, and the Higher Education Funding Council for England. The DSS were produced at the Space Telescope Science Institute under U.S. Government grant NAG W-2166. The images of these surveys are based on photographic data obtained using the Oschin Schmidt Telescope on Palomar Mountain and the UK Schmidt Telescope.

This work is based in part on observations made with the *Spitzer Space Telescope*, which is operated by the Jet Propulsion Laboratory, California Institute of Technology, under a contract with NASA. Support for this work was provided by NASA through an award issued to program 70062 and 80109 by JPL/Caltech. This work is also based in part on observations made with the NASA/ESA *Hubble Space Telescope*, obtained at the Space Telescope Science Institute, which is operated by the Association of Universities for Research in Astronomy, Inc., under NASA contract NAS 5-26555. These observations are associated with programs 12044 and 12330. Support for these programs was provided by NASA through a grant from the Space Telescope Science Institute. Some of the spectroscopic data presented herein were obtained at the W. M. Keck Observatory, which is operated as a scientific partnership among the California Institute of Technology, the University of California and the National Aeronautics and Space Administration. The Observatory was made possible by the generous financial support of the W. M. Keck Foundation. In acknowledgement of our observing time at Keck and the IRTF, we further wish to recognize the very significant cultural role and reverence that the summit of Mauna Kea has always had within the indigenous Hawaiian community. We are most fortunate to have the opportunity to conduct observations from this mountain.

Our research has benefitted from the M, L, and T dwarf compendium housed at http://DwarfArchives.org, whose server was funded by a NASA Small Research Grant, administered by the American Astronomical Society. This research has made use of the NASA/IPAC Infrared Science Archive (IRSA), which is operated by the Jet Propulsion Laboratory, California Institute of Technology, under contract with the National Aeronautics and Space Administration. We are also indebted to the SIMBAD database, operated at CDS, Strasbourg, France.

REFERENCES

Albert, L., Artigau, É., Delorme, P., et al. 2011, AJ, 141, 203
Andersen, M., Meyer, M. R., Greissl, J., & Aversa, A. 2008, ApJ, 683, L183
Artigau, É., Doyon, R., Lafrenière, D., et al. 2006, ApJ, 651, L57
Artigau, É., Radigan, J., Folkes, S., et al. 2010, ApJ, 718, L38
Baraffe, I., Chabrier, G., Barman, T. S., Allard, F., & Hauschildt, P. H. 2003, A&A, 402, 701
Bastian, N., Covey, K. R., & Meyer, M. R. 2010, ARA&A, 48, 339
Batten, A. H. 1998, J. R. Astron. Soc. Can., 92, 231
Beichman, C. A., Gelino, C. R., Kirkpatrick, J. D., et al. 2012, ApJ, submitted
Benedict, G. F., McArthur, B., Chappell, D. W., et al. 1999, AJ, 118, 1086
Bergfors, C., Brandner, W., Janson, M., et al. 2010, A&A, 520, A54
Bessell, M. S. 2005, ARA&A, 43, 293
Beuzit, J.-L., Ségransan, D., Forveille, T., et al. 2004, A&A, 425, 997
Bidelman, W. P. 1985, ApJS, 59, 197
Biller, B. A., Kasper, M., Close, L. M., Brandner, W., & Kellner, S. 2006, ApJ, 641, L141
Boeshaar, P. C., & Tyson, J. A. 1985, AJ, 90, 817
Bouvier, J., Stauffer, J. R., Martin, E. L., et al. 1998, A&A, 336, 490
Boyd, M. R., Henry, T. J., Jao, W.-C., Subasavage, J. P., & Hambly, N. C. 2011, AJ, 142, 92
Burgasser, A. J. 2007, ApJ, 659, 655
Burgasser, A. J., Cushing, M. C., Kirkpatrick, J. D., et al. 2011, ApJ, 735, 116
Burgasser, A. J., Geballe, T. R., Leggett, S. K., Kirkpatrick, J. D., & Golimowski, D. A. 2006a, ApJ, 637, 1067
Burgasser, A. J., Gelino, C. R., Cushing, M. C., & Kirkpatrick, J. D. 2012, ApJ, 745, 26
Burgasser, A. J., Kirkpatrick, J. D., Brown, M. E., et al. 1999, ApJ, 522, L65
Burgasser, A. J., Kirkpatrick, J. D., Brown, M. E., et al. 2002, ApJ, 564, 421
Burgasser, A. J., Kirkpatrick, J. D., Cruz, K. L., et al. 2006b, ApJS, 166, 585
Burgasser, A. J., Kirkpatrick, J. D., Cutri, R. M., et al. 2000a, ApJ, 531, L57
Burgasser, A. J., Kirkpatrick, J. D., McElwain, M. W., et al. 2003a, AJ, 125, 850
Burgasser, A. J., Kirkpatrick, J. D., Reid, I. N., et al. 2003b, ApJ, 586, 512
Burgasser, A. J., Looper, D., & Rayner, J. T. 2010, AJ, 139, 2448
Burgasser, A. J., McElwain, M. W., & Kirkpatrick, J. D. 2003c, AJ, 126, 2487
Burgasser, A. J., McElwain, M. W., Kirkpatrick, J. D., et al. 2004, AJ, 127, 2856
Burgasser, A. J., Reid, I. N., Siegler, N., et al. 2007, in Protostars and Planets V, ed. B. Reipurth, D. Jewitt, & K. Keil (Tucson, AZ: Univ. Arizona Press), 427
Burgasser, A. J., Tinney, C. G., Cushing, M. C., et al. 2008, ApJ, 689, L53
Burgasser, A. J., Wilson, J. C., Kirkpatrick, J. D., et al. 2000b, AJ, 120, 1100
Burgess, A. S. M., Moraux, E., Bouvier, J., et al. 2009, A&A, 508, 823
Burningham, B., Pinfield, D. J., Leggett, S. K., et al. 2008, MNRAS, 391, 320
Burningham, B., Pinfield, D. J., Leggett, S. K., et al. 2009, MNRAS, 395, 1237
Burningham, B., Pinfield, D. J., Lucas, P. W., et al. 2010, MNRAS, 406, 1885
Burrows, A., Marley, M., Hubbard, W. B., et al. 1997, ApJ, 491, 856
Burrows, A., Sudarsky, D., & Lunine, J. I. 2003, ApJ, 596, 587
Burrows, A., & Volobuyev, M. 2003, ApJ, 583, 985
Casewell, S. L., Dobbie, P. D., Hodgkin, S. T., et al. 2007, MNRAS, 378, 1131
Chabrier, G. 2003, PASP, 115, 763
Chiu, K., Fan, X., Leggett, S. K., et al. 2006, AJ, 131, 2722
Chiu, K., Liu, M. C., Jiang, L., et al. 2008, MNRAS, 385, L53
Costa, E., Méndez, R. A., Jao, W.-C., et al. 2005, AJ, 130, 337
Costa, E., Méndez, R. A., Jao, W.-C., et al. 2006, AJ, 132, 1234
Cuby, J. G., Saracco, P., Moorwood, A. F. M., et al. 1999, A&A, 349, L41
Cushing, M. C., Kirkpatrick, J. D., Gelino, C. R., et al. 2011, ApJ, 743, 50
Cushing, M. C., Roellig, T. L., Marley, M. S., et al. 2006, ApJ, 648, 614
Daemgen, S., Siegler, N., Reid, I. N., & Close, L. M. 2007, ApJ, 654, 558
Dahn, C. C., Harris, H. C., Vrba, F. J., et al. 2002, AJ, 124, 1170
Deacon, N. R., Liu, M. C., Magnier, E. A., et al. 2011, arXiv:1109.6319
Delfosse, X., Forveille, T., Beuzit, J.-L., et al. 1999, A&A, 344, 897
Delfosse, X., Forveille, T., Udry, S., et al. 1999, A&A, 350, L39
Delorme, P., Albert, L., Forveille, T., et al. 2010, A&A, 518, A39
Delorme, P., Delfosse, X., Albert, L., et al. 2008, A&A, 482, 961
Drummond, J. D., Christou, J. C., & Fugate, R. Q. 1995, ApJ, 450, 380
Ducourant, C., Dauphole, B., Rapaport, M., Colin, J., & Geffert, M. 1998, A&A, 333, 882
Dupuy, T. J., & Liu, M. C. 2012, arXiv:1201.2465
Eisenhardt, P. R. M., Griffith, R. L., Stern, D., et al. 2010, AJ, 139, 2455
Faherty, J. K., Burgasser, A. J., West, A. A., et al. 2010, AJ, 139, 176
Fazio, G. G., Hora, J. L., Allen, L. E., et al. 2004, ApJS, 154, 10
Festin, L. 1998, A&A, 333, 497
Forveille, T., Beuzit, J.-L., Delfosse, X., et al. 1999, A&A, 351, 619
Garrison, R. F. 1994, in ASP Conf. Ser. 60, The MK Process at 50 Years: A Powerful Tool for Astrophysical Insight, ed. C. Corbally, R. O. Gray, & R. F. Garrison (San Francisco, CA: ASP), 3
Gatewood, G., & Coban, L. 2009, AJ, 137, 402
Geballe, T. R., Knapp, G. R., Leggett, S. K., et al. 2002, ApJ, 564, 466
Geißler, K., Metchev, S., Kirkpatrick, J. D., Berriman, G. B., & Looper, D. 2011, ApJ, 732, 56
Gelino, C. R., Kirkpatrick, J. D., Cushing, M. C., et al. 2011, AJ, 142, 57
Giclas, H. L., Burnham, R., & Thomas, N. G. 1971, in Lowell Proper Motion Survey, Northern Hemisphere. The G numbered stars. 8991 stars fainter than magnitude 8 with motions >0.″26/yr (Flagstaff, AZ: Lowell Observatory)
Giclas, H. L., Burnham, R., Jr., & Thomas, N. G. 1978, Lowell Obs. Bull., 8, 89
Golimowski, D. A., Leggett, S. K., Marley, M. S., et al. 2004, AJ, 127, 3516
Gliese, W. 1956, Z. Astrophys., 39, 1
Gliese, W. 1969, Veroeffentlichungen des Astronomischen Rechen-Instituts Heidelberg, Catalog of Nearby Stars (Karlsruhe: Verlag G. Braun), 22, 1
Gliese, W., & Jahreiß, H. 1979, A&AS, 38, 423
Gliese, W., & Jahreiß, H. 1991, in The Astronomical Data Center CD-ROM: Selected Astronomical Catalogs, Vol. I, ed. L. E. Brotzmann & S. E. Gesser (Greenbelt, MD: NASA/Astronomical Data Center, Goddard Space Flight Center)
Goldman, B., Marsat, S., Henning, T., Clemens, C., & Greiner, J. 2010, MNRAS, 405, 1140
Golimowski, D. A., Henry, T. J., Krist, J. E., et al. 2000, AJ, 120, 2082
Gray, R. O., Corbally, C. J., Garrison, R. F., McFadden, M. T., & Robinson, P. E. 2003, AJ, 126, 2048
Gray, R. O., Corbally, C. J., Garrison, R. F., et al. 2006, AJ, 132, 161
Gray, R. O., Napier, M. G., & Winkler, L. I. 2001, AJ, 121, 214
Griffin, R. F. 1998, Observatory, 118, 273
Hawley, S. L., Gizis, J. E., & Reid, I. N. 1996, AJ, 112, 2799
Hawley, S. L., Gizis, J. E., & Reid, I. N. 1997, AJ, 113, 1458
Heintz, W. D. 1981, ApJS, 46, 247
Henry, T. J., Jao, W.-C., Subasavage, J. P., et al. 2006, AJ, 132, 2360
Henry, T. J., Johnson, D. S., McCarthy, D. W., Jr., & Kirkpatrick, J. D. 1992, A&A, 254, 116
Henry, T. J., Kirkpatrick, J. D., & Simons, D. A. 1994, AJ, 108, 1437
Henry, T. J., & McCarthy, D. W., Jr. 1993, AJ, 106, 773
Henry, T. J., Subasavage, J. P., Brown, M. A., et al. 2004, AJ, 128, 2460
Henry, T. J., Walkowicz, L. M., Barto, T. C., & Golimowski, D. A. 2002, AJ, 123, 2002
Herbst, W., & Layden, A. C. 1987, AJ, 94, 150
Hershey, J. L., & Taff, L. G. 1998, AJ, 116, 1440
Hertzsprung, E. 1907, Zeitschrift für Wissenschaftliche Photographie, Photophysik und Photochemie Zur Strahlung der Sterne, 5, 86
Hertzsprung, E. 1922, Bull. Astron. Inst. Neth., 1, 21
Irwin, A. W., Yang, S. L. S., & Walker, G. A. H. 1996, PASP, 108, 580
Jao, W.-C., Henry, T. J., Subasavage, J. P., et al. 2005, AJ, 129, 1954
Jenkins, J. S., Ramsey, L. W., Jones, H. R. A., et al. 2009, ApJ, 704, 975
Jenkins, L. F. 1952, in General Catalog of Trigonometric Stellar Parallaxes (New Haven, CT: Yale University Observatory)
Karataş, Y., Bilir, S., Eker, Z., & Demircan, O. 2004, MNRAS, 349, 1069
Kasper, M., Biller, B. A., Burrows, A., et al. 2007, A&A, 471, 655
Keenan, P. C., & McNeil, R. C. 1989, ApJS, 71, 245
Khrutskaya, E. V., Izmailov, I. S., & Khovrichev, M. Y. 2010, Astron. Lett., 36, 576
Kirkpatrick, J. D. 1992, PhD thesis (Tucson: Univ. of Arizona)
Kirkpatrick, J. D. 2005, ARA&A, 43, 195
Kirkpatrick, J. D. 2008, in ASP Conf. Ser. 384, 14th Cambridge Workshop on Cool Stars, Stellar Systems, and the Sun, ed. G. van Belle (San Francisco, CA: ASP), 85
Kirkpatrick, J. D., Cruz, K. L., Barman, T. S., et al. 2008, ApJ, 689, 1295
Kirkpatrick, J. D., Cushing, M. C., Gelino, C. R., et al. 2011, ApJS, 197, 19
Kirkpatrick, J. D., Henry, T. J., & McCarthy, D. W., Jr. 1991, ApJS, 77, 417
Kirkpatrick, J. D., Henry, T. J., & Simons, D. A. 1995, AJ, 109, 797
Kirkpatrick, J. D., Looper, D. L., Burgasser, A. J., et al. 2010, ApJS, 190, 100
Kirkpatrick, J. D., & McCarthy, D. W., Jr. 1994, AJ, 107, 333
Kirkpatrick, J. D., Reid, I. N., Liebert, J., et al. 1999, ApJ, 519, 802
Kirkpatrick, J. D., Reid, I. N., Liebert, J., et al. 2000, AJ, 120, 447
Knapp, G. R., Leggett, S. K., Fan, X., et al. 2004, AJ, 127, 3553
Koester, D., Voss, B., Napiwotzki, R., et al. 2009, A&A, 505, 441
Kuiper, G. P. 1942, ApJ, 95, 201
Kuiper, V. G. P. 1943, ApJ, 97, 275
Leggett, S. K., Burningham, B., Saumon, D., et al. 2010, ApJ, 710, 1627
Leggett, S. K., Toomey, D. W., Geballe, T. R., & Brown, R. H. 1999, ApJ, 517, L139
Liu, M. C., Delorme, P., Dupuy, T. J., et al. 2011, ApJ, 740, 108
Liu, M. C., Dupuy, T. J., & Leggett, S. K. 2010, ApJ, 722, 311

Liu, M. C., Leggett, S. K., Golimowski, D. A., et al. 2006, ApJ, 647, 1393
Lodders, K. 1999, ApJ, 519, 793
Lodieu, N., Burningham, B., Hambly, N. C., & Pinfield, D. J. 2009, MNRAS, 397, 258
Lodieu, N., Dobbie, P. D., Deacon, N. R., Venemans, B. P., & Durant, M. 2009, MNRAS, 395, 1631
Lodieu, N., Pinfield, D. J., Leggett, S. K., et al. 2007, MNRAS, 379, 1423
Loh, E. D., Biel, J. D., Chen, J.-J., et al. 2004, Proc. SPIE, 5492, 1644
Looper, D. L., Gelino, C. R., Burgasser, A. J., & Kirkpatrick, J. D. 2008, ApJ, 685, 1183
Looper, D. L., Kirkpatrick, J. D., & Burgasser, A. J. 2007, AJ, 134, 1162
Lucas, P. W., Tinney, C. G., Burningham, B., et al. 2010, MNRAS, 408, L56
Luhman, K. L. 2007, ApJS, 173, 104
Luhman, K. L., Burgasser, A. J., & Bochanski, J. J. 2011, ApJ, 730, L9
Luhman, K. L., Burgasser, A. J., Labbé, I., et al. 2012, ApJ, 744, 135
Luhman, K. L., Patten, B. M., Marengo, M., et al. 2007, ApJ, 654, 570
Luyten, W. J. 1979, in LHS Catalog (2nd ed.; Minneapolis, MN: Univ. Minnesota)
Mainzer, A., Cushing, M. C., Skrutskie, M., et al. 2011, ApJ, 726, 30
Marley, M. S., Saumon, D., & Goldblatt, C. 2010, ApJ, 723, L117
Marocco, F., Smart, R. L., Jones, H. R. A., et al. 2010, A&A, 524, A38
Marsh, K. A., Wright, E. L., Kirkpatrick, J. D., et al. 2012, ApJ, submitted
Martini, P., Persson, S. E., Murphy, D. C., et al. 2004, Proc. SPIE, 5492, 1653
Mason, B. D., McAlister, H. A., Hartkopf, W. I., & Shara, M. M. 1995, AJ, 109, 332
Masters, D., McCarthy, P., Burgasser, A. J., et al. 2012, arXiv:1204.6320
Matthews, K., Nakajima, T., Kulkarni, S. R., & Oppenheimer, B. R. 1996, AJ, 112, 1678
McCarthy, D. W., Jr., Henry, T. J., Fleming, T. A., et al. 1988, ApJ, 333, 943
McCaughrean, M. J., Close, L. M., Scholz, R.-D., et al. 2004, A&A, 413, 1029
McCook, G. P., & Sion, E. M. 2006, VizieR Online Data Catalog, 3235, 0
McLean, I. S., Becklin, E. E., Bendiksen, O., et al. 1998, Proc. SPIE, 3354, 566
McLean, I. S., Graham, J. R., Becklin, E. E., et al. 2000, Proc. SPIE, 4008, 1048
McLean, I. S., McGovern, M. R., Burgasser, A. J., et al. 2003, ApJ, 596, 561
Metchev, S. A., Kirkpatrick, J. D., Berriman, G. B., & Looper, D. 2008, ApJ, 676, 1281
Milligan, S., Cranton, B. W., & Skrutskie, M. F. 1996, Proc. SPIE, 2863, 2
Montagnier, G., Ségransan, D., Beuzit, J.-L., et al. 2006, A&A, 460, L19
Mould, J. R. 1976, A&A, 48, 443
Mould, J. R., & Hyland, A. R. 1976, ApJ, 208, 399
Mugrauer, M., Seifahrt, A., Neuhäuser, R., & Mazeh, T. 2006, MNRAS, 373, L31
Murray, D. N., Burningham, B., Jones, H. R. A., et al. 2011, MNRAS, 414, 575
Nakajima, T., Oppenheimer, B. R., Kulkarni, S. R., et al. 1995, Nature, 378, 463
Perryman, M. A. C., Lindegren, L., Kovalevsky, J., et al. 1997, A&A, 323, L49
Pinfield, D. J., Burningham, B., Tamura, M., et al. 2008, MNRAS, 390, 304
Reid, I. N., & Cruz, K. L. 2002, AJ, 123, 2806
Reid, I. N., Cruz, K. L., & Allen, P. R. 2007, AJ, 133, 2825
Reid, I. N., Cruz, K. L., Allen, P., et al. 2004, AJ, 128, 463
Reid, I. N., Cruz, K. L., Laurie, S. P., et al. 2003, AJ, 125, 354
Reid, I. N., & Gizis, J. E. 1997, AJ, 113, 2246
Reid, I. N., Hawley, S. L., & Gizis, J. E. 1995, AJ, 110, 1838
Reid, I. N., Kilkenny, D., & Cruz, K. L. 2002, AJ, 123, 2822
Reid, I. N., Kirkpatrick, J. D., Liebert, J., et al. 1999, ApJ, 521, 613
Reiners, A., Seifahrt, A., Käufl, H. U., Siebenmorgen, R., & Smette, A. 2007, A&A, 471, L5
Reylé, C., Delorme, P., Willott, C. J., et al. 2010, A&A, 522, A112
Riaz, B., Gizis, J. E., & Harvin, J. 2006, AJ, 132, 866
Riedel, A. R., Murphy, S. J., Henry, T. J., et al. 2011, AJ, 142, 104
Rodgers, A. W., & Eggen, O. J. 1974, PASP, 86, 742
Saumon, D., Marley, M. S., Leggett, S. K., et al. 2007, ApJ, 656, 1136
Schilbach, E., Röser, S., & Scholz, R.-D. 2009, A&A, 493, L27
Schmidt, M. 1968, ApJ, 151, 393
Scholz, R.-D. 2010, A&A, 510, L8
Scholz, R.-D. 2010, A&A, 515, A92
Scholz, R.-D., Bihain, G., Schnurr, O., & Storm, J. 2011, A&A, 532, L5
Scholz, R.-D., Lo Curto, G., Méndez, R. A., et al. 2005a, A&A, 439, 1127
Scholz, R.-D., McCaughrean, M. J., Lodieu, N., & Kuhlbrodt, B. 2003, A&A, 398, L29
Scholz, R.-D., Meusinger, H., & Jahreiß, H. 2005b, A&A, 442, 211
Ségransan, D., Delfosse, X., Forveille, T., et al. 2000, A&A, 364, 665
Seifahrt, A., Röll, T., Neuhäuser, R., et al. 2008, A&A, 484, 429
Shkolnik, E., Liu, M. C., & Reid, I. N. 2009, ApJ, 699, 649
Shkolnik, E. L., Hebb, L., Liu, M. C., Reid, I. N., & Collier Cameron, A. 2010, ApJ, 716, 1522
Simcoe, R. A., Burgasser, A. J., Bochanski, J. J., et al. 2010, Proc. SPIE, 7735, 38
Simcoe, R. A., Burgasser, A. J., Bernstein, R. A., et al. 2008, Proc. SPIE, 7014, 27
Skrutskie, M. F., Cutri, R. M., Stiening, R., et al. 2006, AJ, 131, 1163
Stephens, D. C., & Leggett, S. K. 2004, PASP, 116, 9
Strauss, M. A., Fan, X., Gunn, J. E., et al. 1999, ApJ, 522, L61
Stumpf, M. B., Brandner, W., Henning, T., et al. 2008, arXiv:0811.0556
Stumpf, M. B., Brandner, W., Joergens, V., et al. 2010, ApJ, 724, 1
Subasavage, J. P., Jao, W.-C., Henry, T. J., et al. 2009, AJ, 137, 4547
Sumi, T., Kamiya, K., Bennett, D. P., et al. 2011, Nature, 473, 349
Swaters, R. A., Valdes, F., & Dickinson, M. E. 2009, in ASP Conf. Ser. 411, Astronomical Data Analysis Software and Systems XVIII, ed. D. A. Bohlender, D. Durand, & Patrick Dowler (San Francisco, CA: ASP), 506
Tinney, C. G. 1996, MNRAS, 281, 644
Tinney, C. G., Burgasser, A. J., & Kirkpatrick, J. D. 2003, AJ, 126, 975
Tinney, C. G., Burgasser, A. J., Kirkpatrick, J. D., & McElwain, M. W. 2005, AJ, 130, 2326
Tinney, C. G., Ryder, S. D., Ellis, S. C., et al. 2004, Proc. SPIE, 5492, 998
Tokunaga, A. T., Simons, D. A., & Vacca, W. D. 2002, PASP, 114, 180
Tomkin, J., & Pettersen, B. R. 1986, AJ, 92, 1424
Torres, G., Henry, T. J., Franz, O. G., & Wasserman, L. H. 1999, AJ, 117, 562
Tsvetanov, Z. I., Golimowski, D. A., Zheng, W., et al. 2000, ApJ, 531, L61
van Altena, W. F., Lee, J. T., & Hoffleit, E. D. 1995, in The General Catalog of Trigonometric Stellar Parallaxes (4th ed.; New Haven, CT: Yale Univ. Observatory)
van de Kamp, P. 1930, Pop. Astron., 38, 17
van de Kamp, P. 1940, Pop. Astron., 48, 297
van de Kamp, P. 1945, PASP, 57, 34
van de Kamp, P. 1953, PASP, 65, 73
van de Kamp, P. 1969, PASP, 81, 5
van de Kamp, P. 1971, ARA&A, 9, 103
van Leeuwen, F. 2007, A&A, 474, 653
van Maanen, A. 1917, PASP, 29, 258
van Maanen, A. 1943, Leaflet of the Astronomical Society of the Pacific (San Francisco, CA: ASP), 4, 199
Volk, K., Blum, R., Walker, G., & Puxley, P. 2003, IAU Circ., 8188, 2
Vrba, F. J., Henden, A. A., Luginbuhl, C. B., et al. 2004, AJ, 127, 2948
Warren, S. J., Mortlock, D. J., Leggett, S. K., et al. 2007, MNRAS, 381, 1400
Westphal, J. A. 1969, ApJ, 157, L63
Wilson, O. C., & Vainu Bappu, M. K. 1957, ApJ, 125, 661
Winters, J. G., Henry, T. J., Jao, W.-C., et al. 2011, AJ, 141, 21
Wright, E. L., Eisenhardt, P. R. M., Mainzer, A. K., et al. 2010, AJ, 140, 1868
Wright, E. L., Skrutskie, M. F., Kirkpatrick, J. D., et al. 2012, arXiv:1203.5764
York, D. G., Adelman, J., Anderson, J. E., Jr., et al. 2000, AJ, 120, 1579
Zapatero Osorio, M. R., Béjar, V. J. S., Martín, E. L., et al. 2002, ApJ, 578, 536
Zuckerman, B., & Song, I. 2004, ARA&A, 42, 685